VPS13D IS A REGULATOR OF PINK1-MEDIATED MITOPHAGY AND MEMBRANE CONTACTS

A Dissertation Presented

By

James L. Shen

Submitted to the Faculty of the University of Massachusetts Graduate School of Biomedical Sciences, Worcester in partial fulfillment of the requirements for the degree of

DOCTOR OF PHILOSOPHY

March 29, 2021

MOLECULAR CELL AND CANCER BIOLOGY

VPS13D IS A REGULATOR OF PINK1-MEDIATED MITOPHAGY AND MEMBRANE CONTACTS

A Dissertation Presented

By

James L. Shen

This work was undertaken in the Graduate School of Biomedical Sciences Program in Molecular Cell and Cancer Biology

Eric H. Baehrecke, Ph.D., Thesis Advisor

Cole Haynes, Ph.D., Member of Committee

Junhao Mao, Ph.D., Member of Committee

Dohoon Kim, Ph.D., Member of Committee

Jayanta Debnath, M.D. Ph.D., External Member of Committee

Andreas Bergmann, Ph.D., Chair of Committee

Mary Ellen Lane, Ph.D.,

Dean of the Graduate School of Biomedical Sciences

March 29, 2021

DEDICATION

I dedicate this thesis to my loved ones. You have stuck by me for so long, endured too many “need to go to work”s, and yet still encouraged me. You all know who you are.

ACKNOWLEDGEMENTS

First, I would like to thank my mentor, Dr. Eric H. Baehrecke. He has been incredibly patient, thoughtful and supportive during my time as a student. Whether it was giving advice for experiments, support during this very difficult time to get published (thanks COVID), critiquing my writing, or participating in many of the academic debates we have had on what to include and exclude in manuscripts, he has been an exemplary model of a mentor. I have evolved as a scientist thanks to his mentorship, and as I continue on my professional path as a physician scientist, I doubt I will ever find a mentor as supportive and professional as him. He is more than a great mentor. He is a good one.

I could not have completed this work without the support and advice of past and current members of the Baehrecke lab, including honorary lab members. It has been a wild ride being a member of the Baehrecke lab. Thanks to Liz for being a model bay mate, although to be fair, I deserved a lot more stickers. Thanks to Allyson for starting off this Vps13D project and, while it was brief, doing a remarkable job being the lab bully. Speaking of which, thanks to Johnna for temporarily taking up the mantle of being the lab bully and maintaining the lab's reputation as the "Party Lab." Thanks to Shaowei for being perhaps the most organized fly biologist I have ever known…and making me feel incredibly bad about how disorganized I am in the process. Thanks to Yan for teaching me how to do many Cell Culture techniques that were vital for my manuscripts. And then putting up with me asking how to do the exact same techniques several months later when I forgot I already asked you. Thanks to Panos for having the remarkable ability to answer ANY question that cannot found on Google or Wikipedia. Thanks to Tina for being the lab mom and cleaning up any mess that I was too lazy to clean up or indefinitely put off. Thanks to Ruoxi for the designing countless fly lines that I was either too lazy to design or thought were impossible. I still can't believe you managed to recombine FRT19a with that *pink1*^{B9} allele. Thanks to Fei for all the juicy COVID gossip that made social distancing in the lab more manageable. Thanks to Miaomiao for continuing the Vps13D project and actually making it here. Seriously, I still can't believe you had to go through Cambodia to arrive in the US. And last, but not least, Lucas…Ok, I was actually a little disappointed in your performance as lab bully. But you have been incredibly enthusiastic and helpful with the Vps13D project, and actually decided to join this lab to continue the project even after all my attempts to scare you away on your rotation, so I can respect that.

On a more serious note, I would like to thank my TRAC and thesis committee members. Thank you Andreas for being a superb chair, always asking plenty of thought-provoking questions while we had joint lab meetings and keeping a fine balance between professional and reasonable. Thanks to Junhao for letting me rotate in his lab and

teaching me some very valuable cell culture and mouse model techniques. I would like to thank Cole for putting up with all my mitochondria related questions. Thanks to Jay for letting me present in his lab meetings and providing tons of useful feedback. And lastly, thanks to Do for his thoughtful insight during MCCB seminars…and especially for agreeing to serve on my thesis committee at the last minute!!

Lastly, I would like to thank my family. To my father who is not only supportive, but also secretly helps me with my scientific endeavors as a scientist himself. To my mother, who is always looking for ways to help me, whether it is cooking tons of delicious food or buying me 5 sets of shoes. To my brother, who is one of the few people who understands my awkward sense of humor and is currently struggling to survive as a healthcare provider in a random hospital somewhere (a situation I will soon be accustomed to as well). And finally, to Xiaowen, who has been through so much with me. You have supported me every step of the way. I always look forward to you welcoming me home every day, whether it is with delicious cooking or motivation that just keeps me going. I could not have gotten this far without you.

ABSTRACT

Autophagy is the delivery of cytoplasmic cargo to lysosomes for degradation. Defects in autophagy are responsible for various diseases, including neurodegenerative diseases and cancer. While studies in yeast have largely characterized autophagy in response to nutrient starvation, these elegant studies do not account for autophagy in other contexts, including selective autophagy of organelles. A previous screen identified *Vps13D* as a gene required for the autophagic removal of mitochondria, mitophagy. Vps13D is highly conserved and essential in animals, and *Vps13d* loss-of-function mutants have enlarged mitochondria and mitophagy deficiencies in both cell and animal models. However, the mechanism by which Vps13D regulates these processes has not been defined.

Here, I use mitochondrial clearance in the developing *Drosophila* intestine and fibroblasts from *VPS13D* mutant patients as experimental models to investigate the function of Vps13D. I discover that Vps13D is a regulator of ubiquitin and Atg8a/LC3/GABARAP localization around mitochondria. These functions are dependent on Pink1, a ubiquitin kinase, and the core autophagy machinery, respectively. Furthermore, Vps13D regulates mitochondria and endoplasmic reticulum (ER) contact sites downstream of Vmp1, a repressor of mitochondria and ER contact sites. I find that Marf, a mitochondria and ER tether and regulator of mitochondrial fusion, acts downstream of both Vmp1 and Vps13D. These findings explain the phenotypes in *Vps13d* mutants, as dysregulation of ubiquitin, Atg8a, and mitochondria and ER membrane contact sites impair regulation of both autophagy and mitochondria morphology.

TABLE OF CONTENTS

LIST OF TABLES

Tables in Chapter I

Tables in Chapter II

Tables in Chapter III

Tables in Appendix

LIST OF FIGURES

Figures in Chapter I

Figures in Chapter II

Figures in Chapter III

Figures in Chapter IV

LIST OF ABBREVIATIONS

APF	After prepupae formation
ATG/atg	autophagy-related gene
Atg8a/LC3/GABARAP	Autophagy-related 8a/ Microtubule-associated protein 1A/1B-light chain 3/ Gamma-aminobutyric acid receptor-associated protein
BCL2	B-cell Lymphoma 2
ER	Endoplasmic Reticulum
ESCRT	endosomal sorting complexes required for transport
IM	Isolation Membrane
MAM	Mitochondria associated membranes
MTS	mitochondrial targetting sequence
NDP52	Nuclear domain 10 protein 52
OPTN	Optineurin
P62//Ref2p	Sequestosome-1/refractory to sigma P
PAS	Phagophore Assembly Site
PE	phosphatidylethanolamine
PI3KC3-C1	Class III PI3K complex I
PI3P	Phosphatidylinositol 3-phosphate
PINK1	PTEN-induced putative kinase
PARK2/Park	E3 Parkinson’s Disease 2
ROS	Reactive Oxygen Species
UVRAG	UV radiation resistance-associated gene protein
Vps13D	Vacuolar Protein Sorting 13 Homolog D

PREFACE

The work presented in Chapter II represents unpublished work that is currently in submission.

The work presented in Chapter III represents unpublished work that is under revision at *Current Biology:*

Shen J.L., Fortier T.M., Zhao Y.G., Wang R. Burmeister M., Baehrecke E.H. (2021). A conserved Vps13D pathway regulates organelle contact in development and disease. *Current Biology* (under revision).

CHAPTER I

Introduction

A. Autophagy

Autophagy, or self-eating, is the process by which intracellular contents are degraded by the lysosome. This process was first identified as a potential survival mechanism for cells in response to nutrient deprivation, but has since been found to play more complex roles in metabolism, development and disease (Takeshige et al., 1992; Cecconi and Levine, 2008; Levine and Kroemer 2008). There are three known classes of autophagy: microautophagy, chaperone-mediated autophagy, and macroautophagy (Parzych and Klionsky, 2014). Microautophagy is the process by which the lysosomal membrane engulfs nearby cargo (Mijaljica et al., 2011). Chaperone-mediated autophagy involves using chaperones to target cargo for transport across the lysosomal membrane for delivery (Massey et al., 2004). Macroautophagy is the third and most characterized form of autophagy and will hereby be referred to as “autophagy.” This process is unique in that it involves sequestration of cargo away from the lysosome in a vesicle known as an isolation membrane (IM)/phagophore.

Autophagy involves the targeting of cargo for degradation, the recruitment of the autophagy machinery to the cargo, and finally the processing of the cargo to the lysosome for degradation. Substrates are marked for autophagic degradation through an E1-E2-E3 ubiquitination process. An E1 enzyme activates ubiquitin for transfer onto an E2 enzyme, which then catalyzes the transfer of ubiquitin to an E3. The E3 then transfers the ubiquitin to a cargo substrate (Scheffner et al., 1995). This process links

the lysine residue of a protein with ubiquitin, which in turn can form ubiquitin chains through the addition of more ubiquitin moieties on ubiquitin lysine residues. The type of ubiquitin chain is typically named by which of these lysine residues is conjugated with ubiquitin. For example, K-63 ubiquitin chains are chains where the lysine-63 residue is conjugated with ubiquitin. The types of ubiquitin chains determine the purpose of ubiquitination (Akutsu et al., 2016). While many types of ubiquitin chains exist, in the context of autophagy ubiquitination generally refers to K-63 ubiquitination, which labels cargo for autophagy (Ohtake et al., 2018).

The degradation of protein aggregates, pathogens, and organelles typically involve the use of autophagic cargo receptors, including Ref2p/p62, to link ubiquitinated cargo with the autophagy machinery (Farré and Subramani, 2016). After an IM localizes to the cargo, it expands into a double membrane structure known as an autophagosome. This structure fuses with the lysosome to form an autolysosome, an acidic structure that degrades the cargo. The composition of the autophagosome contains many key autophagy proteins, including Atg8/LC3/GABARAP, and lipids like Phosphatidylinositol 3-phosphate (PI3P) and phosphatidylethanolamine (PE). The formation of this structure is driven by a set of core autophagy genes (*atg*) with distinct roles at the phagophore assembly site (PAS) (Xie and Klionsky, 2007; Shaid and Brandts 2013). These genes involved in the core autophagy machinery are listed in **Table 1-1.**

Table 1-1: Core Autophagy Genes in Various Organisms.

Complex	*S. cerevisiae*	*D. melanogaster*	*H. sapiens*
Atg1/ULK1/2	ATG1	Atg1	ULK1/2
	ATG13	Atg13	ATG13
	ATG17	Atg17	FIP200/RB1CC1
	ATG29		
	ATG31		
		Atg101	ATG101
Atg2/9/18	ATG2	Atg2	ATG2
	ATG9	Atg9	ATG9A, ATG9B
	ATG18	Atg18	WIPI1, WIPI2, WIPI3, WIPI4
PI3KC3-C1	ATG6	Atg6	BECN1
	VPS34	Vps34	VPS34
	ATG14	Atg14	ATG14
	VPS15	Vps15	VPS15
		CG6116	UVRAG
		EndoB	SH3GLB1
		Buffy	BCL2
			AMBRA1
Ubiquitin-like Conjugating System	ATG8	Atg8a, Atg8b	MAP1LC3A, MAP1LC3B, MAP1LC3C, GABARAP, GABARAPL2
	ATG3	Atg3	ATG3
	ATG4	Atg4	ATG4A, ATG4B, ATG4C, ATG4D
	ATG5	Atg5	ATG5
	ATG7	Atg7	ATG7
	ATG10	Atg10	ATG10
	ATG12	Atg12	ATG12
	ATG16	Atg16	ATG16L1, ATG16L2
N/A	TOR1, TOR2	Tor	MTOR
		Ref2p	P62
	TEP1	Pten	PTEN
		Tango5	VMP1
		Epg5	EPG5
		tank	EI24
		Rab7	RAB7
	KOG1	Raptor	RAPTOR
	RHB1	Rheb	RHEB
	TSC11	Rictor	RICTOR

A1. Autophagy Initiation

The initiation of autophagy begins with the recruitment of the Atg1/ULK1/2 complex, which includes Atg1 and other components depending on the organism. Starvation-induced autophagy typically involves signaling through nutrient signals, such as AMP-activated kinase (AMPK) and mechanistic target of rapamycin (mTOR). In mammals, these components include conserved autophagy proteins including ATG13, FIP200/, and ATG101 (Nishimura and Tooze, 2020). Atg1 is a serine/threonine kinase, and is known to phosphorylate many downstream autophagy genes and undergo auto-phosphorylation (Matsuura et al. 1997). Atg13 is phosphorylated by mTOR in nutrient-rich conditions, but is rapidly dephosphorylated in starved conditions and binds with Atg1 to help initiate starvation-induced autophagy (Kamada et al., 2010). FIP200 is important for stabilization and phosphorylation of the Atg1 complex, and is believed to be the homologue of Atg17 in yeast (Hara et al., 2008). ATG101, while lacking a yeast homologue, is believed to play a similar role in stabilization the Atg1 complex (Mercer et al., 2009). The Atg1 complex is responsible for recruiting other core autophagy components to the PAS.

A2. The Atg9-Atg2-Atg18 Complex

The Atg9-Atg2-Atg18 complex is important for the generation of the autophagosome membrane. While the exact role of the proteins in this complex are still being researched, it is thought that Atg9 facilitates the distribution of key lipids and proteins needed for autophagosome assembly. In yeast, it is believed to act as the initial source of membrane for the autophagosome (Nishimura and Tooze, 2020). Atg9 is

phosphorylated by Atg1, allowing Atg9 to recruit Atg2/ATG2 and Atg18/WIPI to the PAS (Araki et al., 2013). This Atg9/Atg2/Atg18 complex facilitates downstream applications in autophagosome nucleation. Current models suggest that Atg2 serves as a lipid transporter and membrane tether, while Atg18 facilitates PI3P transfer to downstream Atg proteins (Nishimura and Tooze, 2020).

A3. The Class III PI3K complex I (PI3KC3-C1)

PI3P and PE make up the primary lipid composition of autophagosome membranes and are crucial for recruitment of other autophagy proteins. These lipids are generated by the PI3KC3-C1 complex, which is comprised of Atg6/BECN1, Vps34/VPS34, Vps15/p150, and Atg14/ATG14L (Nishimura and Tooze, 2020). Another Atg protein, Atg38/NRBF2, is required for stability of this complex (Araki et al., 2013). In addition to autophagy, many of these proteins play important roles in vesicular and protein transport. Vps34 acts as a kinase that phosphorylates phosphatidylinositol to produce PI3P, but requires other proteins to facilitate this process (Nishimura and Tooze, 2020). This is partly achieved by Vps15, which scaffolds Vps34 to other PI3KC3-C1 complex members (Stjepanovic et al., 2017). Atg6 forms an essential regulatory component of this complex. Interestingly, Atg6 can bind with anti-apoptotic protein Bcl-2 to prevent autophagic activity (Pattingre et al., 2005). In addition to autophagy, many of these proteins play important roles in vesicular and protein transport. For example, Atg6 regulates endocytic trafficking through its interactions with UVRAG (Kim et al., 2015).

A4. Atg8a/LC3/GABARAP and the Ubiquitin-like Conjugating System

All of these previously mentioned complexes contain proteins with Atg8a interacting motifs (AIM). Atg8a is an important component of the autophagosome, which is activated through lipidation. Lipidation allows incorporation of Atg8a onto both the inner and outer membranes of the autophagosome in a process similar to the ubiquitination process described previously (see A). As such, multiple autophagy proteins and complexes act as the E1, E2, and E3. This process is summarized in **Figure 1.1.** In Atg8a-lipidation, Atg4 cleaves the C-terminal of Atg8a to expose a terminal glycine, which is transferred by Atg7 (E1-like) to Atg3 (E2-like). Separately, Atg12 conjugates with Atg7 before conjugating with the E2-like Atg10. Atg12 is then transferred to Atg5 and Atg16 to form the Atg5/12/16 complex. The recruited Atg5/12/16 complex then acts as an E3 enzyme for Atg8a, replacing Atg3 with PE to lipidate Atg8a onto the expanding autophagosome membrane. After fusion of the autophagosome with the lysosome and degradation of the cargo, Atg4 cleaves Atg8a on the outer autophagosome membrane for Atg8a recycling (Nishimura and Tooze, 2020).

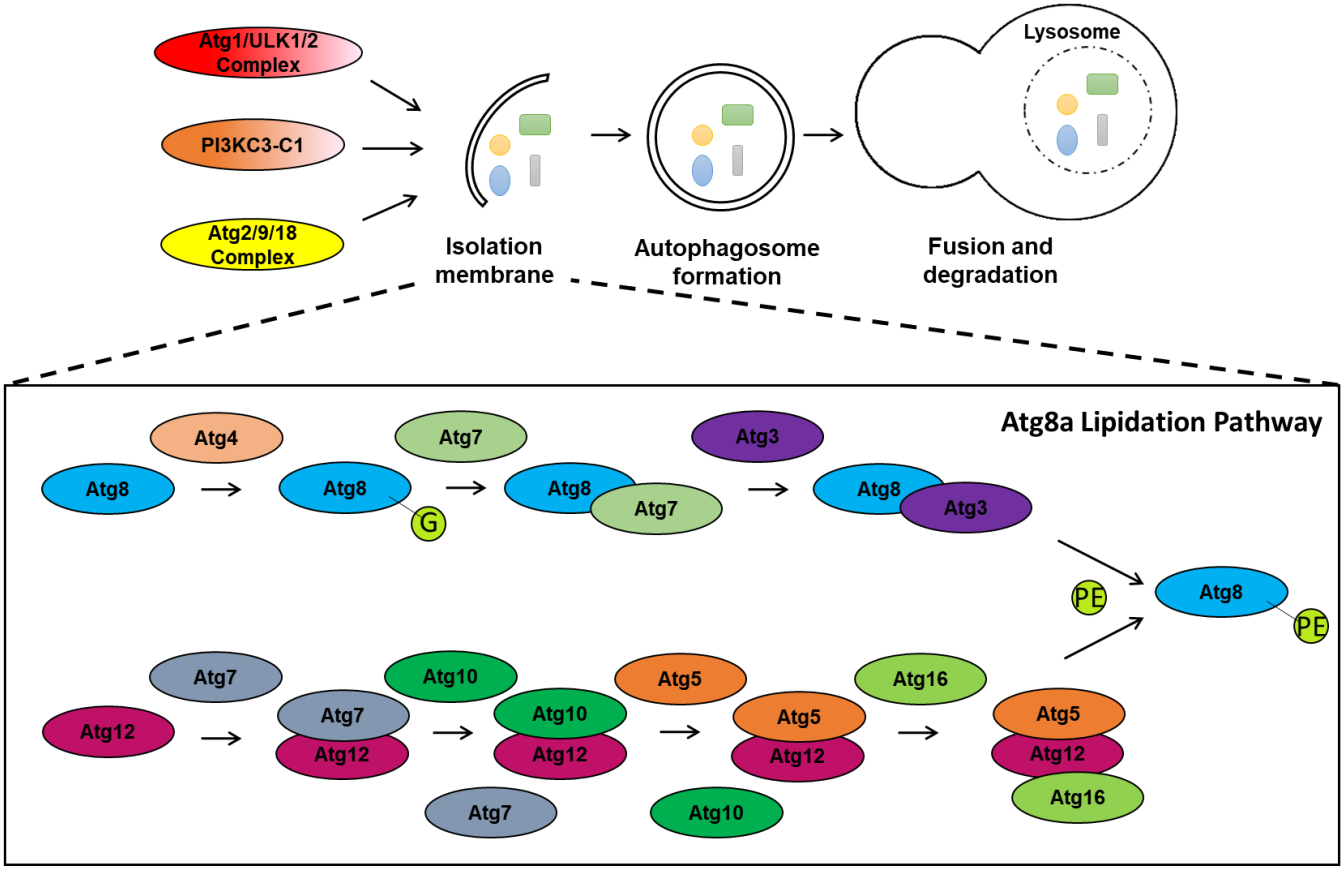

Figure 1-1: The Atg8a Lipidation Pathway. Components in of the Atg8a lipidation pathway. Please refer to text for additional details.

B. Role of Organelles in Autophagy

Before autophagy initiation, the cell must organize and recruit resources required for the formation of autophagy structures, including the autophagosome and lysosome. Vesicles, proteins and lipids required for this process are often sorted by trafficking organelles like the Golgi Body toward the PAS (De Tito et al., 2020). Proteins involved in these processes, including enzymes and ubiquitin, are produced by ribosomes and endoplasmic reticulum (ER). The endosomal sorting complexes required for transport (ESCRT) complex transports endosomes to maturing autophagosomes and lysosomes via the cytoskeleton, which is organized by organelles including the microtubule-organizing center (MTOC) (Schäfer et al., 2020; Ktistakis et al., 2016). Often, the cargo being degraded is the organelle itself, which can require regulation by organelle dependent stress-response pathways. The autophagosome, being a double-membrane structure, also requires a source of membrane from other organelles (Nishimura and Tooze, 2020). Thus, the initiation and regulation of autophagy rely on contributions from many different organelles (Chen et al., 2019).

B1. Autophagosome Membrane Source

There are multiple reported membrane sources for the autophagosome, including the ER, mitochondria, Golgi body, endosomes, ERGIC, the plasma membrane, and lipid droplets (Axe et al., 2008; Hamasaki et al., 2013; Hailey et al., 2010; Ge et al., 2013; Puri et al., 2013; Ravikumar et al., 2010; Dupont et al., 2014; Nascimbeni et al., 2017). Of these, the most established source is the ER. Autophagosomes have been shown to form at subdomains within the ER called omegasomes, which are enriched with PI3P

(Axe et al., 2008). Autophagosomes form at membrane contact sites between the ER and other organelles, such as the mitochondria and plasma membrane (Hailey et al., 2010; Nascimbeni et al., 2017). Thus, it is hypothesized that the ER serves as a platform for the autophagosome to form, and that membrane contacts between the ER and other organelles plays an important role in autophagosome biogenesis. In the context of autophagy, two of the most studied contact sites are the ER/IM and mitochondria/ER contact sites.

B2. ER/IM Contact Sites

Previous studies using three-dimensional (3D) electron tomography of starved kidney cells have shown that the membranes of an IM are sandwiched between two ER cisternae during autophagosome formation (Ylä-Anttila et al., 2009; Hayashi-Nishino et al., 2009). This intimate connection between the ER and IM membrane highlights the importance of the ER/IM membrane microenvironment. These membrane contact sites serve as important platforms for lipid transport and ion signaling in autophagosome biogenesis. First identified in a *C elegans* screen for crucial autophagy genes, EPG-3/VMP1 regulates autophagosome formation by severing ER/IM contact sites through Ca^{2+} signaling. VMP1 binds to and prevents the inhibition of the active form of SERCA, a Ca^{2+} importer on the ER. In *Vmp1* loss-of-function mutants, an increase in Ca^{2+} in the region of the ER/IM contact site prevents dissociation of the membranes, preventing formation of the autophagosome (Zhao et al., 2017). However, key mechanistic questions, such as how local Ca^{2+} levels regulate membrane contacts disassembly, still remain.

B3. Mitochondria/ER Contact Sites

The region of the ER with Mitochondria associated membranes (MAMs) is of particular importance for cellular homeostasis. In addition to being a well-established site for autophagosome formation, MAMs are crucial for inflammation, mitochondrial dynamics (mitochondrial fusion and fission), lipid synthesis and exchange, and intracellular signaling (Moltedo et al., 2019). The importance of these factors in human health are just starting to be appreciated, particularly in aging and neurodegenerative disease (Wilson, E. L. and Metzakopian, 2020). In addition to ER/IM contact sites, loss of VMP1 function has also been shown to increase mitochondria and ER contact sites (Zhao et al., 2017), suggesting that Vmp1 can regulate multiple different membrane contact sites. The autophagosomes that form at these contact sites appear to be responsible for mitophagy, the autophagic degradation of mitochondria (Böckler, S. & Westermann, 2014). The fact that so many processes occur at mitochondria/ER contact sites raises the possibility that these processes are functionally linked.

C. Autophagy in Disease and Development

Autophagy was initially believed to be a non-selective and inducible process responding to nutrition deprivation and stress. However, further studies have shown that there are selective mechanisms that can regulate autophagy during periods of physiological development and differentiation. Defects in these processes can gradually lead to the accumulation of damaged and/or dysregulated cells within an organism, causing death and disease (Anding and Baehrecke, 2015).

C1. Diseases

Dysfunction in autophagy plays a role in many diseases. The role of autophagy in tumorigenesis is complex, with autophagy acting as both a promoter and suppressor of tumorigenesis depending on the context (Yun and Lee, 2018). The depletion of several autophagy genes, including *BECN1* and *UVRAG*, has been observed in several types of cancers (Qu et al., 2003; Takahashi et al., 2007; Liang et al., 1999). A possible model explaining these findings is that the failure to clear detrimental cargo through autophagy, some of which may produce toxins or reactive oxygen species that could damage DNA, helps precipitate the mutagenesis process. Many genes involved in autophagy, including *BECN1*, also act as tumor suppressors independent of autophagy (Morselli et al., 2009). On the other hand, increasing autophagy could also enhance tumorigenesis, providing the tumor cell with the additional energy needed to metastasize and/or survive drug therapies (Yun and Lee, 2018). Ras-driven cancers, for example, have a high level of basal autophagy and inhibition of autophagy impairs tumorigenesis (Goncalves et al., 2016; Zhu et al., 2019). Further investigation is required to better understand the exact role between autophagy and cancer.

Autophagy is also implicated in aging, as studies suggest that dietary restriction enhances longevity at least partly through autophagy (Guarente and Kenyon, 2000; Jia and Levine, 2007). In addition to aging, loss of autophagy also contributes to neurodegenerative disease. Autophagy facilitates removal of aggregates that contribute to the pathology of diseases like Alzheimer's disease, Huntington's disease, and Parkinson's disease (Williams et al., 2006). The loss of *atg* genes in *C elegans*

increases aggregation of the toxic protein polyglutamine, which is responsible for Huntington's disease progression (Jia et al., 2007). Autophagy contributes to the removal of aggregates in other tissues as well. Inhibition of autophagy causes an accumulation of an aggregate prone mutant of α1-antitrypsin Z, which may play an important role in the pathogenesis of liver disease (Kamimoto et al., 2006). The ability to remove toxic or harmful cellular components is not limited to those produced by the cell itself – autophagy is also utilized as a defense mechanism against invading microbes (Levine and Deretic, 2007). These findings illustrate the broad, significant role that autophagy plays in human health and disease.

C2. Development

Autophagy is involved in a process of programmed cell death, termed autophagic cell death. Autophagic cell death often coincides or facilitates other forms of programmed cell death, including apoptosis and necrosis (Denton and Kumar, 2018; Galluzzi et al., 2018). For example, both apoptosis and autophagy are required for degradation of salivary glands during *Drosophila* development (Berry and Baehrecke, 2007). Loss of *atg5* further delays the programmed cell death in the interdigital web cells in apoptosis deficient mice embryos, suggesting that autophagy can compensate for loss of apoptotic function in context-dependent cell death (Arakawa et al., 2017). Autophagy can even regulate cell death in the absence of apoptosis, such as the resveratrol-induced cell death of A549 lung cancer cells (Dasari et al., 2017). The programmed cell death of *Drosophila* intestine cells during pupariation is also an example of autophagy-dependent, apoptosis-independent cell death (Denton et al., 2009).

C3. Autophagic Cell Death in the *Drosophila* Larval Intestine

The fruit fly *Drosophila melanogaster* is a model organism that undergoes numerous metamorphological changes throughout its lifetime. The life cycle of a fruit fly begins as an egg/embryo that is implanted on the surface of food. Shortly after, the eggs hatch into larvae and consume the food they hatched in while transitioning through 3 larval stages (termed 1st, 2nd, and 3rd instar) (Jennings, 2011). During the late 3rd instar stage, hormonal changes, including the expression of the steroid ecdysone, trigger a behavioral and morphological change in the larvae (Lee et al., 2002). This causes the larvae to leave the food and seek a dry area to begin the process of pupation. After finding such a spot, the larvae transform into prepupae. Further hormonal changes continue the process of pupation, turning the prepupa into a pupa. A few days later, an adult fruit fly emerges from the pupal shell. The adult reaches sexual maturity shortly afterwards, and after mating, new eggs are laid to restart the process (Lee et al., 2002; Jennings, 2011).

The process of pupation requires the programmed cell death of many of the larval organs for replacement by adult organs. Autophagic cell death independent of caspase activity plays an important role in many of these processes. One such organ is the larval intestine, which is divided into three regions: the foregut, midgut, and hindgut. Like the mammalian intestine, the *Drosophila* larval intestine contains several layers of cells that coordinate nutritional uptake. The innermost layer of cells is comprised of enterocytes, which have long microvilli to maximize surface area for nutritional absorption. Spaced in between the enterocytes are enteroendocrine cells, which serve

as secretory cells, and stem cells. Surrounding this layer is the basal lamina, followed by a thick layer of smooth muscle, which contract to push food through the intestine. During pupation, the majority of the larval intestine enterocytes, hereby referred as intestine cells, undergo autophagic cell death and the intestine decreases in size while the stem cells proliferate to replace the dying cells with adult intestine cells (Mathur et al., 2010). The enterocytes in particular undergo a drastic cell size reduction, which depends on key autophagy genes, including *atg1* and *atg6*, and ubiquitination pathway components such as *UbaI*, the only E1 in *Drosophila*. Furthermore, the contents within the cell, including organelles, are also removed by autophagy (Chang et al., 2013) **(Figure 1-2)**. This process thus serves as a valuable platform to investigate context-dependent autophagy mechanisms, including the autophagy of certain cargos within the cell.

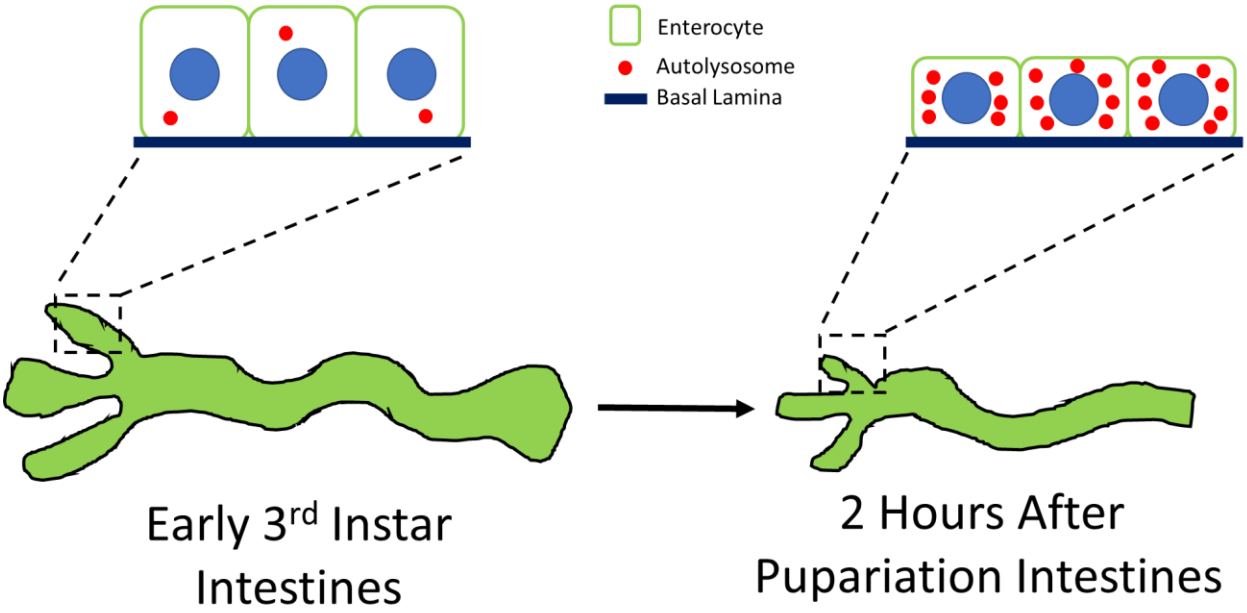

Figure 1-2: Enterocyte Cell Size Reduction During Pupariation in Larval Intestine Cells. Larval intestine enterocytes undergo autophagy-driven cell size reduction during pupation

D. Selective Autophagy

As previous mentioned, autophagy has physiological roles including programed development and cell death (Anding and Baehrecke, 2015). Protein aggregates, which contribute to numerous diseases including neurodegeneration, are degraded through selective autophagy, the autophagic removal of specific cargoes (Deng et al., 2017). Autophagy of Endoplasmic Reticulum (ER) (ER-phagy), ribosomes (ribophagy), lipid droplets (lipophagy), peroxisomes (pexophagy), and other organelles are often regulated by processes that act independently of overall nutritional status (Farré and Subramani, 2016). Here, I will discuss the selective autophagy of mitochondria, also known as mitophagy (Pickles et al., 2018).

D1. Mitophagy

Mitochondria have many diverse roles including energy production, lipid and amino acid production, intracellular signaling, inflammation, and apoptosis. Many of these processes produce waste that can damage the mitochondria and surrounding contents in the cell, particularly the production of reactive oxygen species (ROS) from energy producing superoxide reactions. The failure to remove damaged mitochondria thus leads to unintended consequences for the cell, including cell death and dysfunction (Pickles et al., 2018).

D2. Pink1/Parkin Mitophagy

Damaged and/or depolarized mitochondria can be removed by mitophagy regulated by PTEN-induced putative kinase 1 (Pink1/PINK1) and E3 Parkinson's Disease 2 (Park/PARK2) (Narandra et al., 2008), key proteins involved in Pink1/Parkin-regulated mitophagy **(Figure 1-3).** In the absence of mitochondrial dysfunction, Pink1 localizes to the mitochondria due to a N-terminal mitochondrial targeting sequence (MTS) and is imported by the TIM/TOM complex (Jin et al., 2010). The N-terminal of Pink1 is then cleaved by mitochondrial proteases MPP and PARL, releasing Pink1 from the mitochondria where it is degraded by the proteasomal degradation pathway (Meissner et al., 2011; Deas et al., 2011). However, when mitochondria are damaged or depolarized, Pink1 accumulates on the outer mitochondrial membrane (OMM) and phosphorylates ubiquitin on OMM proteins. Ubiquitin phosphorylation is thought to make the ubiquitin more resistant to deubiquitinating enzymes, allowing ubiquitin chains to form that attract autophagy receptors like Nuclear domain 10 protein 52 (NDP52) and Optineurin (OPTN) which in turn recruit the autophagy machinery (Wauer et al., 2015; Pickles et al., 2018). Curiously, Pink1 stabilized on the OMM also appears to form dimeric structures and undergoes auto-phosphorylation, which may play a role in Pink1 kinase activity and function (Okatsu et al., 2013).

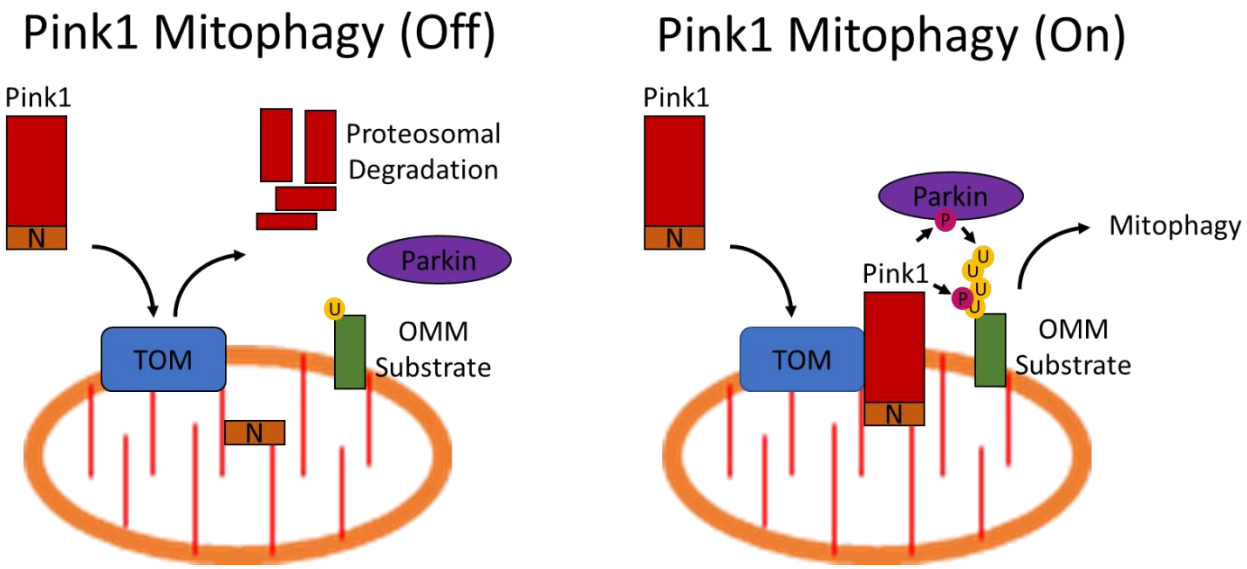

Figure 1-3: Pink1/Parkin Mitophagy. In Pink1/Parkin mitophagy, Pink1 phosphorylates 1) ubiquitin on outer mitochondrial membrane (OMM) substrates and 2) Parkin, an E3 ligase. Phosphorylated Parkin interacts with phosphorylated ubiquitin on the OMM, leading to further ubiquitination of substrates on the OMM and recruitment of the core autophagy machinery to the mitochondria for clearance by mitophagy. Under normal circumstances, Pink1 is imported into the mitochondria and the N terminal is cleaved and released back into the cytoplasm, leading to proteosomal degradation (Off). When mitophagy is induced, such as in the context of response to mitochondrial damage, cleavage of the Pink1 N-terminal is impaired, leading to phosphorylation of Pink1 substrates.

Pink1-mediated phosphorylation leads to increased ubiquitination of OMM substrates largely through activation of Parkin. Pink1 phosphorylates Parkin, increasing Parkin E3 ligase activity and enhances recruitment to the OMM to accelerate the ubiquitination process (Kondapalli et al., 2012; Shiba-Fukushima et al., 2014). Phospho-ubiquitin appears to be important for this process, as Parkin binding with phospho-ubiquitin stabilizes Parkin on the OMM, leading to the rapid formation of ubiquitin chains. These ubiquitin chains serve as additional substrates for Pink1, which leads to further recruitment of Parkin. The end result is a positive feedback loop that marks the

mitochondria with ubiquitin chains for recognition by the autophagy machinery (Koyano et al., 2014; Shiba-Fukushima et al., 2014; Okatsu et al., 2015; Pickles et al., 2018). Pink1/Parkin also appear to play important roles in developmental mitophagy, as Pink1/Parkin are responsible for removal of paternal mitochondria during fertilization (Rojansky et al., 2016).

D3. Pink1/Park Regulation of Mitochondrial Dynamics

Mitochondrial are dynamic organelles that undergo changes in shape, size and organization. These factors are determined by mitochondrial fission (the splitting of a single mitochondrion into two daughter mitochondria) and mitochondrial fusion (the fusing of two mitochondria to make a single mitochondrion). The balance between these two opposing functions is referred to as mitochondrial dynamics (Liesa et al., 2009). Overexpression experiments have suggested that Pink1 promotes mitochondrial fission while inhibiting mitochondrial fusion (Yang et al., 2008; Deng et al., 2008). Pink1 appears to phosphorylate Drp1, a regulator of mitochondria fission, to increase mitochondrial fission activity (Han et al., 2020). At the same time, Pink1 phosphorylates Mfn2, a key mitochondrial fusion regulator, to inhibit Mfn2 activity, likely through Parkin-mediated ubiquitination and degradation (Chen and Dorn, 2013; McLelland et al., 2018). While the purpose of Pink1 regulation of mitochondrial dynamics is still under debate, it has been suggested that this pro-fission function may help facilitate the piecemeal mitophagy of dysfunctional portions of mitochondria (Yang and Yang, 2013). Furthermore, given the large size of mitochondria, preventing mitochondrial fusion and

promoting mitochondrial fission to reduce mitochondrial size may facilitate engulfment of the entire mitochondria by the forming autophagosome.

D4. Pink1/Park Independent mitophagy

There are multiple forms of mitophagy that seem to act independently of Pink1 and Parkin. Furthermore, Pink1-regulated mitophagy does not always require Parkin, and vice versa (Vilain et al., 2012; Yun et al., 2014; Igarashi et al., 2020; Kubli, D. A. et al., 2015; Shiba-Fukushima et al., 2014; Lin et al., 2020). During blood cell differentiation, mitochondria in reticulocytes are removed by Nix/ BNIP3L (Schweers et al., 2007). Interestingly, while mitophagy also relies on the core autophagy machinery, this Nix regulated mitophagy does not seem to require the core autophagy genes *atg5* and *atg7* (Honda et al., 2014). BNIP3, a protein similar in structure to Nix, plays a role in hypoxia-induced mitophagy (Tracy et al., 2007). Both of these mitophagy pathways do not require Pink1 or Parkin. These findings suggest that there are still many regulators of mitophagy yet to be discovered.

D5. Mitophagy in the pupating *Drosophila* larval intestine

As previously mentioned (see C3), the larval intestine can serve as an invaluable tool to screen for genes involved in autophagy (see “Autophagic Cell Death in the *Drosophila* Larval Intestine”). As mitochondria are also cleared by autophagy in this process, this tool can also be applied to look for genes crucial for mitophagy. Indeed, *atg1* and *UBAI* loss-of-function mutants all failed to clear mitochondria during pupation (Chang et al., 2013). However, whether the loss of these genes impairs mitophagy non-specifically due to a general loss of autophagy or if mitophagy specific-programming is impaired is

still unknown. Autophagy in the larval intestine does not require the core autophagy proteins Atg3 and Atg7, hinting at the existence of a potential, non-canonical autophagy pathway regulating larval intestine autophagy (Chang et al., 2013). Indeed, the role of established mitophagy pathways, such as Pink1/Parkin mitophagy, in pupating intestines still remains unanswered. I will now focus on a gene required for autophagy and mitophagy in this process, *vps13d* (Anding et al., 2018).

E. Vacuolar Protein Sorting 13 Homolog D (Vps13D)

Vps13D was found to be essential for autophagy in pupating larval intestines. Knockdown of *vps13d* reduced the puncta formation of autophagy reporter mCherryATG8, which forms bright, large puncta only when autophagy is intact as mCherry accumulates in the autolysosomes (Anding et al., 2018; Lőrincz et al., 2017). Significantly, *vps13d* mutants had large mitochondria with intact cristae and failed to clear mitochondria in pupating larval intestine cells. Additional mechanistic studies revealed that the enlarged mitochondria phenotype in *vps13d* mutants could be suppressed by knockdown of *marf*, a regulator of mitochondrial fusion (Anding et al., 2018). Curiously, depletion of Vps13D did not affect other forms of autophagy, in particular stress and starvation-induced autophagy (Anding et al., 2018). Together, these findings suggested that there may be a unique, context-dependent role of Vps13D in autophagy and mitophagy.

E1. Known roles of Vps13 family members

Vps13D belongs to the highly conserved Vacuolar Protein Sorting 13 (Vps13) protein family. Yeast has a single Vps13 homologue while humans have four, Vps13A-D. The

Vps13 proteins are believed to act as lipid transporters at membrane contact sites (Ugur et al., 2020). In yeast, Vps13 was found to have a redundant relationship to the ER to Mitochondria Encounter Structure (ERMES), which plays an important role in lipid transfer between the ER and mitochondria (Lang et al., 2015). Furthermore, Vps13 family members contain a conserved Chorein_N domain, which has high homology with the Chorein_N domain on Atg2, which is required for lipid transport function in autophagy (Valverde et al., 2019). These findings are supported by structural studies into the N terminal of Vps13 in *Chaetomium thermophilum,* which resembles a basket with interior hydrophobic patches that may serve to shuttle lipids from one membrane to another (Li et al., 2020).

The diversification of Vps13 in yeast into four orthologues in humans likely arose to fulfill specialized functions and/or function at specific intracellular locations. Vps13A and Vps13C both localize to ER and lipid droplet contact sites, with Vps13A also localizing to contact sites between ER and mitochondria and Vps13C to ER and endosome contact sites (Kumar et al., 2018). Localization data for Vps13B has been lacking, although it has been suggested to localize to the Golgi Apparatus Vps13D (Seifert et al., 2011). Localization studies in flies have suggest Vps13D localizes to endosomes/lysosomes, while studies in mammalian culture have suggested it may also localize to mitochondria and ER membrane contact sites due to interactions with proteins that localize to this site (Anding et al., 2018; Hung et al., 2017; Antonicka et al., 2020). While these orthologues are all believed to retain their function as lipid transporters, it is still unknown what the specific roles are (Ugur et al., 2020).

E2. Vps13 Disease Associations

Mutations in *VPS13A* cause a unique form of neurodegenerative condition called chorea-acanthocytosis. This disease presents with chorea, dystonia, behavior changes, and seizures (Peikert et al., 2018). These neurodegenerative signs are also seen in *Vps13a* mutant models of mice and *Drosophila* as well. *Vps13a* mutants generally have altered mitochondrial morphology, with phenotypes associated with mitochondrial disorders such as sperm immotility and motor deficits (Yeshaw et al., 2019; Nagata et al., 2019; Vonk et al., 2017).

VPS13B mutations are known to cause Cohen Syndrome, a disease manifesting usually within the first two years of life with microcephaly, retinal abnormalities, mental/psychomotor difficulties, hypotonia, truncal obesity, neutropenia, joint hypermobility, and failure to thrive (Cohen et al., 1973). These symptoms are believed to be due to defects in the Golgi Apparatus, as fibroblasts from Cohen Syndrome patients have fragmented Golgi bodies that are organized into multiple mini-stacks (Seifert et al., 2011). Likewise, this may contribute to the abnormal protein glycosylation and impaired endocytic trafficking pathways seen in *VPS13B* mutant cells (Duplomb et al., 2013).

VPS13C mutations are associated with an early onset, rapidly progressive form of Parkinson's disease. Patients with mutations in this gene have tremor, dystonia and early cognitive decline. Curiously, these patients also have increased Pink1/Parkin mitophagy, suggesting that the Pink1/Parkin pathway can be utilized to compensate for loss of Vps13C function (Lesage et al., 2016). Immunofluorescence studies suggest that

Vps13C localizes mainly to ER/endosome and ER/lipid droplet contact sites (Kumar et al., 2018). It is currently unknown how this localization can explain the mitophagy role of Vps13C.

E3. Vps13D and Outstanding Questions

Of all the Vps13 family proteins, Vps13D is perhaps the most enigmatic. It is the only Vps13 family member that is essential (Wang et al., 2015; Blomen et al., 2015; Meyers et al., 2017). Vps13D is associated with numerous diseases, including cancer, septic shock, and most notably a hereditary neurological movement disorder involving dystonia, chorea, hypotonia, vision disturbances, and microcephaly (Seong et al., 2018; Gauthier et al., 2018; Bousquet et al., 2016; Nakada et al., 2015). Furthermore, it is the only Vps13 family member required for autophagy in *Drosophila* and has an ubiquitin-associating (UBA) domain **(Figure 1.4)**.

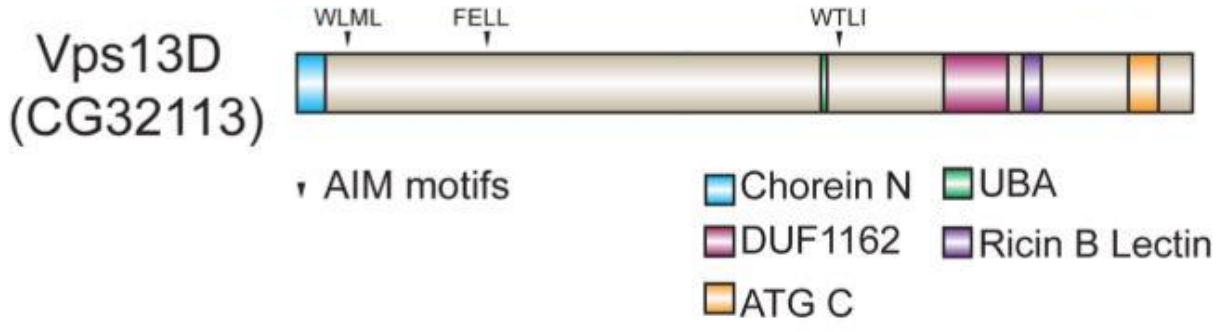

Figure 1-4. ***Drosophila* Vps13D Protein Domains.** Schematic of known functional domains on Vps13D. UBA = Ubiquitin-associating domain, AIM = Atg8a Interacting. Adapted from (Anding et al., 2018).

Loss-of-function mutants in other *Vps13* family members have fragmented mitochondria. In contrast, loss of Vps13D results in large mitochondria with intact cristae. Deletion of the ubiquitin binding UBA domain is sufficient to produce this phenotype (Anding et al., 2018). These findings suggest that Vps13D has a unique function compared to other Vps13 family members. In addition, the mechanism linking Vps13D with autophagy, and well-known mitophagy regulatory pathways, remains unknown.

In this thesis, I will use the pupating *Drosophila* larval intestine to define the role of Vps13D in autophagy, mitophagy, and membrane contact regulation. I will 1) Describe the role of Vps13D in the core autophagy machinery and Pink1-mediated mitophagy and 2) Investigate the relationship between Vps13D and Vmp1, a regulator of mitochondria and ER membrane contact.

Chapter II

Vps13d Functions in a Pink1-Dependent and Parkin-Independent Mitophagy Pathway

James L. Shen[1], Tina M. Fortier[1], Ruoxi Wang[1], and Eric H. Baehrecke[1]

[1] Department of Molecular, Cell and Cancer Biology, University of Massachusetts Medical School, Worcester, MA 01605 USA

Keywords: Vps13D, Pink1, Parkin, autophagy, mitochondria, mitophagy, *Drosophila*

Running title: Vps13d Functions in Pink1-Regulated Mitophagy

ABSTRACT

Defects in autophagy cause problems in metabolism, development, and disease. The autophagic clearance of mitochondria, mitophagy, is impaired by the loss of Vps13D. Here we discover that Vps13D regulates mitophagy in a pathway that depends on the core autophagy machinery by regulating Atg8a and ubiquitin localization. This process is Pink1-dependent, with loss of *pink1* having the same autophagy and mitochondrial defects as loss of *vps13d*. The role of Pink1 has largely been studied in tandem with Park/Parkin, an E3 ubiquitin ligase that is widely considered to be crucial in Pink1-dependent mitophagy. Surprisingly, we find that loss of *park* does not exhibit the same autophagy and mitochondrial deficiencies as *vps13d* and *pink1* mutant cells, and contributes to mitochondrial clearance through a pathway parallel to *vps13d.* These findings provide a Park-independent pathway for Pink1-regulated mitophagy, and help explain how Vps13D regulates autophagy, mitochondrial morphology and contributes to neurodegenerative diseases.

INTRODUCTION

Autophagy, the delivery of intracellular cargo to lysosomes, plays an important role in cell homeostasis and health. Cells utilize autophagy as a way to recycle intracellular contents and waste for energy maintenance. Various human diseases, including neurodegenerative conditions and cancer, have been linked to defects in autophagy (Jiang and Mizushima, 2014). For example, a decrease in autophagic flux and failure to clear autophagy substrates contributes to Parkinson's Disease and Amyotrophic lateral sclerosis pathogenesis (Hou et al., 2020; Vicencio et al., 2020). Knowledge of the role of autophagy in the development of these diseases, however, is limited by an incomplete understanding of the molecular mechanisms and factors that regulate autophagy.

Elegant studies in yeast characterized a core autophagy machinery that is comprised of the autophagy-related (Atg) genes that are functionally conserved in higher eukaryotes. This autophagy machinery regulates the engulfment of intracellular cargoes, often marked by ubiquitination, through the formation of a double membrane autophagosome structure. Autophagosomes fuse with lysosomes to degrade the engulfed cargoes, completing the autophagy process (Nakatowwa et al., 2009). While most studies have characterized the role of autophagy in starvation and cell stress, they are not able to account for the role of autophagy in other processes, such as development and cell death. For example, it has been reported that autophagy can occur without core autophagy machinery components such as *atg6/BECN1*, *atg3* and *atg7* (Scarlatti et al., 2008; Chang et al., 2013; Tsuboyama et al., 2016). This is

surprising as these genes are crucial for starvation-induced autophagy (Nakatowwa et al., 2009). Furthermore, selective forms of autophagy that recruit specific intracellular cargoes possess unique regulatory pathways that are unaccounted for in the current model of the core autophagy machinery (Lazarou et al., 2015; Rakovic et al., 2019; Chino and Mizushima, 2020).

Selective autophagy is important for the removal of specific organelles (Anding and Baehrecke, 2017). One such organelle that is removed by autophagy is the mitochondrion, which has crucial roles in cell metabolism and death (Friedman and Nunnari, 2014). The Pink1/Parkin pathway regulates mitophagy, the autophagic removal of mitochondria. Pink1 acts as a Ser-Thr kinase that phosphorylates ubiquitin chains on the outer mitochondrial membrane and recruits the E3 ubiquitin ligase Park/Parkin to mitochondria, marking mitochondria for degradation through the autophagy pathway (Ordureau et al., 2014; Koyano et al., 2014; Wauer et al., 2015). Studies of this pathway in cell lines have expanded our understanding of mitophagy and how this process contributes to multiple diseases, such as Parkinson's disease and Alzheimer's disease (Palikaras et al., 2018, Wang et al., 2019). However, the initial mechanistic studies of Pink1/Parkin-dependent mitophagy were conducted in HeLa cells, which required exogenous expression of Parkin (Lazarou et al., 2015). Mitophagy under physiological conditions in animals is more complex and often utilizes different mechanistic pathways that cannot be explained by these existing models. For example, *pink1*- and *parkin*-independent mitophagy is known to occur in multiple cell lines and tissues (Lee et al., 2018; Bhujabal et al., 2017; McWilliams et al., 2018; Allen et al., 2013; von Stockum et al., 2018). These studies reveal that there is much to learn

regarding the relationship between Pink1, Parkin, and mitophagy under physiological conditions.

The context-dependent removal of specific autophagic cargoes is important for animal development and health. For example, macrophages must specifically target foreign microbes for autophagy following phagocytosis to control infection, and utilizes regulatory pathways not utilized in starvation-induced autophagy (Pilli et al., 2012). This example demonstrates the need to investigate selective autophagy in the context of appropriate physiological stimuli. The development of *Drosophila* larvae to prepupae involves the autophagic removal of larval organs (Chang et al., 2013). In larval intestine cells, mitochondria are rapidly cleared through mitophagy, and previous studies have utilized this system to screen for genes required for mitophagy under physiological conditions. One gene required for this process is *vps13d,* which is required for proper mitochondrial morphology and clearance (Anding et al., 2018). *vps13d* is an essential gene, with *vps13d* loss-of-function mutants being lethal during development in both flies and mammals (Anding et al., 2018). *vps13d* also ranks as one of the most important genes for survival in cells lines (Blomen et al., 2015; Wang et al., 2015; Dempster et al., 2019; Meyers et al., 2017). Furthermore, mutations in *vps13d* have been linked to several diseases, most notably a familial neurological movement disorder involving chorea, dystonia and ataxia (Seong et al., 2018; Gauthier et al., 2018; Nakada et al., 2015; Bousquet et al., 2016; Anderson et al., 2010). In contrast to other Vps13 family members, only Vps13D is required for autophagy in flies, is essential, and contains a ubiquitin binding (UBA) domain that is required for proper mitochondrial morphology and clearance (Anding et al., 2018). However, the functional role that Vps13D plays in the

autophagic machinery, and the relationship to any well-defined mitophagy pathways, is currently unknown.

Here we identify a context-dependent function of Vps13D in the core autophagy machinery as a regulator of ubiquitin and Atg8a localization. We find that in the developing *Drosophila* larval intestine, Pink1 regulates mitochondrial clearance upstream of Vps13D. Unlike Pink1, Parkin does not regulate mitophagy in a Vps13D-dependent manner, and instead influences mitochondrial clearance through a parallel pathway that is required for the clearance of a smaller subset of mitochondria within the cell. Importantly, our findings characterize a new form of Pink1-dependent and Parkin-independent mitophagy regulated by Vps13D. These results establish a mechanistic model for the role that Vps13D plays in mitophagy, and help explain the function of *vps13d* in development and disease.

RESULTS

Vps13D regulates Atg8a and ubiquitin localization during developmental autophagy

Autophagy genes are required for the clearance of intracellular cargoes, including mitochondria, in *Drosophila* larval intestine cells (Chang et al., 2013; Anding et al., 2018). The poorly understood role of Vps13D in autophagy prompted us to consider how Vps13D interacts with the autophagy machinery to influence this process in larval intestine cells.

Atg8a (LC3/GABARAP in mammals) is an important regulator of autophagosome formation and influences the recruitment of mitochondria to autophagosomes during

mitophagy (Lazarou et al., 2015). We thus sought to examine the localization of Atg8a and mitochondria in *vps13d* mutants. *vps13d (MiMic)* loss-of-function intestine cells that lack red fluorescent protein (RFP) were generated through mosaic cell clone induction. Intestines were then stained with an antibody specific for endogenous Atg8a **(Figure 2-1A)** 2 hours after prepupa formation.

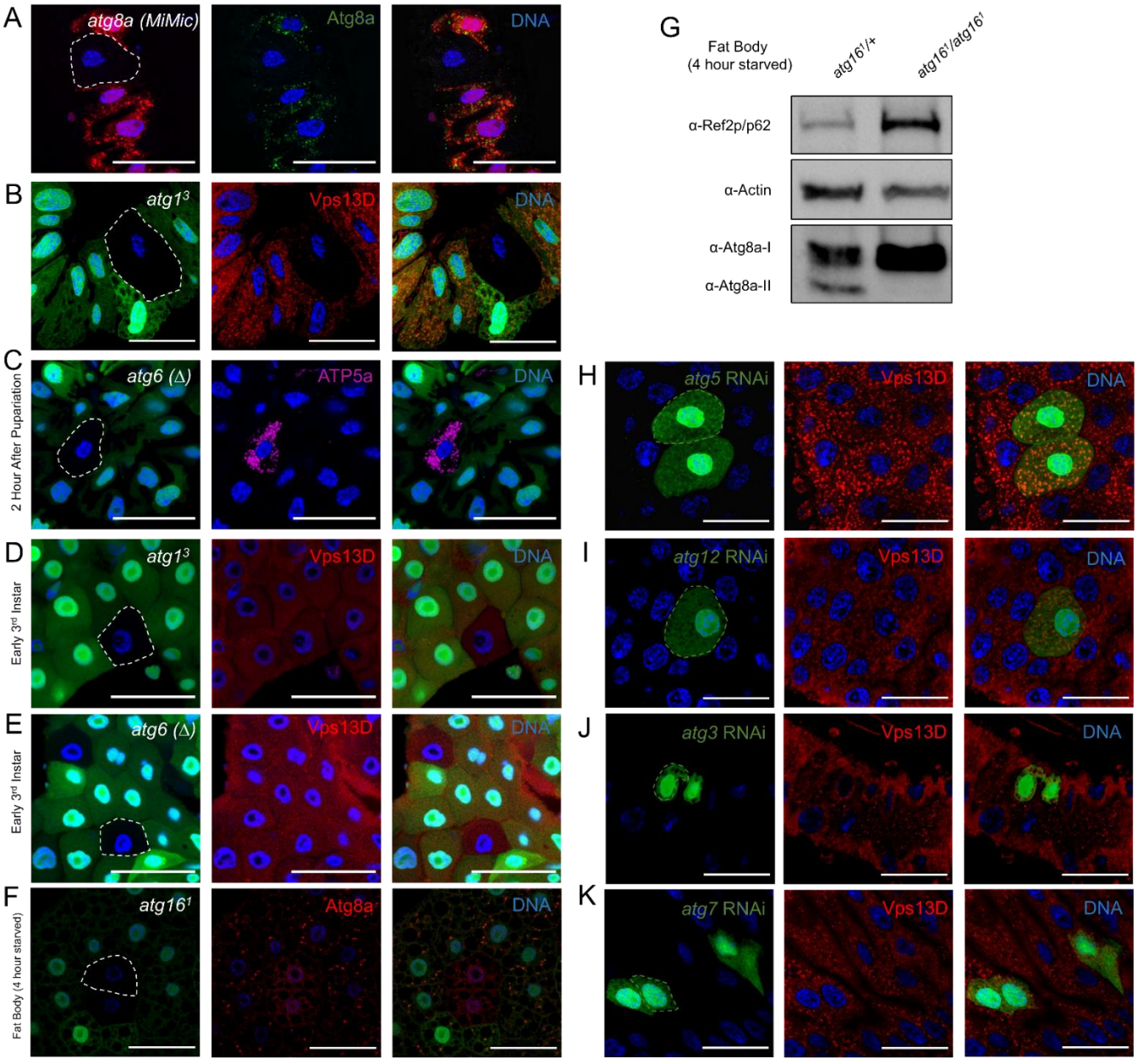

Figure 2-1: Vps13D puncta localization is not affected in early third instar larvae autophagy mutant cells or by loss of Atg8a conjugating pathway components. A) *atg8a (MiMic)* intestine cells (non-red) stained with Atg8a-specific antibody have depleted Atg8a puncta (green) compared to heterozygous control cells (red) 2 hours after pupariation. B) *atg1*^{3} loss-of-function intestine cells (non-green) have less Vps13D puncta (red) compared to neighboring heterozygous control cells (green) 2 hours after pupariation. C) *atg6 (*Δ*)* loss-of-function intestine cells (non-green) retain ATP5a puncta (purple) compared to neighboring heterozygous control cells (green) 2 hours after pupariation. (D) *atg1*^{3} loss-of-function mutant intestine cells (non-green) from early third instar larvae do not have altered Vps13D puncta (red) compared to neighboring heterozygous control cells (green). E) *atg6 (*Δ*)* loss-of-function mutant intestine cells from early third instar larvae (non-green) do not have altered Vps13D puncta (red) compared to neighboring heterozygous control cells (green). F) *atg16*^{1} fat body cells (non-green) from early third instar larvae starved for 4 hours have decreased Atg8a puncta (red) compared to neighboring heterozygous control cells (green). G) Fat body dissected from homozygous *atg16*^{1}*/ atg16*^{1} mutant early third instar larvae starved for 4 hours have increased Ref2p/p62, increased Atg8a-I, and decreased Atg8a-II compared to heterozygote *atg16*^{1}/+ controls. H) *atg5* RNAi-expressing intestine cells (green) do not have altered Vps13D puncta (red) compared to neighboring control cells (non-green) 2 hours after pupariation. I) *atg12* RNAi-expressing intestine cells (green) do not have altered Vps13D puncta (red) compared to neighboring control cells (non-green) 2 hours after pupariation. J) *atg3* RNAi-expressing intestine cells (green) do not have altered Vps13D puncta (red) compared to neighboring control cells (non-green) 2 hours after pupariation. K) *atg7* RNAi-expressing intestine cells (green) do not have altered Vps13D puncta (red) compared to neighboring control cells (non-green) 2 hours after pupariation. Scale bars in (A-F) and (H-K) represent 40μm. Representative of 3 or more independent biological experiments.

Compared to RFP-labeled heterozygous control cells, *vps13d* loss-of-function mutant intestine cells had an abnormal retention and localization of Atg8a. Atg8a puncta in these mutant cells were enlarged and seemed to localize around ATP5a-labeled mitochondria that failed to be degraded **(Figure 2-2A and B).**

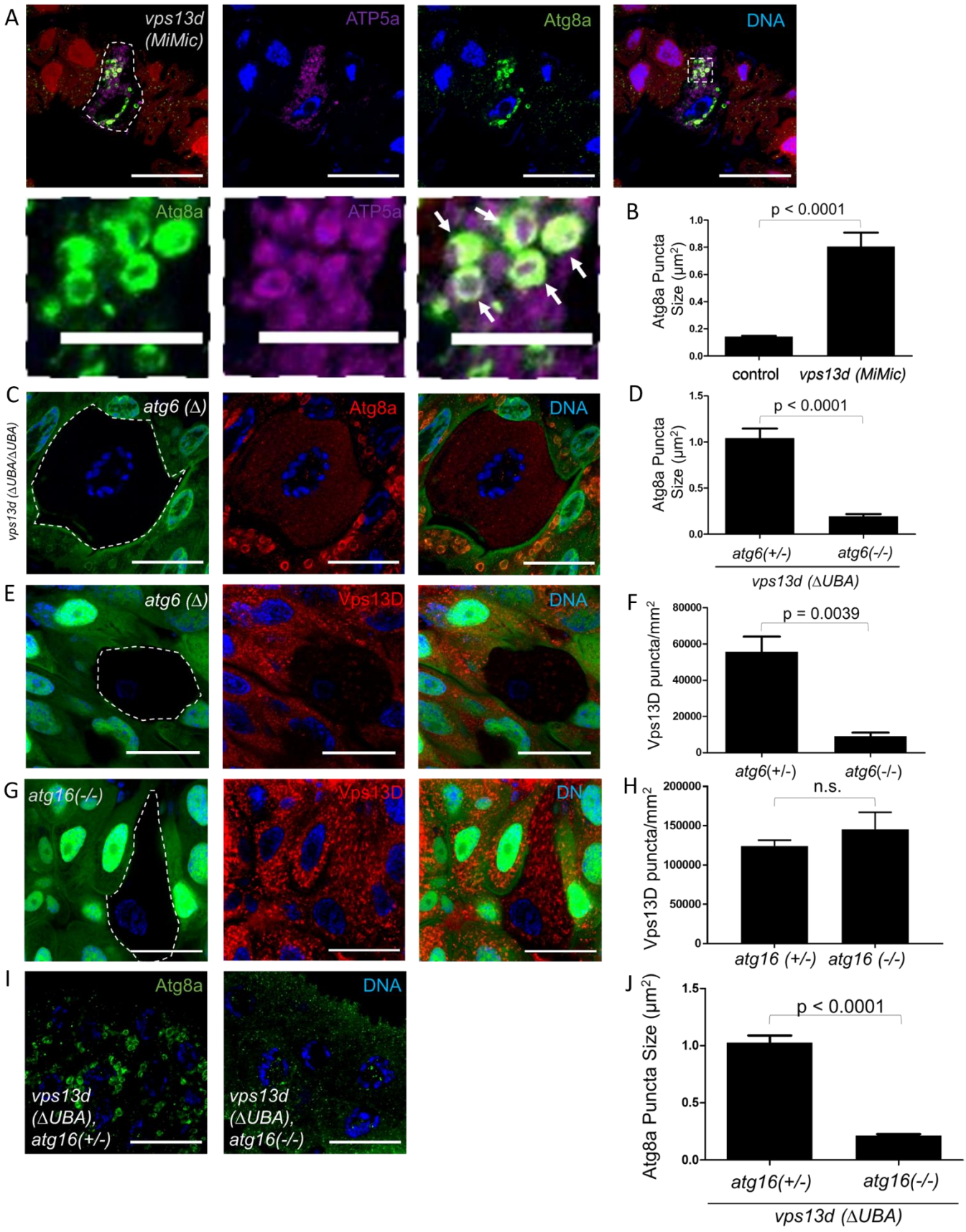
A
vps13d (MiMic)
ATP5a
Atg8a
DNA
Atg8a
ATP5a
B
p < 0.0001
Atg8a Puncta Size (μm²)
control
vps13d (MiMic)
C
vps13d (ΔUBA/ΔUBA)
atg6 (Δ)
Atg8a
DNA
D
p < 0.0001
Atg8a Puncta Size (μm²)
atg6(+/-)
atg6(-/-)
vps13d (ΔUBA)
E
atg6 (Δ)
Vps13D
DNA
F
p = 0.0039
Vps13D puncta/mm²
atg6(+/-)
atg6(-/-)
G
atg16(-/-)
Vps13D
DN
H
n.s.
Vps13D puncta/mm²
atg16 (+/-)
atg16 (-/-)
I
Atg8a
DNA
vps13d (ΔUBA), atg16(+/-)
vps13d (ΔUBA), atg16(-/-)
J
p < 0.0001
Atg8a Puncta Size (μm²)
atg16(+/-)
atg16(-/-)
vps13d (ΔUBA)

Figure 2-2: Vps13D regulates Atg8a localization around mitochondria during autophagy A) *vps13d (MiMic)* loss-of-function intestine cells (non-red) from 2-hour old prepupae have increased mitochondrial ATP5a puncta (purple) and enlarged Atg8a (green) puncta compared to neighboring control cells (red) (top panels). Atg8a puncta tend to surround the ATP5a puncta in *vps13d (Mimic)* mutant cells (bottom panel). B) Quantification of the size of Atg8a puncta surrounding ATP5a puncta in *vps13d (MiMic)* intestine cells (n=6) compared to heterozygote controls (n=22). C) ***atg6*** *(∆), vps13d (∆UBA/∆UBA)* double mutant intestine cells (non-green) 2 hours after pupariation have suppressed formation of enlarged Atg6a puncta (red) seen in control neighboring *atg6 (∆)/+, vps13d (∆UBA/∆UBA)* single mutant cells (green). D) Quantification of Atg8a puncta size in ***atg6*** *(∆), vps13d (∆UBA/∆UBA)* double mutant cells (n=7) compared to *atg6 (∆)/+, vps13d (∆UBA/∆UBA)* single mutant cells (n=20). E) ***atg6*** *(∆)* loss-of-function intestine cells (non-green) stained with antibody against Vps13D (red) were compared to neighboring heterozygous control cells (green) in 2-hour old prepupae. F) Quantification of the amount of Vps13D puncta in ***atg6*** *(∆)* loss-of-function intestine cells (n=5) compared to neighboring control cells (n=13). G) $atg16^{1}$ loss-of-function intestine cells (non-green) have similar levels of Vps13D puncta (red) compared to neighboring heterozygote control cells (green) in 2-hour old prepupae. H) Quantification of Vps13D puncta in $atg16^{1}$ cells (n=9) compared to neighboring heterozygous control cells (n=22). I) $atg16^{1}$*, vps13d (∆UBA/∆UBA)* double mutant intestines cells have suppressed formation of enlarged Atg8a puncta compared to $atg16^{1}$*/+, vps13d (∆UBA/∆UBA)* single mutant cells 2 hours after pupariation. J) Quantification of Atg8a puncta size in $atg16^{1}$*, vps13d (∆UBA/∆UBA)* double mutant intestines cells (n=19) compared to $atg16^{1}$*/+, vps13d (∆UBA/∆UBA)* single mutant cells (n=14). Scale bars in A), C), E), G), and I) are 40µm. Columns in B), D), F), H), and J) were compared using two-tailed student t-test without Welch's correlation with error bars representing SEM. Representative of 3 or more independent biological experiments.

To determine if the Atg8a localization phenotype in *vps13d* mutant cells was due to a defect in the autophagy machinery, we investigated if this phenotype was influenced by loss of any core autophagy genes. *atg6* loss-of-function mutants, ***atg6*** *(∆),* were generated in intestine cells that were homozygous for the *vps13d (∆UBA)* mutant allele that lacks the ubiquitin binding (UBA) domain. Staining with the Atg8a antibody revealed that loss of *atg6* in the cells lacking green fluorescent protein (GFP), which were therefore *atg6* and *vps13d* double mutants, suppressed the altered Atg8a localization phenotype compared to neighboring *vps13d (ΔUBA)* control cells

expressing GFP **(Figure 2-2C and D).** These data indicate that the unique Atg8a localization phenotype in *vps13d* mutant cells requires the Atg6 upstream regulator of autophagy, and suggest that a functional link exists between the core autophagy machinery and Vps13D. Consistent with this hypothesis, ***atg6 (Δ)*** mutant cells that lack GFP exhibit a significant decrease in Vps13D protein puncta in intestine cells 2 hours after prepupa formation **(Figure 2-2E and F).** Like Atg6, Atg1/ULK acts an initiator of autophagy early in the core autophagy machinery (Suzuki et al., 2007). Consistent with these findings, *atg1*^{3} loss-of-function mutant cells lacking GFP also had decreased Vps13D protein puncta **(Figure 2-1B).**

Autophagy is required for removal of mitochondria from *Drosophila* larval intestine cells (Chang et al., 2013). Consistent with these previous findings, ***atg6 (Δ)*** mutant intestine cells lacking GFP were unable to clear mitochondria 2 hours after prepupa formation **(Figure 2-1C).** Generation of *atg1*^{3} and ***atg6 (Δ)*** mutants in intestine cells in early 3rd instar larvae, before the onset of pupariation and autophagy in the larval intestine (Chang et al., 2013), did not affect Vps13D puncta levels **(Figure 2-1D and E)**, suggesting a context- and stage-specific relationship between Vps13D and these core autophagy genes.

The Atg5/12/16 complex is required for lipidation of Atg8a and recruitment to the forming autophagosome (Shpilka et al., 2011). We used TALENs to generate a frameshift mutation in all isoforms of Atg16, resulting in a strong loss-of-function mutant allele *atg16*^{1}. Cells lacking *atg16*^{1} accumulated the autophagy cargo receptor Ref2p and possessed decreased Atg8a lipidation and puncta formation in starved fat body cells **(Figure 2-1F and G).** Unlike *atg1* and *atg6* loss of function mutants, which act early in

the core autophagy machinery (Suzuki et al., 2007), *atg16*^{1} mutant cells lacking GFP did not affect Vps13D puncta 2 hours after prepupa formation **(Figure 2-2G and H).** Knockdown of other components of the Atg8a conjugation machinery, including *atg3, atg7, atg5,* and *atg12*, also did not affect Vps13D localization 2 hours after prepupa formation **(Figure 2-1H-K).** These findings suggest that while Vps13D puncta formation depends on Atg1 and Atg6, it either does not require or functions upstream of core autophagy machinery components required for Atg8a conjugation. To determine which of these possibilities was more likely, we conducted double mutant analyses between the *vps13d (*Δ*UBA)* mutant and *atg16*$^{1.}$ Compared to *vps13d* (Δ*UBA)* single mutants that possess enlarged Atg8a puncta, loss-of-*atg16* suppressed the Atg8a localization phenotype **(Figure 2-2I and J).** Taken together, these findings suggest that Vps13D acts downstream of Atg1 and Atg6, but upstream of Atg8a conjugation pathways in *Drosophila* intestine cells 2 hours after puparium formation.

The functional requirements of both the ubiquitin E1 activating enzyme Uba1 and ubiquitin binding domain encoding Vps13D protein for autophagy illustrate the importance of ubiquitin in *Drosophila* intestine cells (Chang et al., 2013; Anding et al., 2018). Therefore, we investigated the relationship between ubiquitin and Vps13D during autophagy in intestine cells. As expected, we detected an increase in the amount of

ubiquitinated proteins in whole animal lysates between early third instar larvae and 2 hours after puparium formation **(Figure 2-3A).**

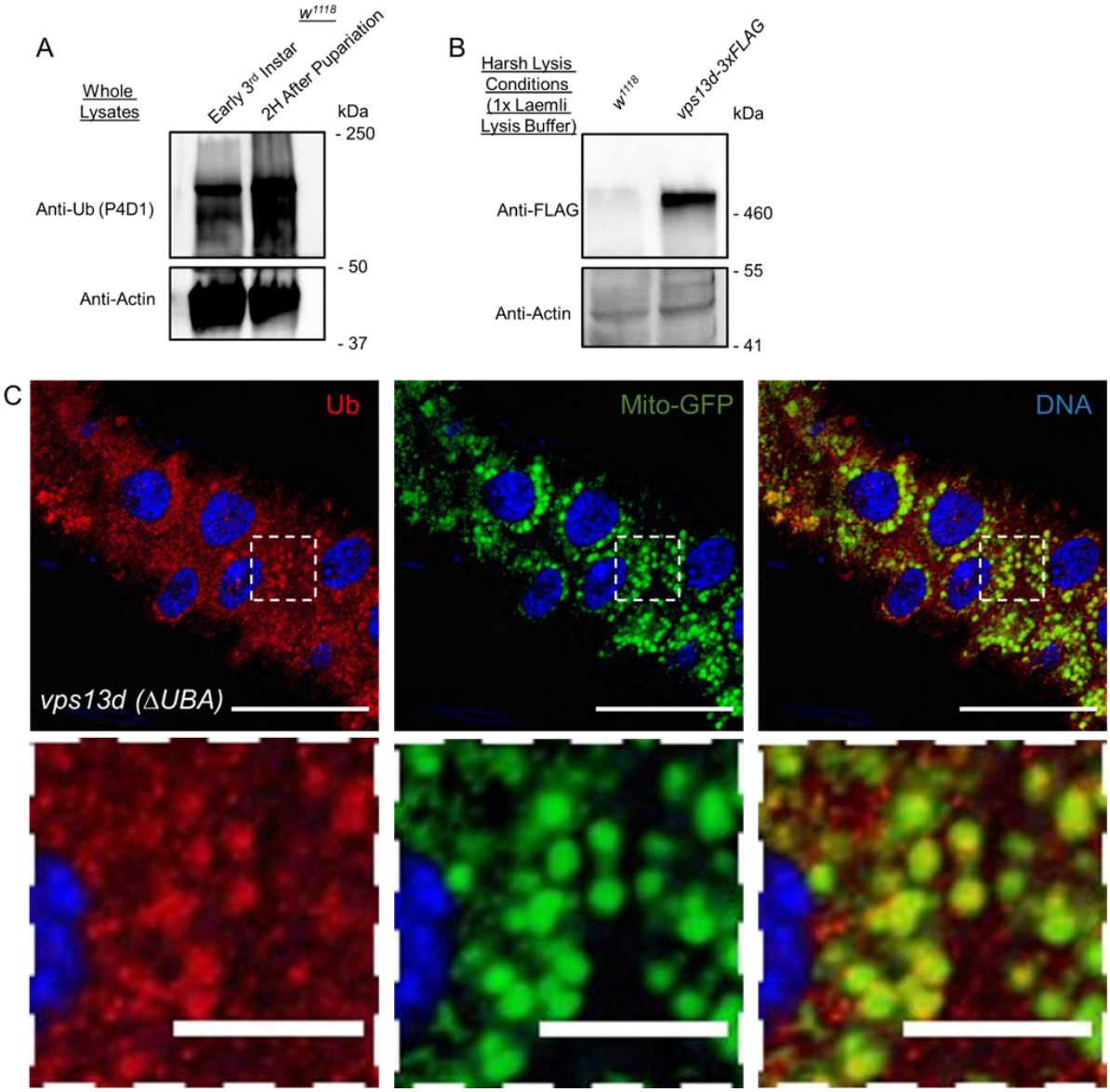

Figure 2-3: Proteins are ubiquitinated during pupariation in *Drosophila* and lysis of Vps13d-3xFLAG requires harsh conditions. A) Whole animal lysates from early 3rd instar larval and 2 hours after pupariation were lysed in harsh lysis conditions (1X Laemli buffer) and immunoblotted with antibody against Ub and Actin. B) Control *w1118* and *vps13d-3xFLAG* 2-hour old prepupae were lysed in harsh lysis conditions and immunoblotted with antibody against FLAG and Actin. C) *vps13d (ΔUBA)* intestines expressing mitochondrial localized mito-GFP (green) throughout the intestine 2 hours after pupariation were stained with a pan-ubiquitin specific antibody (red). Scale bars in C) represent 40μm with the exception of enlarged images, which represent 10μm.

The Vps13D ubiquitin-binding UBA domain preferentially interacts with K63 ubiquitin *in vitro* (Anding et al., 2018). To verify that Vps13d interacts with ubiquitin *in vivo*, we used a *Drosophila* strain in which the *vps13d* gene was endogenously tagged with *3xFLAG* on the C terminus, *vps13d-3xFLAG*. Unlike *vps13d* mutants, these flies are viable, fertile, complement the early lethal phenotype of *vps13d (MiMic)* flies. Importantly, immunoblotting revealed a distinct band in the *vps13d-3xFLAG* lysates at the predicted size of Vps13D-3xFLAG that was absent in the w^{1118} control lysates **(Figure 2-3B).** Immunoprecipitation of the FLAG epitope followed by western blot analysis of the eluate using a ubiquitin antibody did not reveal ubiquitinated protein binding with Vps13D-3xFLAG in the early third instar stage in either the control w^{1118} or *vps13d-3xFLAG* lysates **(Figure 2-4A).**

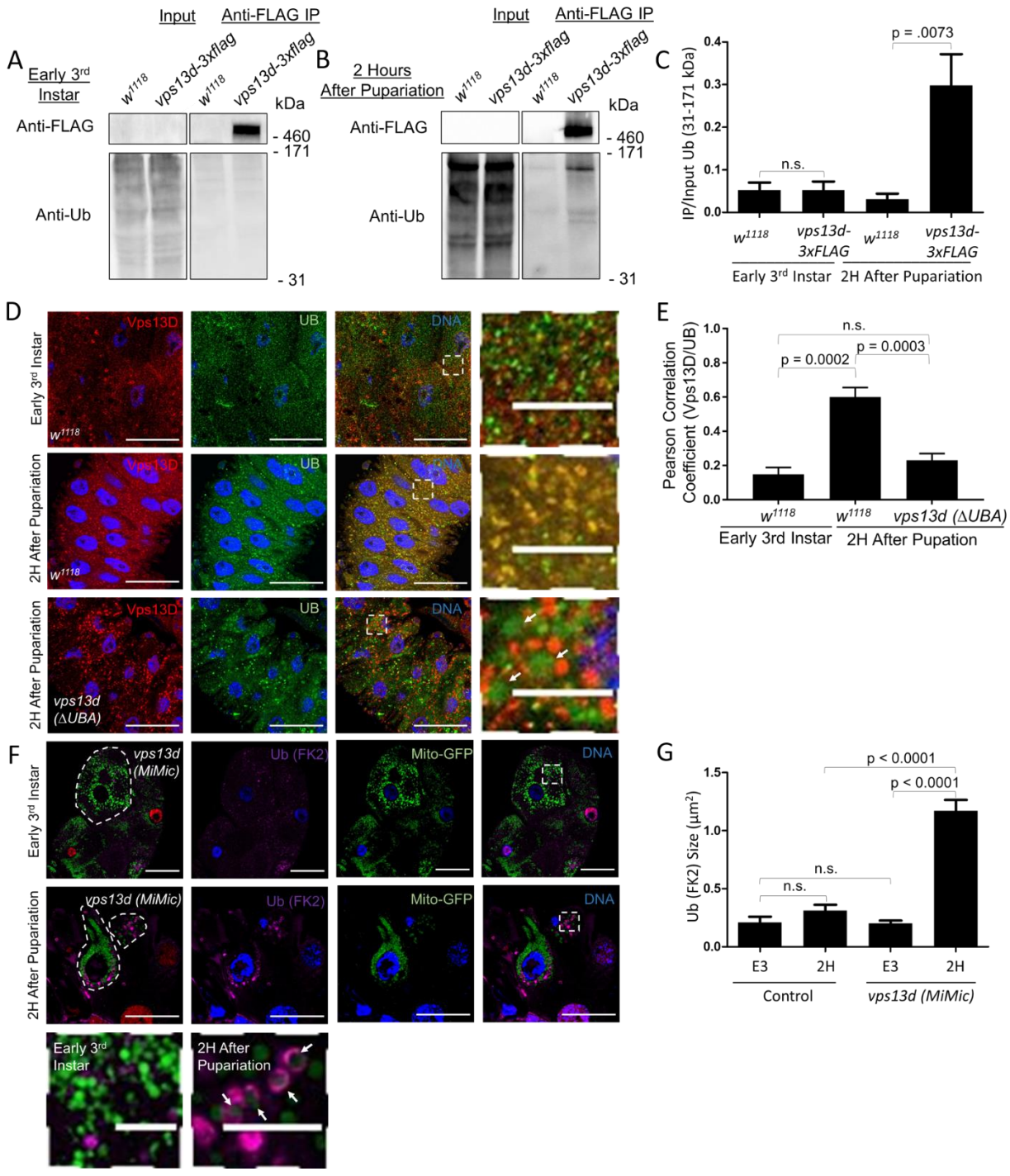
A
Early 3rd Instar
Input
Anti-FLAG IP
w1118
vps13d-3xflag
w1118
vps13d-3xflag
kDa
Anti-FLAG
- 460
- 171
Anti-Ub
- 31
B
2 Hours After Pupariation
Input
Anti-FLAG IP
w1118
vps13d-3xflag
w1118
vps13d-3xflag
kDa
Anti-FLAG
- 460
- 171
Anti-Ub
- 31
C
p = .0073
n.s.
IP/Input Ub (31-171 kDa)
0.4
0.3
0.2
0.1
0.0
w1118
vps13d-3xFLAG
w1118
vps13d-3xFLAG
Early 3rd Instar
2H After Pupariation
D
Early 3rd Instar
Vps13D
UB
DNA
w1118
2H After Pupariation
Vps13D
UB
DNA
w1118
2H After Pupariation
Vps13D
UB
DNA
vps13d (ΔUBA)
E
n.s.
p = 0.0003
p = 0.0002
Pearson Correlation Coefficient (Vps13D/UB)
1.0
0.8
0.6
0.4
0.2
0.0
w1118
w1118
vps13d (ΔUBA)
Early 3rd Instar
2H After Pupation
F
Early 3rd Instar
vps13d (MiMic)
Ub (FK2)
Mito-GFP
DNA
2H After Pupariation
vps13d (MiMic)
Ub (FK2)
Mito-GFP
DNA
Early 3rd Instar
2H After Pupariation
G
p < 0.0001
p < 0.0001
n.s.
n.s.
Ub (FK2) Size (μm2)
1.5
1.0
0.5
0.0
E3
2H
E3
2H
Control
vps13d (MiMic)

Figure 2-4: Vps13D interacts with and regulates ubiquitin localization. A) Western blot of input and eluates from a FLAG immunoprecipitation of control *w*^{1118} and *vps13d-3xflag* early third instar larvae extracts that were probed with antibodies against ubiquitin. B) Western blot of input and eluates from a FLAG immunoprecipitation of control *w*^{1118} and *vps13d-3xflag* 2-hour old prepupal extracts that were probed with antibodies against ubiquitin. Vps13D-3xFLAG levels were too low to be detected in the input with lysate conditions suitable for immunoprecipitation, but was present in lysates from harsher lysis conditions (Figure 2-3B). C) Quantification of the ratio of ubiquitinated proteins from 31kDa to 171kDa in the immunoprecipitation compared to input for *w*^{1118} and *vps13d-3xFLAG* lysates (n=6 independent experiments). D) *w*^{1118} and *vps13d (*∆*UBA)* intestines were dissected from early third instar and 2-hour after pupariation stage animals and co-stained with antibodies against Vps13D (red) and ubiquitin (green). *vps13d (*∆*UBA)* intestines had larger and more spherical ubiquitin puncta (arrows). E) Quantification of the Pearson Correlation Coefficient between Vps13D and ubiquitin in *w*^{1118} early third instar intestine cells (n=25), 2-hour after pupariation *w*^{1118} (n=50) and *vps13d (*∆*UBA)* (n=44) intestine cells. F) *vps13d (MiMic)* loss-of-function intestine cells (lacking red nuclei) have similar conjugated ubiquitin (purple) localization to neighboring heterozygote control cells (red nuclei) (top panels) in early third instar larvae. By contrast, *vps13d (MiMic)* cells have enlarged conjugated ubiquitin (FK2) puncta compared to neighboring control cells (middle panel) in 2-hour-old prepupae. A portion of these puncta tend to encircle the mitochondria (green) in *vps13d (MiMic)* mutant cells at 2-hours after pupariation (lower panels). G) Quantification of the size of conjugated ubiquitin (FK2) puncta in *vps13d (MiMic)* intestine cells in early third instar (E3) and 2-hour after pupariation (2H) (E3 and 2H, n=6) intestines cells compared to control cells (E3 n=12, 2H n=15). Scale bars in D) and F) represent 40µm with the exception of the enlarged images, which represent 10µm. Columns in C), E), and G) were compared using two-tailed student t-test without Welch's correlation with error bars representing SEM. Representative of 3 or more independent biological experiments.

By contrast, in 2-hour old prepupae we detected a significant increase in ubiquitinated protein interacting with Vps13D-3xFLAG compared to the control *w*^{1118} eluate **(Figure 2-4B and C).** Consistent with these biochemical results, Vps13D and ubiquitin co-localized to a greater extent at 2 hours after pupariation than in early third instar *w*^{1118} intestines **(Figure 2-4D and E).** Significantly, deletion of the ubiquitin-binding UBA domain in *vps13d* suppressed the co-localization of Vps13D and ubiquitin **(Figure 2-4D and E).** Additionally, ubiquitin puncta in *vps13d (ΔUBA)* mutant cells were larger than

ubiquitin puncta in control intestine cells under identical conditions **(Figure 2-4D).** These enlarged ubiquitin puncta co-localized with mito-GFP, a marker for mitochondria **(Figure 2-3C).**

Ubiquitin is associated with cargoes that are targeted to autophagosomes for degradation, including mitochondria (Nakatogawa et al., 2009). Therefore, we hypothesized that the increased size of ubiquitin puncta in *vps13d* mutant cells could be explained by changes in protein bound to ubiquitin (conjugated ubiquitin) on mitochondria because of a failure in the clearance of these autophagic substrates. To test this possibility, we compared *vps13d (MiMic)* loss-of-function mutant intestine cells stained with an antibody specific for conjugated ubiquitin, the ubiquitin (FK2) antibody. In early third instar larvae, we did not detect a significant difference in conjugated ubiquitin between *vps13d* mutant cells (lacking nuclear RFP) and control cells **(Figure 2-4F and G).** By contrast, conjugated ubiquitin puncta were enlarged in *vps13d* mutant compared to control cells 2 hours after puparium formation **(Figure 2-4F and G).** Interestingly, the co-localization of conjugated ubiquitin with mito-GFP revealed ubiquitin puncta that appeared to encircle mitochondria that failed to be cleared in *vps13d* mutant cells **(Figure 2-4F and G),** a localization pattern that is similar to Atg8a **(Figure 2-2A).** These results indicate that Vps13D influences the localization of Atg8 and conjugated ubiquitin that are associated with mitochondrial clearance.

Vps13D regulates mitophagy through a Pink1-dependent mechanism

The influence of Vps13D on Atg8a, ubiquitin and clearance of mitochondria prompted us to consider if established mitophagy pathway genes have phenotypes that are similar to *vps13d* in intestine cells. Pink1 functions as a mitochondrial stress-sensing kinase that facilitates the targeting of mitochondrial-associated proteins for ubiquitination by Parkin and clearance during mitophagy (Lazarou et al., 2015). To determine if Pink1 is required for mitochondrial clearance by autophagy in intestine cells, we generated *pink1*^{B9} loss-of-function mutant cell clones (lacking RFP), and stained with antibodies specific for the autophagy cargo receptor Ref2p/p62 and mitochondrial ATP5a. Cells lacking *pink1* function had increased Ref2p/p62 and ATP5a puncta compared to neighboring control cells **(Figure 2-5A, B, D, and E).**

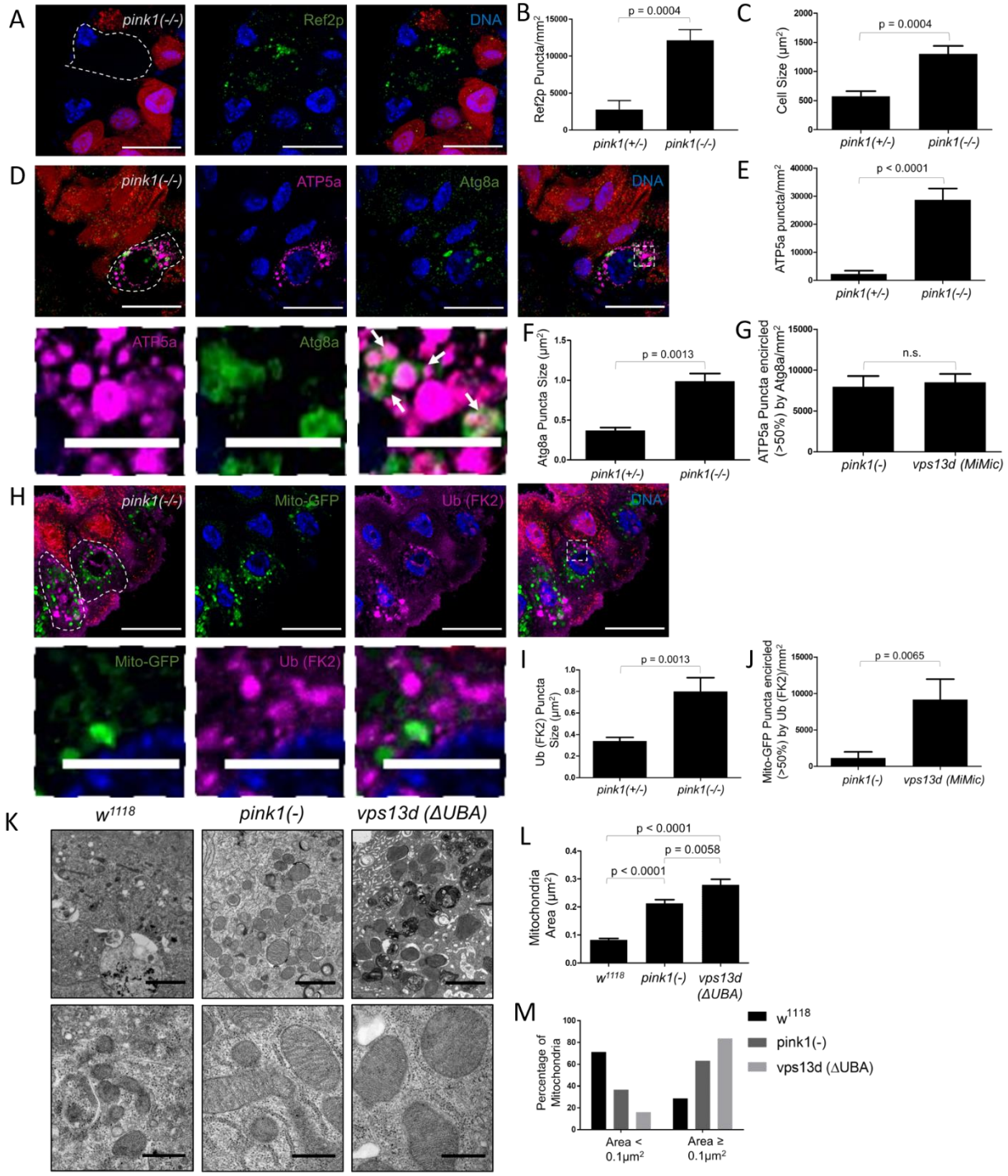
A
pink1(-/-)
Ref2p
DNA
B
p = 0.0004
Ref2p Puncta/mm²
pink1(+/-)
pink1(-/-)
C
p = 0.0004
Cell Size (µm²)
pink1(+/-)
pink1(-/-)
D
pink1(-/-)
ATP5a
Atg8a
DNA
E
p < 0.0001
ATP5a puncta/mm²
pink1(+/-)
pink1(-/-)
F
p = 0.0013
Atg8a Puncta Size (µm²)
pink1(+/-)
pink1(-/-)
G
n.s.
ATP5a Puncta encircled (>50%) by Atg8a/mm²
pink1(-)
vps13d (MiMic)
H
pink1(-/-)
Mito-GFP
Ub (FK2)
DNA
I
p = 0.0013
Ub (FK2) Puncta Size (µm²)
pink1(+/-)
pink1(-/-)
J
p = 0.0065
Mito-GFP Puncta encircled (>50%) by Ub (FK2)/mm²
pink1(-)
vps13d (MiMic)
K
w1118
pink1(-)
vps13d (ΔUBA)
L
p < 0.0001
p = 0.0058
p < 0.0001
Mitochondria Area (µm²)
w1118
pink1(-)
vps13d (ΔUBA)
M
Percentage of Mitochondria
Area < 0.1µm²
Area ≥ 0.1µm²
w1118
pink1(-)
vps13d (ΔUBA)

Figure 2-5: *pink1* mutant cells have autophagy and mitochondrial phenotypes that are similar to *vps13d* mutant cells. A) *pink1^{B9}* loss-of-function mutant (-/-) intestines cells (non-red) fail to reduce in size and have increased Ref2p puncta (green) compared to neighboring control *pink1^{B9}*/+ heterozygous (+/-) cells (red) 2 hours after pupariation. B) Quantification of Ref2p puncta in *pink1^{B9}* mutant (-/-) cells (n=6) compared to heterozygous control (+/-) cells (n=15). C) Quantification of cell size in *pink1^{B9}* mutant (-/-) cells (n=9) compared to control (+/-) cells (n=11). D) *pink1^{B9}* loss-of-function mutant (-/-) intestines cells (non-red) have increased mitochondrial ATP5a (purple) puncta and exhibit enlarged Atg8a puncta (green) compared to heterozygous (+/-) control cells (red) 2 hours after pupariation (top panels). Atg8a puncta in mutant cells tend to encircle mitochondrial ATP5a puncta (bottom panels). E) Quantification of the amount of ATP5a puncta in *pink1^{B9}* mutant (-/-) cells (n=9) compared to neighboring control (+/-) cells (n=11). F) Quantification of the size of Atg8a puncta in *pink1^{B9}* mutant (-/-) cells (n=7) compared to neighboring control (+/-) cells (n=13) G) Quantification of the number of ATP5a puncta having at least half of the perimeter encircled by Atg8a in *pink1^{B9}/pink1^{B9}* mutant (-/-) cells (n=7) compared to *vps13d (MiMic)* mutant intestine cells (n=6). H) *pink1^{B9}/pink1^{B9}* loss-of-function mutant (-/-) intestine cells (non-red) have enlarged conjugated ubiquitin (FK2) puncta (purple) compared to heterozygous neighboring control cells (red) 2 hours after pupariation (top panels). These enlarged puncta do not seem to encircle mitochondria labeled by mito-GFP (green) (bottom panels). I) Quantification of conjugated ubiquitin (FK2) puncta size in *pink1^{B9}/pink1^{B9}* mutant (-/-) cells (n=9) compared to control (+/-) cells (n=11). J) Quantification of the number of mito-GFP puncta having a perimeter at least halfway encircled by conjugated ubiquitin in *pink1^{B9}/pink1^{B9}* mutant (-/-) cells (n=9) compared to *vps13d (MiMic)* mutant cells (n=6). K) Representative TEM images from sections of control *w^{1118}, pink1^{B9} (-),* and *vps13d (ΔUBA)* male larval intestine cells 2 hours after pupariation. Images on top and bottom are lower and higher resolution images, respectively. L) Quantification of mitochondria area in *w^{1118}* (n=202), *pink1^{B9}* (n=188), and *vps13d (ΔUBA)* (n=185) intestine cells 2 hours after pupariation. M) Quantification of the percentage of mitochondria smaller and equal to or larger than 0.1 μm in *w^{1118}* (n=202), *pink1^{B9} (-)* (n=188), and *vps13d (ΔUBA)* (n=185) intestine cells 2 hours after pupariation. Fisher exact test values are as follows: *w^{1118}* vs. *pink1^{B9},* $p < 0.0001$; *w^{1118}* vs. *vps13d (ΔUBA)*, $p < 0.0001$; *pink1^{B9}* vs. *vps13d (ΔUBA)*, $p < 0.0001$. Scale bars in A), D), and H), represent 40μm with the exception of the enlarged images in D) and H), which represent 10μm. Scale bars in K) represent 2.0μm (top panels) and 0.5μm (bottom panels). Columns in B), C), E), F), G), I), J), and (L) were compared using two-tailed student t-test without Welch's correlation with error bars representing SEM. Representative of 3 or more independent biological experiments.

In addition, *pink1* mutant cells also failed to reduce in size **(Figure 2-5C),** an indicator of autophagy deficiency in intestine cells (Chang et al., 2013). Combined, these data

indicate that *pink1* influences markers of autophagy and mitochondrial clearance in a manner that is similar to loss of *vps13d.*

We next investigated the influence of *pink1* function on the localization of Atg8a and ubiquitin with ATP5a as a marker of mitochondria. Antibody staining against Atg8a revealed enlarged puncta surrounding enlarged mitochondrial ATP5a puncta **(Figure 2-5D-G)**, and these Atg8a puncta could be suppressed by knockdown of *atg6* **(Figure 2-6)**, similar to *vps13d* mutant cell Atg8a puncta **(Figure 2-2C and D).**

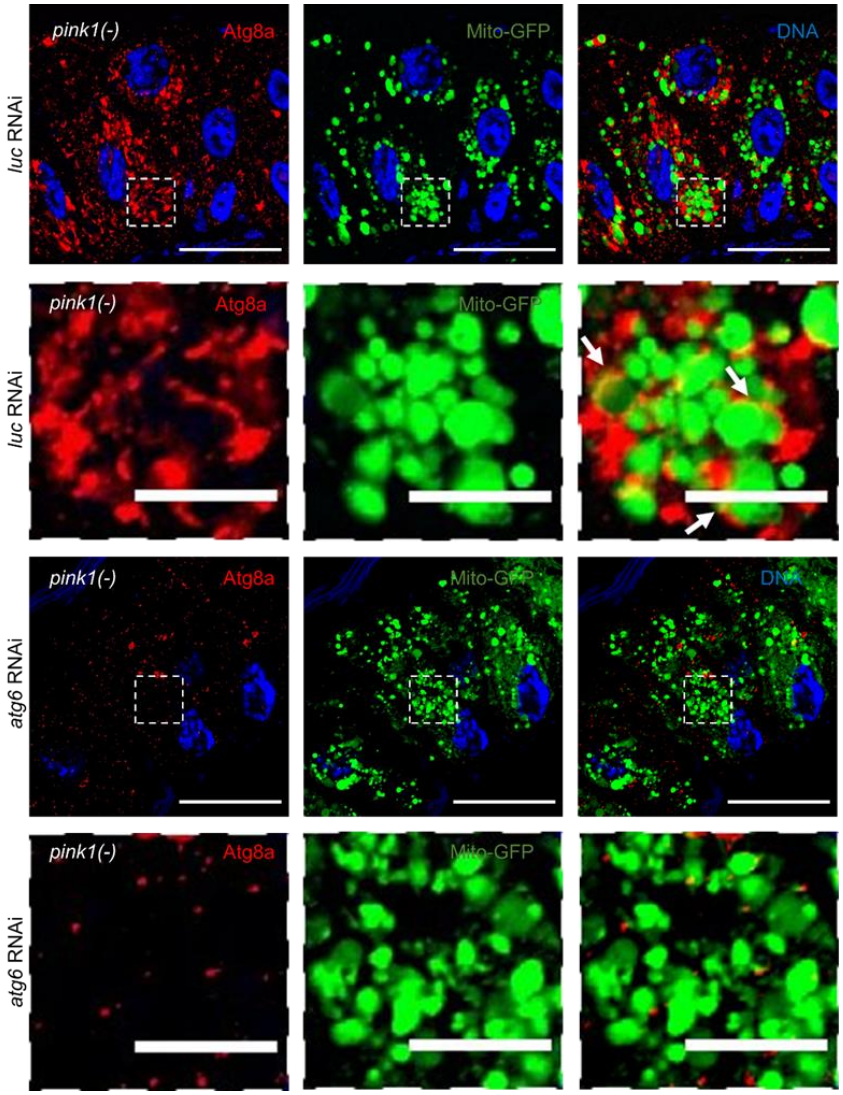

Figure 2-6: Loss of *atg6* suppresses the *pink1* loss-of-function Atg8a puncta phenotype. *atg6* RNAi-expressing *pink1^{B9} (-)* intestine cells have suppression of the enlarged, Atg8a puncta (red) that encircle mito-GFP (green) compared to control *luc* RNAi-expressing *pink1^{B9} (-)* mutant cells (white arrows) 2 hours after pupariation. Scale bars represent 40μm with the exception of enlarged figures, which represent 10μm. Representative of 3 or more independent biological experiments.

Antibody staining against conjugated ubiquitin also revealed that *pink1* mutant cells had enlarged conjugated ubiquitin puncta **(Figure 2-5H and I).** In contrast to *vps13d* mutant cells, *pink1* mutant cell puncta did not localize to the periphery of mitochondria **(Figure 2-5J),** suggesting potential differences between Pink1 and Vps13D.

Transmission electron microscopy (TEM) was used to investigate mitochondrial clearance and ultrastructure in control *w^{1118}*, *pink1* loss-of-function mutant, and *vps13d (ΔUBA)* mutant intestine cells 2 hours after prepupa formation. Both *pink1* and *vps13d (ΔUBA)* mutant cells possessed uncleared mitochondria that were larger than *w^{1118}* controls, which possess mitochondria with an area of approximately 0.1μm^2 **(Figure 2-5K and L).** *vps13d (ΔUBA)* mutant mitochondria were on average larger than *pink1* mutant mitochondria **(Figure 2-5K and L).** In addition, *pink1* mutant cells possessed a larger percentage of mitochondria having an area less than 0.1μm^2 than *vps13d (ΔUBA)* mutants **(Figure 2-5M).**

The similarities in *vps13d* and *pink1* mutant cell phenotypes prompted us to investigate their functional relationship. Therefore, we conducted double mutant genetic analyses to determine if *vps13d* and *pink1* are in a common pathway that regulates mitochondria structure and removal. We compared mitochondrial size in TEM sections

of *pink1* mutant with *pink1* and *vps13d* double mutant intestine cells. These mutants had similar mitochondria area 2 hours after puparium formation **(Figure 2-7A and B).**

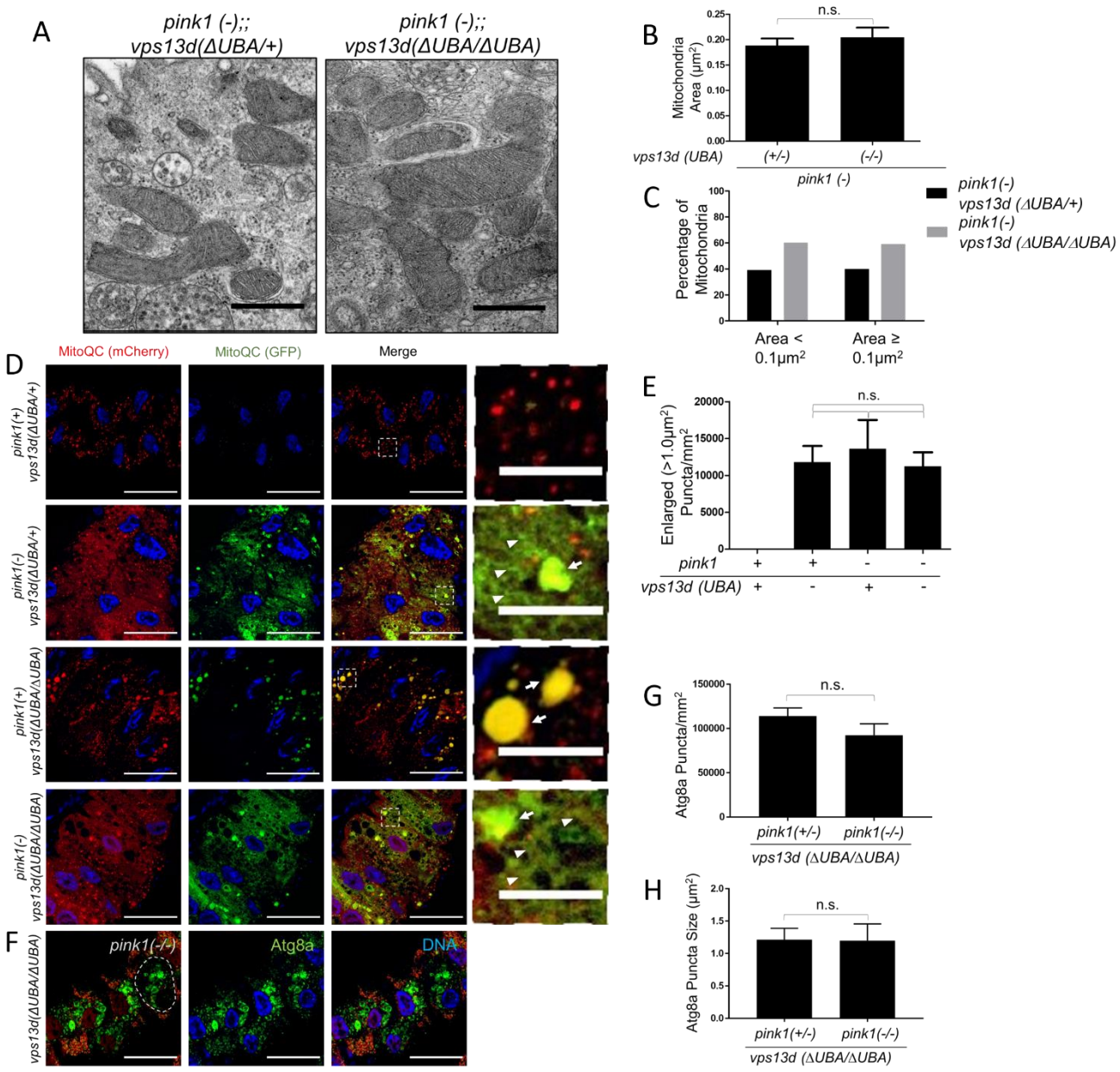

Figure 2-7: Vps13D functions in a mitophagy pathway with Pink1. A) Representative TEM images of male *pink1^{B9} (-), vps13d (ΔUBA/+)* single mutant and *pink1^{B9} (-), vps13d (ΔUBA/ΔUBA)* double mutant intestine cells 2 hours after puparation. B) Quantification of mitochondria area in *pink1^{B9} (-), vps13d (ΔUBA/+)* single mutant (n=187) and *pink1^{B9}, vps13d (ΔUBA/ΔUBA)* double mutant (n=181) intestine cells 2 hours after puparation. C) Quantification of the percentage of

mitochondria smaller and equal to or larger than 0.1 μm in *pink1^{B9} (-), vps13d (ΔUBA/+)* single mutant (n=187) and *pink1^{B9} (-), vps13d (ΔUBA/ΔUBA)* double mutant (n=181) intestine cells 2 hours after pupariation using Fisher exact test (p = 0.7507). D) Mito-QC was expressed in *pink1^{B9} (-)* and *vps13d (ΔUBA)* mutant intestine cells from 2-hour old male prepupae. *pink1 (+), vps13d (*Δ*UBA)/+* heterozygote control cells possessed mostly red puncta without corresponding green puncta, reflecting mitochondria in autolysomes (mitolysosomes). By contrast, *pink1^{B9} (-)*, *vps13d (*Δ*UBA)/+* single mutant, *pink1 (+), vps13d (*Δ*UBA/*Δ*UBA)* single mutant, and *pink1^{B9} (-), vps13d (*Δ*UBA)/*Δ*UBA)* double mutant intestine cells all exhibited red and green structures, reflecting mitochondria that failed to be cleared by mitophagy. These structures were either filamentous (arrowheads) or enlarged and puncta (white arrows). Enlarged punctate structures were defined as having an area of at least 1.0μm^2. E) Quantification of the amount of red and green structures that presented as enlarged punctate in *pink1 (+), vps13d (*Δ*UBA)/+* heterozygote control (n=17), *pink1^{B9} (-), vps13d (*Δ*UBA)/+* single mutant (n=14), *pink1 (+), vps13d (*Δ*UBA/*Δ*UBA)* single mutant, and *pink1^{B9} (-), vps13d (*Δ*UBA)/*Δ*UBA)* double mutant (n=14) cells 2 hours after pupariation. F) *pink1^{B9}/pink1^{B9} (-/-), vps13d (*Δ*UBA/*Δ*UBA)* double mutant intestine cells (non-red) have similar levels and size of Atg8a puncta (green) compared to *pink1^{B9}/+ (+/-), vps13d (*Δ*UBA/*Δ*UBA)* single mutant cells (red) 2 hours after pupariation. G) Quantification of Atg8a puncta number in *pink1^{B9}/pink1^{B9} (-/-), vps13d (*Δ*UBA/*Δ*UBA)* double mutant cells (n=11) compared to neighboring *pink1^{B9}/+ (+/-), vps13d (*Δ*UBA/*Δ*UBA)* single mutant cells (n=15). H) Quantification of Atg8a puncta size in *pink1^{B9}/pink1^{B9} (-/-), vps13d (*Δ*UBA/*Δ*UBA)* double mutant cells (n=11) compared to *pink1^{B9}/+ (+/-); vps13d (*Δ*UBA/*Δ*UBA)* single mutant cells (n=15). Scale bars in A) represent 0.5μm. Scale bars in D) and F) represent 40μm with the exception of the enlarged images in D), which represent 10μm. Columns in B), E), G), and H) were compared using two-tailed student t-test without Welch's correlation with error bars representing SEM. Representative of 3 or more independent biological experiments.

Furthermore, these single and double mutant genotypes had a similar proportion of remaining mitochondria that are smaller than 0.1μm^2 **(Figure 2-7C),** even though *vps13d (ΔUBA)* single mutants have larger mitochondria and fewer mitochondria that are smaller than 0.1μm^2 than control and *pink1^{B9}* single mutant intestines **(Figure 2-5K-M).** These data indicate that the combined loss of both *vps13d* and *pink1* fails to enhance single mutant mitochondrial size phenotype, thus suggesting that Vps13D functions in the same pathway as Pink1 in the regulation of mitochondrial size.

We sought to determine if Vps13D and Pink1 act within the same pathway to regulate mitophagy. We used the Mito-QC system to analyze mitophagy, which utilizes a mitochondria-localized tandem mCherry and GFP fluorescent tags to label mitochondria outside of autolysosomes with both mCherry and GFP (yellow) and mitochondria inside autolysosomes with only red mCherry as the acidic environment of the autolysosome quenches GFP signal (McWilliams et al., 2016; Lee et al., 2018). In control cells that are wildtype for *pink1* and heterozygous for *vps13d*, most of the GFP signal from the MitoQC was quenched leaving only red mCherry puncta 2 hours after prepupa formation **(Figure 2-7D and E),** indicating that mitophagy was active. By contrast, *pink1* mutants and *pink1* and *vps13d* double mutants retained both GFP and mCherry (yellow) signal that was absent in the control **(Figure 2-7D and E),** indicating that mitophagy was impaired. However, it is worth noting that the morphology of the retained GFP and mCherry (yellow) signal differed between these single and double mutants. The *pink1* mutants appeared as either filamentous structures or large, round, and punctate structures. By contrast, *vps13d* mutants only had the enlarged punctate structures **(Figure 2-7D).** Importantly, the distribution of the large and round yellow puncta were the same in *pink1* and *pink1* and *vps13d* double mutant cells **(Figure 2-7D and E).** Together with our TEM data **(Figure 2-7A-C),** these findings suggest that Vps13D and Pink1 function in a common pathway to regulate mitochondrial morphology and clearance.

To further investigate the relationship between Vps13D and Pink1, we determined how they influence Atg8a puncta in intestine cells 2 hours after puparium formation. Like *vps13d* mutant intestine cells **(Figure 2-2A and B),** *pink1* mutant

intestine cells possess abnormal and enlarged Atg8a localization **(Figure 2-5D, F and G).** Both *vps13d* mutant (labeled by nuclear RFP) and *pink1* and *vps13d* double mutant (lacking nuclear RFP) intestine cells possessed similar Atg8a puncta size and amounts **(Figure 2-7F-H).** These findings suggest that *pink1* and *vps13d* function in the same pathway to regulate Atg8a localization.

Pink1 senses mitochondrial stress and facilitates ubiquitination of mitochondria-associated proteins to facilitate mitophagy (Ordureau et al., 2014; Koyano et al., 2014; Wauer et al., 2015). In contrast to Atg8a localization, *pink1* and *vps13d* single mutant intestine cells differ in conjugated ubiquitin localization **(Figures 2-4F and G, 2-5H and J).** To further examine the relationship between these 2 regulators of mitochondrial clearance, we compared conjugated ubiquitin localization in either *pink1* mutant, *vps13d* mutant, or *pink1* and *vps13d* double mutant cells. In contrast to *vps13d* mutant cells, *pink1* and *vps13d* double mutant cells exhibited the same pattern of conjugated ubiquitin localization as *pink1* single mutant cells that was not associated with the perimeter of mitochondria **(Figure 2-8A and B).**

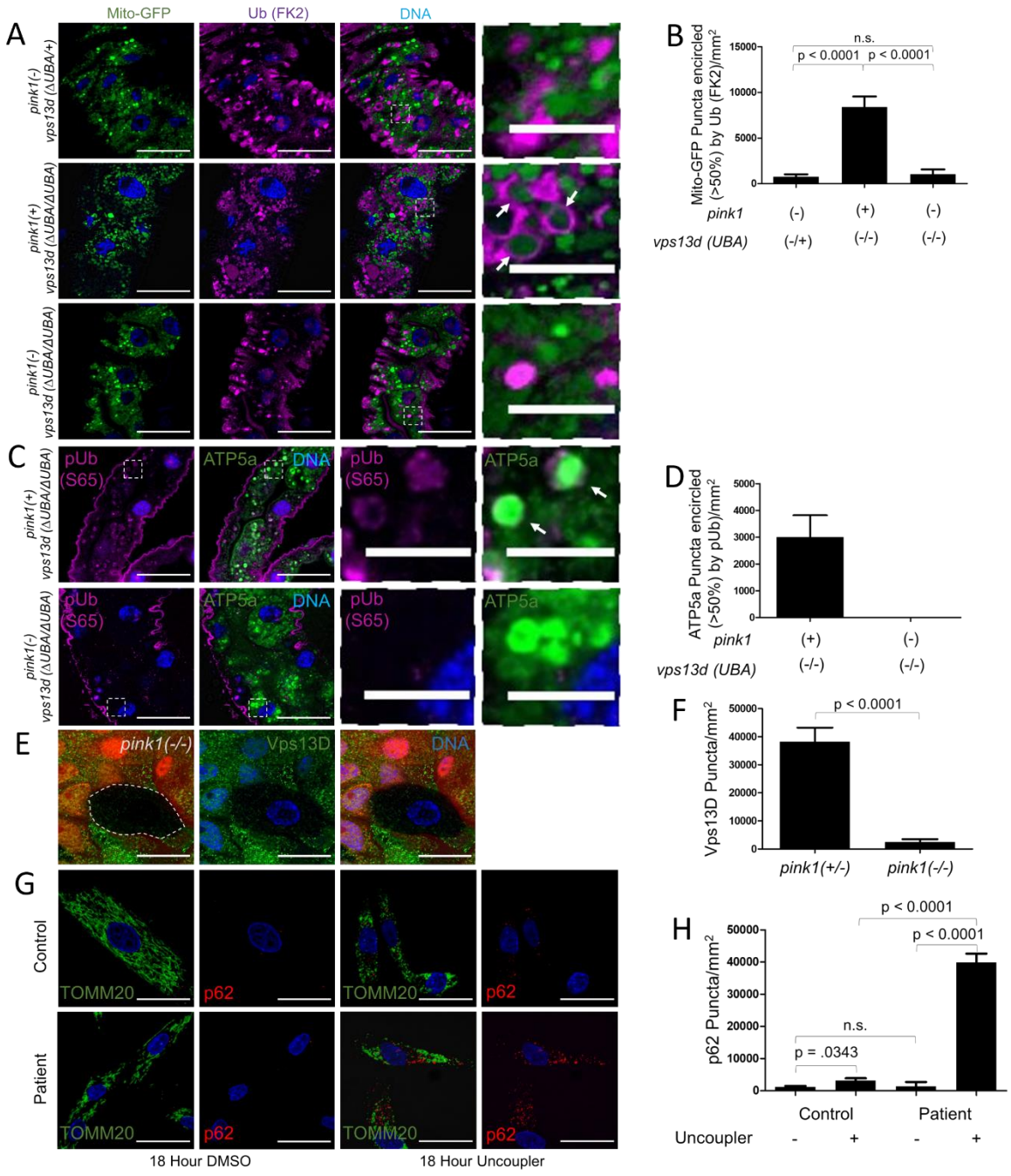

Figure 2-8: Loss of Pink1 suppresses ubiquitin localization to mitochondria in *vps13d* mutant cells. A) *pink1^{B9} (-), vps13d (ΔUBA/+)* single mutant intestine cells have conjugated ubiquitin puncta (purple) that do not encircle mitochondria labeled by mito-GFP (green) as frequently as intestines from *pink1 (+), vps13d (ΔUBA/ΔUBA)* single mutants 2 hours after prepupae formation (top panels). Loss of Pink1 in a *vps13d (ΔUBA/ΔUBA)* background, resulting in a *pink1^{B9} (-), vps13d (ΔUBA/ΔUBA)* double mutant (bottom panels), suppresses the conjugated ubiquitin localization to

mitochondria phenotype in *vps13d* mutant intestine cells (middle panels) 2 hours after pupariation. B) Quantification of the number of mito-GFP puncta with at least 50% of the perimeter encircled by conjugated ubiquitin in *pink1^{B9} (-), vps13d (ΔUBA/+)* (n=15), *pink1 (+), vps13d (ΔUBA/ΔUBA)* (n=11), and *pink1^{B9} (-), vps13d (ΔUBA/ΔUBA)* (n=12) mutant intestines 2 hours after pupariation. C) *pink1 (+), vps13d (ΔUBA/ΔUBA)* single mutant intestine cells have Ser65 phosphorylated ubiquitin puncta (purple) surrounding mitochondria labeled by ATP5a (green) 2 hours after puparium formation. *pink1^{B9} (-), vps13d (ΔUBA/ΔUBA)* double mutant intestine cells do not have Ser65 phosphorylated ubiquitin puncta surrounding mitochondria 2 hours after prepupae formation. D) Quantification of the number of ATP5a puncta with at least 50% of the perimeter encircled Ser65 phosphorylated ubiquitin in *pink1 (+), vps13d (ΔUBA/ΔUBA)* (n=15) single mutant and *pink1^{B9}, vps13d (ΔUBA/ΔUBA)* (n=15) double mutant intestines 2 hours after pupariation. E) *pink1^{B9}/pink1^{B9}* mutant (-/-) intestine cells (non-red) have decreased Vps13D puncta (green) compared to *pink1^{B9}*/+ (+/-) heterozygous control neighboring cells (red). F) Quantification of Vps13D puncta in *pink1^{B9}/pink1^{B9} (-/-)* cells (n=6) compared to control (+/-) cells (n=14). G) Fibroblasts from a patient with trans-heterozygous mutations in *VPS13D (*G1190D/Q1106*) (patient) and a relative who is heterozygous for *VPS13D* mutations (G1190D/+) (control) were stained with antibodies for mitochondrial TOMM20 (green) and autophagy cargo receptor p62 (red) after 18-hour incubation with mitochondrial uncoupler (10μM FCCP, 1μM Antimycin A, and 10μM Oligomycin) or vehicle DMSO control. H) Quantification of the number of p62 puncta in patient and control fibroblasts with DMSO or uncoupler (n=10/condition). Scale bars in A), C), E), and G) represent 40μm with the exception of the enlarged images in A) and C), which represent 10μm. Columns in B), F), and H) were compared using two-tailed student t-test without Welch's correlation with error bars representing SEM. Representative of 3 or more independent biological experiments.

Pink1 can directly phosphorylate ubiquitin conjugated to proteins at the Ser65 residue, resulting in a conformation change that inhibits de-ubiquitination and can lead to further ubiquitination (Ordureau et al., 2014; Koyano et al., 2014; Wauer et al., 2015). *vps13d* mutant intestine cells were stained with an antibody specific for ubiquitin phosphorylated at the Ser65 site. Like conjugated ubiquitin, phosphorylated ubiquitin localized around the periphery of the mitochondria (labeled by ATP5a) in *vps13d* mutants, but was absent in *pink1* and *vps13d* double mutants **(Figure 2-8C and D).** These data indicate that *pink1* function is required for localization of conjugated and

phosphorylated ubiquitin near perimeter of mitochondria in *vps13d* mutant cells, and suggests that *pink1* is upstream of *vps13d*. To test this hypothesis, we analyzed Vps13D protein puncta localization in *pink1* mutant intestine cells. *pink1* mutant cells (lacking RFP) had reduced Vps13D protein puncta compared to neighboring RFP-labeled control cells **(Figure 2-8E and F).** Like with loss of core autophagy proteins, loss of Pink1 did not affect Vps13D puncta in early third instar larval intestine cells **(Figure 2-9),** suggesting that the relationship between Pink1 and Vps13D is stage- and context-dependent. Taken together, these results suggest that Pink1 and Vps13D can function in a common pathway to regulate mitophagy with Pink1 acting upstream of Vps13D.

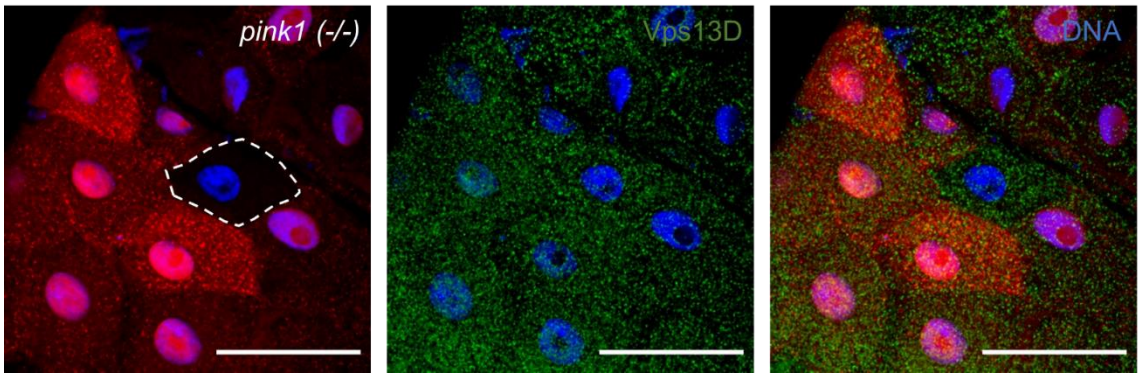

Figure 2-9: Loss of *pink1* in early third instar intestine cells do not have altered Vps13D puncta. *pink1^{B9}/pink1^{B9} (-/-)* loss-of-function mutant intestine cells (non-red) in early third instar larvae do not have altered Vps13D puncta (green) compared to heterozygous control (+/-) cells (red). Scale bars represent 40μm. Representative of 3 or more independent biological experiments.

We next tested if Pink1 and Vps13D could function in a common pathway in human cells. Since Pink1 can be activated through the addition of mitochondrial

uncoupling reagents (Jin et al., 2010; Rakovic et al., 2011), we tested the influence of Pink1 activation in fibroblasts that were derived from a patient with neurological symptoms driven by *VPS13D* mutations (G1190D/Q1106*) and heterozygous control fibroblasts from a relative of the patient (G1190D/+) (Seong et al., 2018). These fibroblasts were incubated with either the uncoupler reagents FCCP, Antimycin A, and oligomycin to induce Pink1-dependent mitophagy (Vives-Bauza et al., 2010) or DMSO as a vehicle control. TOMM20 antibody staining revealed that patient-derived G1190D/Q1106* fibroblasts without any uncoupler had mitochondria that were more round and less filamentous than control G1190D/+ fibroblasts, and that they had comparable amounts of p62 **(Figure 2-8G and H).** While both cell lines had an increase of p62 puncta consistent with the induction of mitophagy by the addition of uncoupler, the patient-derived G1190D/Q1106* fibroblasts had a greater accumulation of p62 puncta than control fibroblasts **(Figure 2-8G and H).** Taken together, these findings indicate that Vps13D functions downstream of Pink1 in conditions that induce mitophagy.

Vps13D and Parkin function in parallel pathways downstream of Pink1

Pink1 phosphorylates both ubiquitin and Parkin, leading to ubiquitination of mitochondrial-associated proteins and recruitment of the core autophagy machinery for mitophagy (Ordureau et al., 2014; Koyano et al., 2014; Wauer et al., 2015; Lazarou et al., 2015). The relationship between Pink1 and Vps13D prompted us to hypothesize that Vps13D and Park, the *Drosophila* homolog of Parkin, function in the same pathway to

regulate mitophagy. We expected *park*^{25} loss-of-function mutant intestine cells to have the same phenotype as *pink1* and *vps13d* mutant cells 2 hours after prepupa formation. While *park*^{25} mutant cells failed to clear mitochondria as indicated by abundant ATP5a staining compared to heterozygous control cells, homozygous *park* mutant cells had neither enlarged ATP5a puncta nor abnormal Atg8a as were detected in *vps13d* mutant cells **(Figure 2-10A-C).** In addition, *park* mutant cells lacked the enlarged conjugated ubiquitin puncta that were observed in homozygous *vps13d* mutant cells **(Figure 2-10D-E).** Furthermore, the ATP5a puncta size was smaller in *park* mutants than in *pink1* mutants ($p = 0.0019$) **(Figure 2-5I and 2-10E).** Significantly, unlike *pink1* mutants, *park* mutants did not affect Vps13D puncta in intestine cells **(Figure 2-10F and G).** Combined, these data suggest that Vps13D and Park act in parallel pathways to regulate mitophagy.

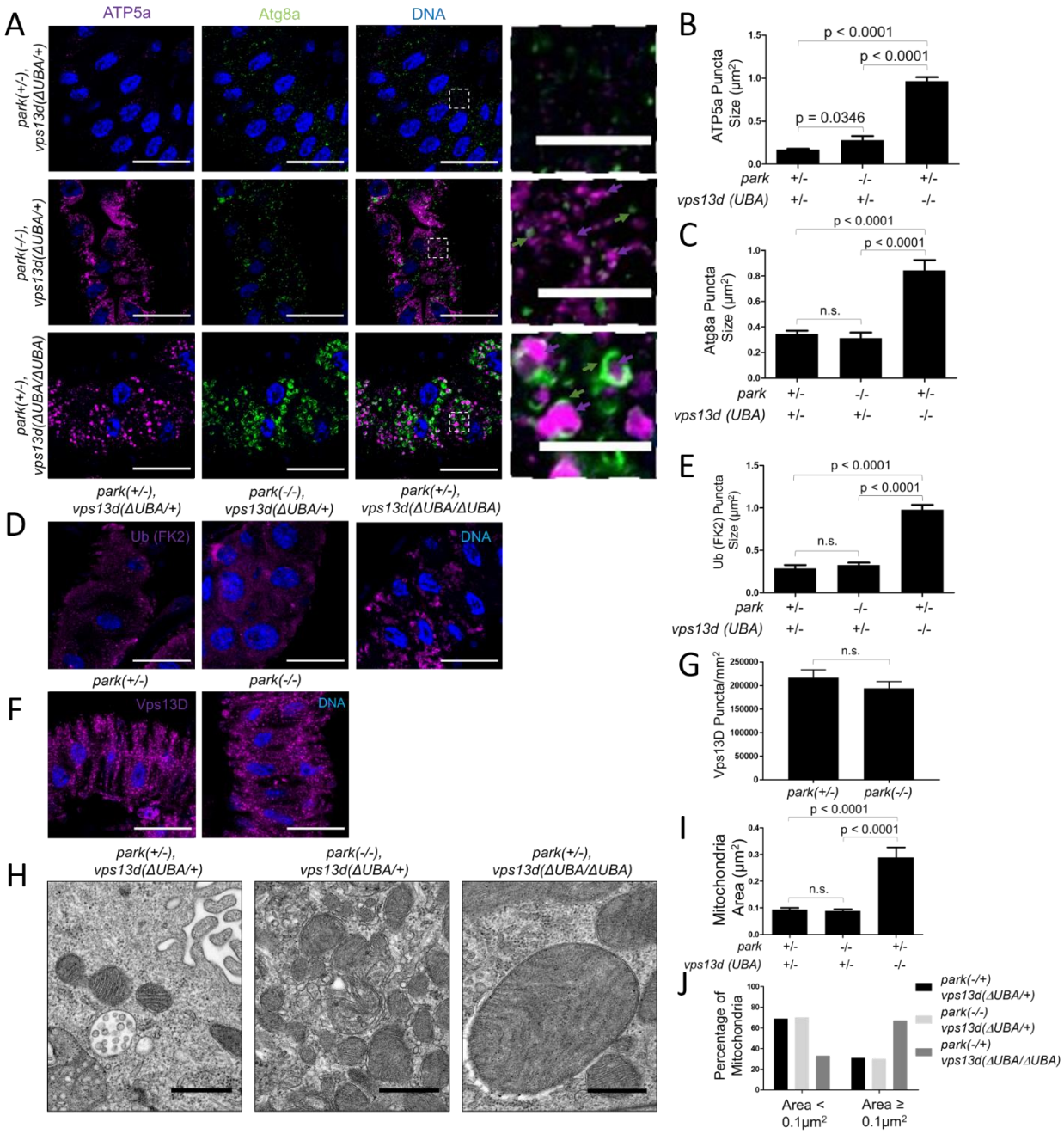

Figure 2-10: Vps13D and Park function in separate mitochondrial clearance pathways. A) *park*^{25}*/park*^{25} *(-/-), vps13d (ΔUBA/+)* (middle panels) single mutant intestine cells and *park*^{25}*/+ (+/-), vps13d (ΔUBA/ΔUBA)* (bottom panels) single mutant intestine cells 2 hours after pupariation are unable to clear mitochondria as shown by ATP5a staining (purple) compared to *park*^{25}*/+ (+/-), vps13d (ΔUBA/+)* heterozygous control cells (top panels). *vps13d (ΔUBA)* mutants have ATP5a that appear larger and less filamentous (purple arrows) and larger Atg8a puncta (green arrows) encircling the

enlarged ATP5a puncta (purple arrows), which are not present in the *park*^{25} mutant cells. B) Quantification of ATP5a puncta size in *park*^{25}*/+ (+/-), vps13d (ΔUBA/+)* heterozygous control (n=13), *park*^{25}*/park*^{25} *(-/-), vps13d (ΔUBA)/+* (n=12), and *park*^{25}*/+ (+/-), vps13d (∆UBA/∆UBA)* (n=12) intestine cells. C) Quantification of Atg8a puncta size in *park*^{25}*/+ (+/-), vps13d (ΔUBA/+)* heterozygous control (n=13), *park*^{25}/park^{25} (-/-), *vps13d (ΔUBA)/+* (n=12), and *park*^{25}*/+ (+/-), vps13d (∆UBA)* (n=12) intestine cells. D) *park*^{25}*/+ (+/-), vps13d (∆UBA/∆UBA)* single mutant cells have larger conjugated ubiquitin (FK2) puncta (purple) than *park*^{25}*/park*^{25} *(-/-), vps13d (∆UBA/+)* single mutant and *park*^{25}*/+ (+/-), vps13d (∆UBA/+)* heterozygous control intestine cells 2 hours after pupariation. E) Quantification of conjugated ubiquitin (FK2) size in *park*^{25}*/+ (+/-), vps13d (∆UBA/+)* heterozygous control (n=11), *park*^{25}*/park*^{25} *(-/-), vps13d (ΔUBA)/+* (n=12), and *park*^{25}*/+ (+/-), vps13d (∆UBA/∆UBA)* (n=11) intestine cells 2 hours after pupariation. F) *park*^{25}*/park*^{25} mutant (-/-) intestine cells have similar levels of Vps13D puncta (purple) compared to heterozygous *park*^{25}*/+* (+/-) control intestine cells 2 hours after pupariation. G) Quantification of Vps13D puncta in *park*^{25}*/park*^{25} *(-/-)* mutant intestine cells (n=11) compared to *park*^{25}*/+ (+/-)* control cells (n=13). H) Representative TEM images of *park*^{25}*/+ (+/-), vps13d (ΔUBA)/+* heterozygous control, *park*^{25}*/park*^{25} *(-/-), vps13d (ΔUBA/+)* single mutant, and *park*^{25}*/+ (+/-), vps13d (ΔUBA/ ΔUBA)* single mutant intestine cells 2 hours after pupariation. I) Quantification of mitochondrial area from TEM images of *park*^{25}*/+ (+/-), vps13d (ΔUBA)/+* heterozygous control cells (n=192), *park*^{25}*/park*^{25} *(-/-), vps13d (ΔUBA/+)* single mutant (n=186), and *park*^{25}*/+ (+/-), vps13d (ΔUBA/ ΔUBA)* single mutant (n=184) intestine cells 2 hours after pupariation. J) Quantification of the percentage of mitochondria smaller and equal to or larger than 0.1 µm from TEM images from *park*^{25}*/+ (+/-), vps13d (ΔUBA)/+* heterozygous control (n=192), *park*^{25}*/park*^{25} *(-/-), vps13d (ΔUBA/+)* single mutant (n=186), and *park*^{25}*/+ (+/-), vps13d (ΔUBA/ ΔUBA)* single mutant (n=184) intestine cells 2 hours after pupariation. *vps13d* mutant intestine cells have larger mitochondria and fewer remaining mitochondria less than or equal to 0.1µm^2 than *park* mutant and control intestine cells. Columns were compared using Fisher exact test with the following values: *park*^{25}*/+, vps13d (ΔUBA)/+* vs. *park*^{25}*/park*^{25}*, vps13d (ΔUBA/+),* $p = 0.9109$; *park*^{25}*/+, vps13d (ΔUBA)/+* vs. *park*^{25}*/+, vps13d (ΔUBA/ ΔUBA),* $p < 0.0001$; *park*^{25}*/park*^{25}*, vps13d (ΔUBA/+)* vs. *park*^{25}*/+, vps13d (ΔUBA/ ΔUBA),* $p < 0.0001$. Scale bars in A), D), and F) represent 40µm with the exception of the enlarged images in A), which represent 10µm. Scale bars in H) represent 0.5µm. Columns in B), C), E), G), and I) were compared using two-tailed student t-test without Welch's correlation with error bars representing SEM. Representative of 3 or more independent biological experiments.

TEM was used to study the influence of Park on mitochondria size. *vps13d* mutant intestine cells had larger mitochondria and a higher proportion of mitochondria remaining with an area greater or equal to 0.1µm^2 compared to *park* mutant intestine

cells 2 hours after prepupa formation **(Figure 2-10H-J).** Significantly, *park* mutant intestine cells had smaller mitochondria than *pink1* mutant cells ($p < 0.0001$), and had a smaller proportion of mitochondria with an area greater or equal to $0.1\mu m^2$ ($p < 0.0001$) **(Figure 2-5K-M, 2-10H-J).** While both Park and Vps13D regulate mitochondrial clearance, these data indicate that they function in parallel pathways.

Park functions downstream of Pink1 (Narendra et al., 2010; Youle and Narendra, 2011). In addition, Vps13D appears to act downstream of Pink1 and in parallel to Park **(Figures 2-8 and 2-10).** Thus, we hypothesized that Pink1 regulates both Vps13D- and Park- mediated clearance of mitochondria in intestine cells. We used MitoQC to investigate the functions of *vps13d* and *park* in mitophagy. The early lethality of *vps13d (ΔUBA)* and $park^{25}$ double mutants required the use of *park* mutants expressing *vps13d* RNAi in intestine cells for these analyses. While *park* heterozygous control intestine cells did not retain GFP indicating active mitophagy 2 hours after prepupa formation, *park* mutant intestine cells retained GFP signal in a filamentous distribution **(Figure 2-11A)**. In contrast to *park* mutant cells, cells with reduced *vps13d* function retained GFP signal in enlarged, round puncta **(Figure 2-11A),** similar to the MitoQC phenotype in *vps13d* mutant cells **(Figure 2-7C and D).** Importantly, intestine cells with reduced function of both *park* and *vps13d* had an additive phenotype with both filamentous and enlarged round puncta **(Figure 2-11A and B).** This phenotype is similar to the MitoQC phenotype in *pink1* mutant intestine cells **(Figure 2-7C and D).** To verify that the Mito-QC distribution we detected in different mutants were representative of mitochondria in intestine cells, we stained Mito-QC expressing intestine cells with antibody against mitochondrial ATP5a protein, and detected Mito-QC and ATP5a co-localization **(Figure**

2-12A). These findings are consistent with Pink1 regulating mitophagy upstream of parallel Vps13D and Park pathways.

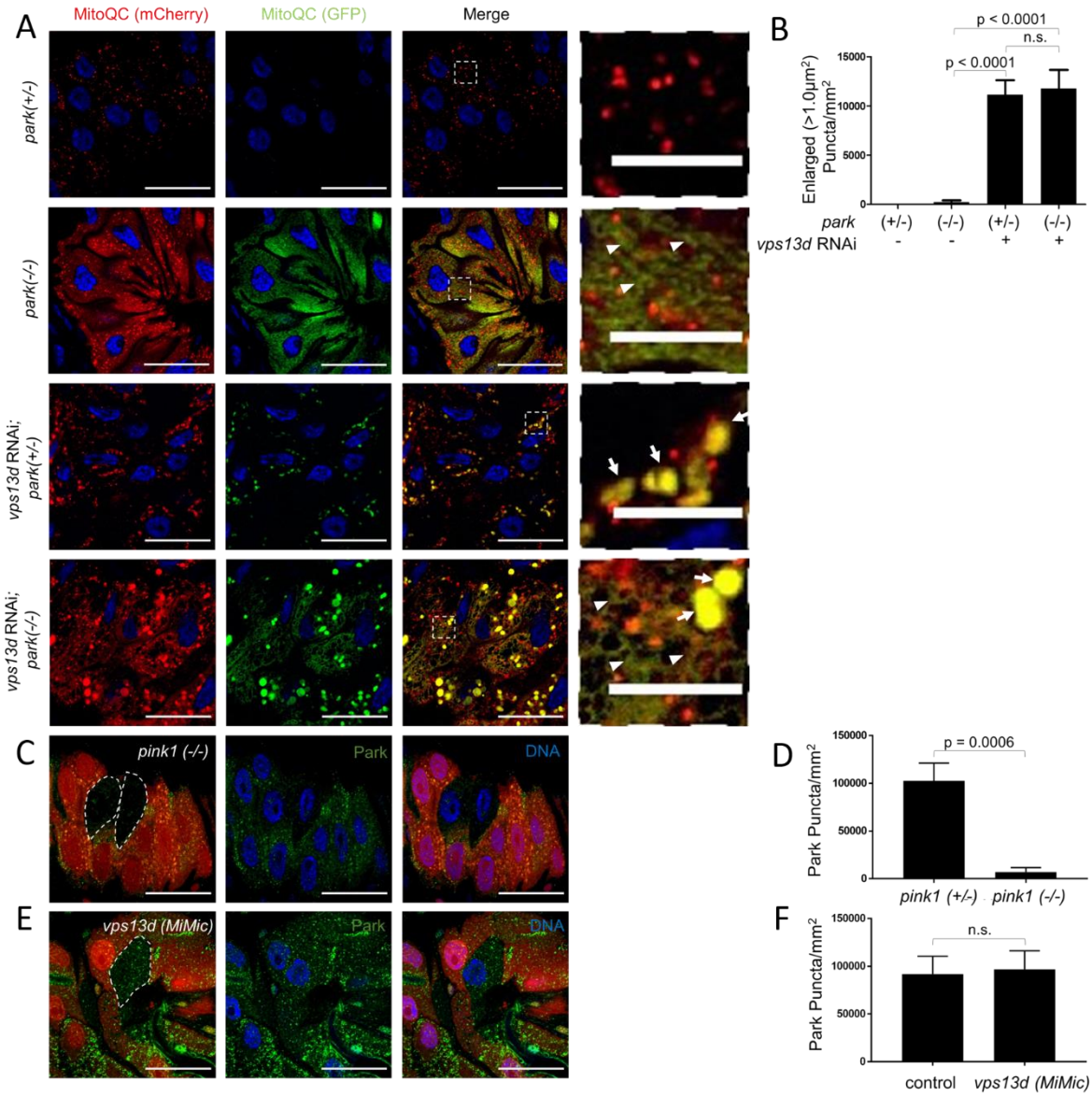

Figure 2-11: Vps13D and Park function in parallel Pink1-regulated mitophagy pathways. A) Mito-QC was expressed in intestine cells from *park^{25}/park^{25} (-/-)* prepupae with and without expression of *vps13d* RNAi. *park^{25}/+ (+/-)* heterozygous control cells expressing control *uas-flp* (to account for off-target effects of UAS expression) possessed mostly red puncta without corresponding green puncta, reflecting mitochondria in autolysomes (mitolysosomes). By contrast, *park^{25}/park^{25} (-/-)* expressing *flp, park^{25}/+ (+/-)* expressing *vps13d* RNAi, and *park^{25}/park^{25} (-/-)* expressing *vps13d*

RNAi intestine cells all exhibited red and green structures 2 hours after pupariation, reflecting mitochondria that failed to be cleared by mitophagy. *park^{25}/park^{25} (-/-)* cells had almost exclusively filamentous structures (arrowheads), *park^{25}/+ (+/-)* expressing *vps13d* RNAi cells had almost exclusively enlarged punctate structures (white arrows), and *park^{25}/park^{25} (-/-)* expressing *vps13d* RNAi intestine cells had both filamentous and enlarged punctate structures. B) Quantification of the number of enlarged (> 1.0 μm^2) punctate structures in *park^{25}/+ (+/-)* heterozygous control (n=24), *park^{25}/park^{25} (-/-)* expressing *flp* (n=16)*, park^{25}/+ (+/-)* expressing *vps13d* RNAi (n=15), and *park^{25}/park^{25} (-/-)* expressing *vps13d* RNAi (n=15) intestine cells. C) *pink1^{B9}/pink1^{B9} (-/-)* loss-of-function mutant intestine cells (non-red) have reduced Park protein puncta (green) compared to neighboring *pink1^{B9}*/+ (+/-) heterozygous control cells (red) 2 hours after pupariation. D) Quantification of Park protein puncta in *pink1^{B9}/pink1^{B9} (-/-)* intestine cells (n=9) compared to neighboring *pink1^{B9}/+ (+/-)* control cells (n=15). E) *vps13d (MiMic)* loss-of-function mutant intestine cells (non-red) have similar levels of Park protein puncta (green) compared to neighboring heterozygous control (red) cells 2 hours after pupariation. F) Quantification of Park protein puncta in *vps13d (MiMic)* intestine cells (n=9) compared to heterozygous control cells (n=11). Scale bars in A), C), and E) represent 40μm with the exception of the enlarged images in A), which represent 10μm. Columns in B), D) and F) were compared using two-tailed student t-test without Welch's correlation with error bars representing SEM. Representative of 3 or more independent biological experiments.

To further explore the relationship between Pink1, Vps13D and Park, we analyzed Park protein puncta localization. While *pink1* loss-of-function (lacking RFP) and *park* loss-of-function mutant cells each had a significant decrease in Park protein puncta **(Figures 2-11C and D, 2-12B),** *vps13d (MiMic)* loss-of-function mutant cells (lacking RFP) had no impact on Park puncta **(Figure 2-11E and F).** Since both Park and Vps13D protein puncta are reduced in *pink1* mutant cells, these data are consistent with Pink1 regulation of mitophagy upstream of both Vps13D and Park.

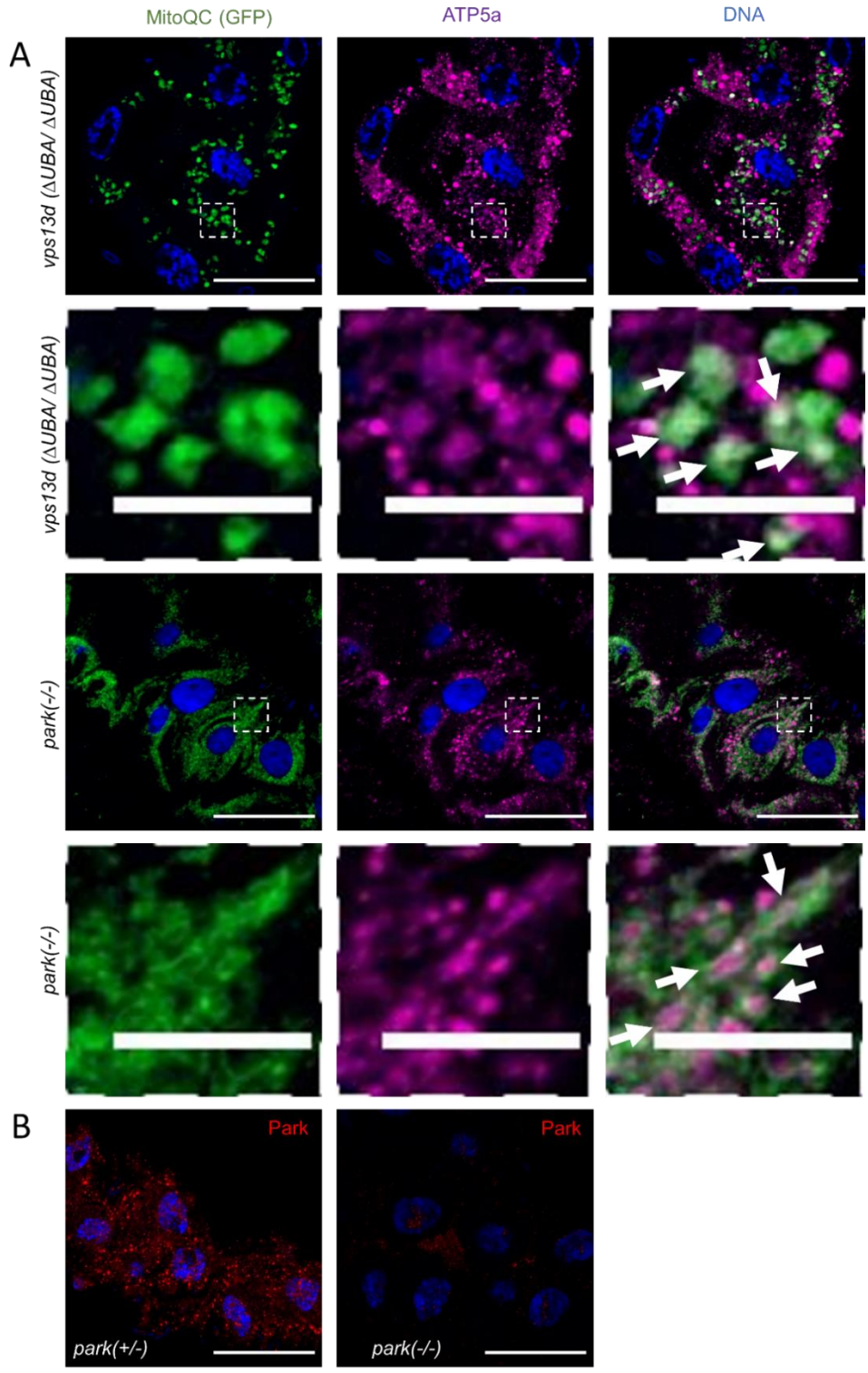

Figure 2-12: MitoQC represents retained mitochondria in *vps13d* and *park* mutants. (A) Localization of the MitoQC GFP component (green), representing mitochondria that have not reached the autolysosome, expressed in *vps13d*

(ΔUBA/ΔUBA) and *park^{25}/park^{25} (-/-)* mutant intestine cells 2 hours after pupariation was compared with ATP5a localization (purple). In both mutant intestines, ATP5a co-localized with non-autolysosomal MitoQC puncta (GFP). (B) *park^{25}/park^{25} (-/-)* loss-of-function mutant intestine cells 2 hours after pupariation probed with a Park specific antibody (Poole et al., 2010) had reduced Park puncta compared to heterozygote *park^{25}*/+ (+/-) control cells. Scale bars represent 40μm with the exception of enlarged images, which represent 10μm. Representative of 3 or more independent biological experiments.

DISCUSSION

Vps13D plays an important role in mitochondrial morphology and mitophagy during development (Anding et al., 2018). Mutations in Vps13D have also been identified as causes of familial neurological movement disorders (Seong et al., 2018; Gauthier et al., 2018). However, little is known about the mechanistic relationship between Vps13D and the regulation of autophagy, mitophagy and associated diseases. Here, we identify a role of Vps13D in the core autophagy machinery and Pink1-regulated mitophagy. Vps13D functions downstream of Pink1 to regulate ubiquitin and Atg8a localization around mitochondria during mitophagy. Thus, we define a new form of Pink1-regulated mitophagy that acts through Vps13D.

Ubiquitin and regulators of ubiquitin localization and conjugation are involved in the regulation of autophagy. In response to mitochondrial damage, Pink1 phosphorylates ubiquitin and Parkin, leading to expansion of ubiquitinated chains on the mitochondrial outer membrane (Ordureau et al., 2014; Koyano et al., 2014; Wauer et al., 2015). Autophagy receptors, including p62 and OPTN, are able to interact with ubiquitinated chains on mitochondria, and through physical interactions with Atg8a function as bridges between mitochondria and the autophagic machinery to facilitate

mitophagy (Lazarou et al., 2015; Kirkin and Rogov, 2019). We show that Vps13D interacts with ubiquitinated proteins and regulates ubiquitin localization in a context-dependent manner. In *vps13d* mutants, ubiquitin is able to localize to mitochondria. The accumulation of enlarged conjugated ubiquitin puncta around mitochondria suggests a problem with the processing of ubiquitin after localization to cargo. In addition, Pink1 is required for the localization of conjugated and phosphorylated ubiquitin around mitochondria in Vps13D mutants **(Figure 2-8A-D).** Thus, Vps13D seems to play a role that is downstream of Pink1 activity, but upstream of the clearance of ubiquitinated mitochondria.

Previous work suggests that the recruitment of the core autophagy machinery to mitochondria during mitophagy depends on ubiquitination of mitochondrial outer membrane proteins following Pink1 recruitment (Lazarou et al., 2015). By contrast, we observed that recruitment of Atg8a to mitochondria is independent of Pink1 function **(Figure 2-5D and G).** These findings indicate that Pink1-regulated ubiquitination and Atg8a recruitment can act in separate pathways. Vps13D appears to function downstream of these biochemical changes during mitophagy, as Vps13D mutant cells accumulate conjugated ubiquitin and Atg8a around the periphery of mitochondria **(Figure 2-2A, 2-4F, 2-5G and J).** Thus, Vps13D could act as a mediator between ubiquitinated cargo and the core autophagy machinery once localized to mitochondria.

It remains unclear how loss of Vps13D results in accumulation of Atg8a and conjugated ubiquitin around mitochondria. Studies of yeast *vps13*, which is highly conserved with *vps13d*, suggest that the *vps13* family of proteins serve as lipid

transporters between membranes at organelle contact sites (Lang et al., 2015). Furthermore, proteins in the Vps13 family all contain conserved Chorein_N domains with strong homology to the Chorein_N domain of Atg2 (Kumar et al., 2018), a core autophagy protein that acts as a tether between the endoplasmic reticulum (ER) and the forming autophagosome known as the phagophore. Atg2 facilitates the transfer of phospholipids to the expanding autophagosome membrane (Osawa and Noda, 2019). Replacement of the Atg2 Chorein_N domain with the Chorein_N domain of Vps13 resulted in the same autophagic activity as wild-type Atg2 (Osawa et al., 2019). However, the presence of this Chorein_N domain in all members of the Vps13 family is not sufficient to explain an autophagy-specific function, as Vps13D is the only member of the Vps13 family that is required for autophagy in flies. Rather, Vps13D is the only Vps13 family member with a ubiquitin binding UBA domain (Anding et al., 2018), and this UBA domain is required for clearance of mitochondria **(Figure 2-10A and C).** Although speculative, it is possible that Vps13D binds to ubiquitinated cargo, in this case Pink1-regulated ubiquitination of factors that are juxtaposed to mitochondria, and then this proximity could allow the transfer of lipids to the growing autophagosome membranes around mitochondrial cargoes. Without Vps13D, autophagosome components such as Atg8a simply accumulate in the vicinity of mitochondria.

Pink1-mediated phosphorylation of ubiquitin and Parkin leads to the rapid ubiquitination of outer mitochondrial membrane proteins, leading to local recruitment of the autophagy machinery (Ordureau et al., 2014; Koyano et al., 2014; Wauer et al., 2015). While phosphorylation of both ubiquitin and Parkin are required for Parkin-mediated mitophagy (Koyano et al., 2014), it is unknown if this is the sole purpose of

ubiquitin phosphorylation. The accumulation of phosphorylated ubiquitin around mitochondria in *vps13d* mutants is consistent with Pink1 regulating Vps13D-mediated mitophagy through phosphorylation of ubiquitin **(Figure 2-8C and D).** Structural studies of phosphorylated ubiquitin chains suggest that phosphorylated ubiquitin is more resistant to deubiquitinating enzymes, suggesting that Pink1 phosphorylation of ubiquitin chains on outer mitochondrial membrane proteins by Pink1 can enhance protein ubiquitination even without Parkin (Wauer et al., 2015). Thus, one possible model is that phosphorylation of outer mitochondrial membrane ubiquitin chains by Pink1 stabilizes these ubiquitin chains. Vps13D then interacts with these chains and facilitates further processing through the autophagic machinery. Without Vps13D, these conjugated ubiquitin chains accumulate on the outer mitochondrial membrane, consistent with the conjugated ubiquitin phenotype observed in Vps13D mutant cells **(Figure 2-4F and G, 2-8A and B).** Another potential Pink1 substrate could be Vps13D itself, as phosphorylation of Vps13D was significantly decreased in a *pink1* mutant mouse model for Parkinson's disease (Auburger et al., 2019).

Pink1 can recruit proteins to mitochondria in a Parkin-independent manner (Lazarou et al., 2015). Furthermore, Pink1 physically interacts with and recruits Atg6 to mitochondria and endoplasmic reticulum (ER) membrane contacts to mediate mitophagy (Michiorri et al., 2010). Significantly, this recruitment of Atg6 is independent of Parkin (Gelmetti et al., 2017). In addition, proteomic studies have suggested that Vps13D interacts with proteins present at the mitochondria and ER interface (Hung et al., 2017; Antonicka et al., 2020). Thus, Vps13D puncta could reflect recruitment to the mitochondria and ER interface that is driven by Pink1 and Atg6.

Mutations in *pink1* and *vps13d* are both associated with neurological disease and abnormal mitochondrial morphology. These diseases also share some symptoms, such as tremors and dystonia (Seong et al., 2018; Gauthier et al., 2018; Armstrong and Okun, 2020). Fibroblasts from patients who are suffering from these symptoms also have autophagy deficiencies in response to mitochondrial depolarization, consistent with a role of Vps13D in Pink1-mediated mitophagy **(Figure 2-8G and H).** These findings suggest that there may be a link between the pathology of Vps13D and Pink1 related diseases. However, thorough comparisons are difficult since only 19 patients from 12 families with confirmed *vps13d*-associated neurological symptoms have been characterized (Seong et al., 2018; Gauthier et al., 2018). A more thorough characterization of *vps13d* patient symptoms and clinical findings will be required to fully understand the clinical implications of the relationship between Pink1 and VPS13D.

MATERIALS AND METHODS

Drosophila strains

Drosophila melanogaster strains used in this study are listed in the key resources table **(Table 2-1)**. w^{1118} were used as controls. All flies were raised on standard cornmeal/molasses/agar media at 25ºC.

Cell Lines

All cells used in this study are listed in the key resources table. Cells were cultured at 37°C in 5% CO_2 in DMEM supplemented with 5% FBS and Penicillin/Streptomycin, as previously described (Anding et al., 2018).

atg16^{1} and *vps13d-3xFLAG* design

The *atg16*^{1} loss-of-function mutant was designed using TALEN (Katsuyama et al., 2013). The *vps13d-3xFLAG* strain was edited using CRISPR/Cas9 (Gratz et al., 2014). All germline injections were done by the UMass Medical School CRISPR Core. For *atg16*^{1}, the following template DNA sequence was used (5' to 3'): TCGCCGATGAGGCCGCCAACGAACTGGGCGGGACTGGAGTTGCGCTGCAAGGA to produce a 5 base pair deletion of CCCAG (2870-2874 in the genomic region), producing frameshift in the 244th amino acid of Atg16 and affecting all isoforms of Atg16. A single female fly containing the insertion was collected, and validated by DNA sequencing. For vps13d-3xflag, the following sgRNA targeting sequence was used (5' to 3'): TTTATAAAATGCAATAGGT. A 2kb region flanking the C terminal of genomic *vps13d* was amplified by PCR and site-directed mutagenesis was used to insert the 3xflag sequence in frame immediately before the stop codon. This fragment was inserted into a TOPO vector via TOPO cloning and sequenced to ensure no additional mutations were present and was used to tag the C terminal of vps13d with 3xflag. A single female fly containing the insertion was collected and validated by DNA sequencing.

Induction of mosaic RNAi and mutant cell clones

Mosaic fluorescent-negative mutant cell clones were induced as described (Anding et al., 2018). To induce mosaic *pink1^{B9}, atg1^{3}, atg6 (Δ), atg16^{1}, and vps13d(MiMic)* loss-of-function mutant cell clones, we used the *hsflp, FRT19A, mRFP; hsflp;;FRT2A, Ubi-nlsRFP, hsflp;;FRT82B, Ubi-nlsGFP, and hsflp;;FRT80B, ubi-nlsGFP* flies and crossed them with the mutant alleles with the respective FRT site. 8-hour eggs lays were heat shocked for 90 minutes at 37°C. Mosaic analyses were conducted only where indicated, otherwise, whole mutant animal or midgut specific RNAi was used. In experiments where entire *pink1^{B9}* mutant animals was used, only males were selected and compared to ensure no sex-specific differences. Unless otherwise stated, in all experiments where mutant or RNAi-expressing phenotypes were compared with other single or double mutant cell phenotypes, either a heterozygous mutant genetic background or background expressing a non-target UAS element was used as a control.

Dissection and immuno-labeling of Drosophila larval intestines and Cultured Cells

White prepupae were collected and allowed to develop on wet filter paper for 2 hours prior to dissection. Intestines were immuno-stained as previously described with modifications (Anding et al., 2018). Intestines were removed in cold PBS before being placed in 4% paraformaldehyde solution for fixation at 4°C overnight. Where applicable, RNAi was expressed throughout the entire intestine using the Myo31DFNP0001 driver. For Atg8a/GABARAP staining, samples were placed in 1:1 4% paraformaldehyde:

heptanes for 20 minutes before being incubated in methanol for 1 minute at room temperature. Intestines were washed twice with PBS and then twice with 0.1% PBSTx before blocking in 5% normal goat serum for 90 minutes and incubation with primary antibody in 0.1% PBSTx overnight. Intestines were then stained with secondary antibody for 3 hours before nuclei staining and mounting. For cell culture, cells were washed and fixed in pre-warmed 4% paraformaldehyde for 30 minutes at room temperature, then permeabilized with 10µg/mL digitonin for 15 minutes, then blocked in 5% normal goat serum in PBS for 1 hour before incubation overnight with primary antibody at 4°C. Cells were then washed, incubated with secondary antibody for 1 hour, and mounted in vectashield with DAPI. The following primary antibodies were used: rabbit anti-ref(2)p (1:1000, from Gabor Juhasz), mouse anti-ATP synthase complex V (1:1000, Abcam #ab14748), rabbit anti-ubiquitin (1:1000, Abcam #ab19247), mouse anti-ubiquitin-FK2 (1:100, Enzo Life Sciences, #-PW8810), rabbit anti-Atg8a/GABARAP (1:100, Cell Signaling #13733), rabbit anti-Park (1:100, from Alex Whitworth), rabbit anti-pSer65 Ubiquitin (1:100, Millipore Sigma # ABS1513-I), mouse anti-Vps13D (1:50) (Anding et al., 2018), rabbit anti-TOMM20 (1:200, Abcam # ab78547), and mouse anti-p62/SQSTM1 (1:100, Santa Cruz #28359). The following secondary antibodies were used: anti-mouse AlexaFluor 647 (Invitrogen #A-21235), anti-rabbit Alexafluor 546 (Invitrogen # A-11035), anti-rabbit Oregon Green 488 (Molecular Probes, # O-6381), and anti-mouse AlexaFluor 546 (Invitrogen #A-11030). Nuclei were stained with Hoescht (Invitrogen) and samples were mounted with Vectashield (Vector Lab). Images were acquired using a Zeiss LSM 700 confocal microscope.

Transmission electron microscopy

Transmission electron microscopy (TEM) was conducted as previously described with modifications (Anding et al., 2018). Intestines were dissected in PBS (GIBCO) 2 hours after pupariation and fixed in a solution of 2.5% glutaraldehyde and 2% paraformaldehyde in 0.1M sodium cacodylate buffer, pH 7.4 (Electron Microscopy Sciences) for 1 hour at room temperature followed by overnight fixation at 4°C in fresh fix. Intestines were washed in 0.1M sodium cacodylate buffer, pH 7.4, post-fixed in 1% osmium tetroxide in distilled water for 1 hour at room temperature and washed in distilled water. Preparations were stained en bloc in 1% aqueous uranyl acetate overnight at 4°C in the dark, washed in distilled water, dehydrated through a graded ethanol series, treated with propylene oxide and infiltrated in SPI-pon/Araldite for embedding. Ultrathin sections were cut on a Leica UC7 microtome. Sections were stained with uranyl acetate and lead citrate and examined on a Phillips CM10 TEM. Images were taken down the length of the anterior region of the midgut to ensure an unbiased approach. For each genotype, at least 3 intestines were embedded and sectioned for analyses and quantification. We reviewed all images and selected representative images for analyses.

Western blot and immunoprecipitation

Tissue was lysed in 1X Laemli sample buffer diluted in RIPA lysis buffer (10mM Tris-Cl PH 8.0, 1mM EDTA PH 8.0, 0.5mM EGTA, 2.4mM Sodium Deoxycholate 140mM Sodium Chloride) at a ratio of 10µL lysis buffer per intestine and 30µL per whole

prepupa. Samples were homogenized in solution using a plastic pestle for 30 seconds before being boiled at 99°C for 6 minutes. Samples were run on 7.5% polyacrylamide gel, transferred onto 0.45µm PVDF membranes (Millipore Sigma), and probed with antibodies using standard protocols. Cells were cultured in 24 well plates and lysed at 80-90% confluency using the same 1X Laemli sample buffer by removing media, washing with PBS, and incubating with 150µL lysis buffer for 15 minutes with rotation. Primary antibodies used were mouse anti-FLAG (1:1000, Millipore Sigma), anti-ubiquitin-P4D1 HRP (Santa Cruz, sc-8017 HRP), rabbit anti-Atg8a/GABARAP (1:1000, Cell Signaling #13733), mouse anti-Actin (1:1000, Proteintech), mouse anti-ATP5a (1:1000, Abcam).

For immunoprecipitations, 2-hour-old prepupae were lysed in RIPA lysis buffer supplemented with 1mM NEM, 1mM PMSF and Halt Protease Inhibitor Cocktail (Thermo Fisher) at a ratio of 16 prepupae per 250µL lysis buffer. Prepupae were crushed with a plastic pestle for 30 seconds and incubated on ice for 30 minutes before being centrifuged at 4°C at 13,000rpm for 10 minutes. Supernatant was filtered through 0.45µm Cellulose Acetate filters (Millipore Sigma). 30µL of filtered supernatant was diluted in 10µL of 4x Laemli sample buffer (Biorad), boiled for 6 minutes at 99°C and used as input. 200µL of filtered supernatant (approximately 1mg protein) was used for immunoprecipitation. 40µL of anti-FLAG M2 magnetic bead slurry (Millipore Sigma) warmed to room temperature was washed twice with RIPA buffer before incubation with filtered supernatant for 2 hours at 4°C on a rotator. For all control lysates, 1µg of 3xFLAG peptide was added to account for nonspecific binding due to the 3xFLAG epitope. Following incubation, supernatant was discarded and beads were washed 4

times with 1mL 0.1% PBST. Beads were eluted with 20µL 1X Laemli sample buffer diluted in RIPA lysis buffer and boiled for 6 minutes at 99°C. 20µL of input and eluate was run on 7.5% polyacrylamide gel for western blot analysis.

Quantification and Statistical Analyses

All quantification of cell size and puncta in immunofluorescence images were conducted using ImageJ, as described previously (Anding et al. 2018). Sample sizes (n) in immunofluorescence image quantifications represent number of cells. For quantification of puncta number, size, and number of puncta encircled, images were first threshholded to the brightest 2.5% of puncta with the exception of conjugated ubiquitin (FK2) puncta, which was thresholded to the brightest 5.0% puncta due to more dull puncta in control cells.

TEM analyses of mitochondria area was manually calculated by individually analyzing mitochondria using ImageJ. Regions for analyses were randomly selected from sections for each sample. For each analysis, at least 100 mitochondria from at least 20 sections from 3 individual animals were used for quantification. Sample sizes (n) in TEM quantifications represent number of mitochondria.

All experiments are representative of 3 independent replicates. No statistical methods were used to predetermine sample sizes. Preliminary experiments were conducted to achieve similar sample sizes as previous published studies using our model systems. Animals were not excluded for statistical analyses. Researchers were

not blinded. Unless otherwise stated, p values were calculated using the two-tailed student t-test without Welch's correlation. p values greater than 0.05 were considered non-significant (n.s.). All bars are means and error bars are SEM unless otherwise stated.

Table 2-1: Key Resources Table

REAGENT or RESOURCE	SOURCE	IDENTIFIER
Antibodies		
Vps13D	Eric Baehrecke	(Anding et al,. 2018)
ref(2)p	Gabor Juhasz	(Pircs et al., 2012)
ATP synthase complex V	Abcam	Ab14748
Atg8a/GABARAP	Cell Signaling	13733
FLAG	Millipore Sigma	F1804
Actin	Proteintech	60008-1-Ig
Park	Alex Whitworth	(Ziviani et al., 2010)
Ubiquitin	Abcam	ab19247
Conjugated ubiquitin (FK2)	Enzo Life Sciences	PW8810
Anti-phospho-Ubiquitin (Ser65)	Millipore Sigma	ABS1513-I
Ubiquitin (P4D1)	Santa Cruz	sc-8017 HRP
TOMM20	Abcam	ab78547
SQSTM1/p62	Santa Cruz Biotechnology	sc-28359
anti-mouse AlexaFluor 647	Invitrogen	A-21235
anti-rabbit Alexafluor 546	Invitrogen	A-11035
anti-chicken AlexaFluor 488	Invitrogen	A-11039
anti-mouse Alexa Fluor 488	Invitrogen	A-11029
Oregon Green 488 goat anti-rabbit	Molecular Probes	O-6381
anti-mouse AlexaFluor 546	Invitrogen	A-11030
Bacterial and Virus Strains		
E. coli/One Shot TOP10	Invitrogen	C404010
E. coli/ C25H3.11/vps-13d	Hong Zhang	N/A
E. coli/ HT115	Hong Zhang	N/A
Biological Samples		
Chemicals, Peptides, and Recombinant Proteins		
PBS	GIBCO	70011
25% Glutaraldehyde	Electron Microscopy Sciences	16220
Sodium cacodylate	Electron Microscopy Sciences	11650
osmium tetroxide	SPI	2601
propylene oxide	SPI	75-56-9
SPI-pon/Araldite 6005 epoxy embedding kit	SPI	02635-AB

paraformaldehyde	Electron Microscopy Sciences	15710
Triton x-100	Sigma	T8787
Digitonin	Sigma	D141
Vectashield	Vector Laboratories	H-1200
Tris-HCl	Sigma	T3253
NaCl	Fisher	BP358-212
Goat serum	Sigma	G9023
EDTA	Quality Biological	351-027-101
7.5% Mini-PROTEAN® TGX™ Precast Protein Gels, 10-well, 30 µl	Biorad	4561023
12% Mini-PROTEAN® TGX™ Precast Protein Gels, 10-well, 30 µl	Biorad	4561043
HiMark™ Pre-stained Protein Standard	Invitrogen	LC5699
Precision Plus Protein™ Dual Color Standards	Biorad	1610374
4x Laemmli Sample Buffer	Biorad	1610747
Glycine (certified)	Fisher	BP381-1
PMSF (phenylmethane sulfonyl flouride) (PMSF)	Sigma	329-98-6
N-Ethylmaleimide (NEM)	Sigma	E3876
Thermo Scientific™ Halt™ Protease Inhibitor Cocktail	Thermo Scientific	PI78430
EGTA	Sigma	324626-25GM
Sodium Deoxycholate	Sigma	D6750-100G
0.45µm PVDF Membranes	Millipore Sigma	IPVH00010
0.45µm Cellulose Acetate filters	Millipore Sigma	CLS8163-100EA
anti-FLAG M2 magnetic bead	Millipore Sigma	M8823-1ML
Tween-20	Fisher	BP337-100
3X FLAG® Peptide	Sigma Aldrich	F4799-4MG
Critical Commercial Assays		
Deposited Data		
Experimental Models: Cell Lines		
Patient Fibroblasts (G1190D/Q1106*): UM1.2	Margit Burmeister	(Seong et al., 2018)
Heterozygote Fibroblasts (Q1106*/+): UM1.17	Margit Burmeister	(Seong et al., 2018)
Experimental Models: Organisms/Strains		
Drosophila Melanogaster/*w*^{1118}	Bloomington *Drosophila* stock center	5905
Drosophila Melanogaster/ w1118; P{GD10464}v41792	VDRC	v41792
Drosophila Melanogaster/ y^1 sc* v^1 sev21; P{TRiP.HMS01784}attP2	Bloomington *Drosophila* stock center	38320
Drosophila Melanogaster/ y^1 v^1; P{TRiP.JF01355}attP2	Bloomington *Drosophila* stock center	31603
Drosophila Melanogaster/ y^1 sc* v^1 sev^{21}; P{TRiP.HMS05713}attP40	Bloomington *Drosophila* stock center	67852

Drosophila Melanogaster/ y^1 w*; Mi{MIC}Vps13DMI11101	Bloomington *Drosophila* stock center	56282
Drosophila Melanogaster/w*; P{w[+mW.hs]=FRT(w[hs])}2A	Bloomington *Drosophila* stock center	1997
Drosophila Melanogaster /y^1 w1118 P{neoFRT}19A	Bloomington *Drosophila* stock center	1744
Drosophila Melanogaster /P{hsFLP}12, y1 w*; snaSco/CyO	Bloomington *Drosophila* stock center	1929
Drosophila Melanogaster/ P{Ubi-mRFP.nls}1, w*, P{hsFLP}12 P{neoFRT}19A	Bloomington *Drosophila* stock center	31418
Drosophila Melanogaster/y1 w*; P{neoFRT}82B Sb1/TM6	Bloomington *Drosophila* stock center	2051
Drosophila Melanogaster/w*; P{neoFRT}82B P{Ubi-GFP.D}83	Bloomington *Drosophila* stock center	5188
Drosophila Melanogaster/w*; *; P{ry[+t7.2]=neoFRT}80B, *atg1*^{3}	Toshifumi Tomoda	(Toda et al., 2008)
Drosophila Melanogaster /w^{1118}; P{Ubi-mRFP.nls}3L P{neoFRT}80B	Bloomington *Drosophila* stock center	30852
Drosophila Melanogaster/w*; P{w[+mC]=UAS-FLP.D}JD2	Bloomington *Drosophila* stock center	4540
Drosophila Melanogaster/w*;; P{neoFRT}82B, *atg6(*Δ*)*	Eric Baehrecke	(Shravage et al., 2013)
Drosophila Melanogaster/y^1 w* Mi{MIC}Atg8aMI13726/Binsinscy	Bloomington *Drosophila* stock center	59357
Drosophila Melanogaster/w*; P{GawB}Myo31DFNP0001 / CyO, P{UAS-lacZ.UW14}UW14	*Drosophila* Genetic Resource Center	112001
Drosophila Melanogaster/ P{UAS-mito-QC}attP16	Alexander J. Whitworth	(Lee et al., 2018)
Drosophila Melanogaster/ *vps13d (ΔUBA)/TM6B*	Eric Baehrcke	(Anding et al., 2018)
Drosophila Melanogaster/ w* Pink1B9/FM7i, P{ActGFP}JMR3	Bloomington *Drosophila* stock center	(Park et al., 2006), 34749
Drosophila Melanogaster/w*;;*park*^{25}*/TM3 Sb*^{1}	Leo Pallank	(Greene et al, 2003)
Drosophila Melanogaster/*w*;;atg16*^{1}	This paper	N/A
Drosophila Melanogaster/*w*;;vps13d-3xFLAG*	This paper	N/A
Oligonucleotides (5’ to 3’)		
Primers to check *atg16*^{1}: CGCGTGCGACTCGTTCTCGT CGGACCATTTAGACGAATCT	Integrated DNA Technologies	N/A

Primers to screen *atg16*[1]: TTGCAGCGCAACTCCAGTCCCGCC TTGACTTTGCGATCAGCGCCACCG	Integrated DNA Technologies	N/A
Oligonucleotide to design *atg16*[1]*: TCGCCGATGAGGCCGCCAACGAACTGGGCGGGAC TGGAGTTGCGCTGCAAGGA*	Integrated DNA Technologies	N/A
Primer used to amplify 5' of genomic fragment used to design donor fragment for *vps13d-3xflag*: gagtttggtgaaaaatgttacgc	Integrated DNA Technologies	N/A
Primer used to amplify 3' of genomic fragment used to design donor fragment for *vps13d-3xflag*: ctactggcaaaggctcgagag	Integrated DNA Technologies	N/A
5' primer used to clone *3xflag* into donor fragment: tcatgacatcgattacaaggatgacgatgacaagtaaaatgcaataggtcg gttcg	Integrated DNA Technologies	N/A
3' primer used to clone *3xflag* into donor fragment: tctttataatcaccgtcatggtctttgtagtccattaaaacggcatgttcacgttc	Integrated DNA Technologies	N/A
5' primer used to screen and sequence *3xflag* insertion: atgcggctgcaattttgg	Integrated DNA Technologies	N/A
3' primer used to screen and sequence *3xflag* insertion: gattgatttagataagctgctcg	Integrated DNA Technologies	N/A
Recombinant DNA		
Plasmid: U6droBsagRNA	Drosophila Genomics Resource Center	1341
Plasmid: pCR™2.1-TOPO® vector	Thermo Fisher Scientific	K450002
Software and Algorithms		
ImageJ	NIH	https://imagej.nih.gov/ij/
Zen Black	Zeiss	N/A
Prism	Graphpad Software, Inc.	https://www.graphpad.com/scientific-software/prism/
Other		

ACKNOWLEDGEMENTS

We thank the Baehrecke laboratory, M. Burmeister, G. Juhasz, L. Pallanck, T. Tomoda, A.J. Whitworth, the Vienna Drosophila Resource Center, the Bloomington Stock Center, the Kyoto Drosophila Genetic Resource Center, and the Electron Microscopy Core

Facility at UMass Medical School for advice, flies, antibodies, cell lines and technical support. This work was supported by R35GM131689 to E.H.B. and F30CA239374 to J.L.S.

AUTHOR CONTRIBUTIONS

J.L.S. and E.H.B. designed experiments, J.L.S. and T.M.F. performed experiments, R.W. provided resources, J.L.S. and E.H.B. wrote the manuscript and all authors commented on it.

DECLARATION OF INTERESTS

The authors declare no competing interests.

Chapter III

A conserved Vps13D pathway

regulates organelle contact in development and disease

James L. Shen[1], Tina M. Fortier[1],Yan G. Zhao[1], Ruoxi Wang[1], Margit Burmeister[2], and Eric H. Baehrecke[1]

[1] Department of Molecular, Cell and Cancer Biology, University of Massachusetts Medical School, Worcester, MA 01605 USA

[2] Michigan Neuroscience Institute and Dept of Computational Medicine & Bioinformatics, University of Michigan, Ann Arbor, MI 48109, USA

Keywords: Vps13D, Vmp1, autophagy, mitochondria, *Drosophila*, membrane contact

ABSTRACT

Mutations in *Vps13D* cause defects in autophagy, clearance of mitochondria and human movement disorders. Here we discover that Vps13D functions in a pathway downstream of Vmp1 and upstream of Marf/Mfn2. Like *vps13d*, *vmp1* mutant cells exhibit defects in autophagy, mitochondrial size and clearance. Through the relationship between *vmp1* and *vps13d*, we reveal a novel role for Vps13D in the regulation of mitochondria and endoplasmic reticulum (ER) contact. Significantly, the function of Vps13D in mitochondria and ER contact is conserved between fly and human cells, including fibroblasts derived from patients suffering from *VPS13D* mutation-associated neurological symptoms. *vps13d* mutants have increased levels of Marf/MFN2, a regulator of mitochondrial fusion. Importantly, loss of *marf/MFN2* suppresses *vps13d* mutant phenotypes, including mitochondria and ER contact. These findings indicate that Vps13d functions at a regulatory point between mitochondria and ER contact, mitochondrial fusion and autophagy, and help to explain how Vps13D contributes to disease.

INTRODUCTION

Autophagy, the lysosome-dependent clearance of intracellular contents, plays important roles in organism development and health. The failure to remove mitochondria by autophagy, or mitophagy, results in defects in cellular homeostasis and health, and contributes to multiple diseases (Palikaras et al., 2018). For example, mutations in genes responsible for mitophagy manifest as inheritable forms of Parkinson's disease and Alzheimer's disease (Wang et al., 2019). As a result, it is becoming clear that understanding the mechanisms that regulate mitophagy under different cellular contexts is crucial to our understanding of biology and health.

The mechanisms underlying mitophagy in animals have been defined through studies of derived cell lines (Narendra et al., 2010). Although these elegant studies of PINK1- and Parkin-dependent mitophagy have significantly advanced our understanding of this important process, studies in animals indicate that the clearance of mitochondria in cells and tissues under physiological conditions do not always utilize the same regulatory pathways (McWilliams et al., 2018; Lee et al., 2018). During *Drosophila* development, the larval intestine undergoes an autophagy driven remodeling process where cells reduce in size and mitochondria are cleared by mitophagy (Chang et al., 2013).This system allowed us to identify *vps13d* and other genes as regulators of autophagy under physiological conditions (Chang et al., 2013; Anding et al., 2018). Importantly, *vps13d* is an essential and conserved gene that regulates mitochondrial clearance, mitochondrial morphology, and has been implicated in human movement disorders (Anding et al., 2018; Seong et al., 2018; Gauthier et al., 2018).

Vacuolar protein sorting 13 (*vps13*) was discovered in yeast, and animals possess four evolutionarily conserved Vps13 family members *Vps13A-D (*Brickner and Fuller, 1997; Velayos-Baeza et al., 2004). Yeast VPS13, as well as mammalian Vps13A and C, have been implicated in the regulation of inter-organelle contact and lipid transport (Kumar et al., 2018; John Peter et al., 2017). However, these studies fail to address if loss of these human paralogs either repress or enhance membrane contacts. Furthermore, no study has linked VPS13D specifically to regulation of membrane contacts.

Members of the Vps13 family possess unique functional requirements. In contrast to *VPS13A-C, VPS13D* is one of the most vital genes for survival in human cell lines (Wang et al., 2015; Blomen et al., 2015), and is essential for *Drosophila* development (Anding et al., 2018). Vps13D is the only Vps13 family member that contains a ubiquitin binding domain, which is required for proper mitochondrial morphology and clearance. Vps13D is also the only Vps13 family member in flies that is required for autophagy (Anding et al., 2018). Significantly, mutations in *VPS13D* have been associated with multiple diseases, including altered septic shock mortality and a unique group of familial neurological movement disorders involving ataxia, chorea and dystonia (Seong et al., 2018; Gauthier et al., 2018; Nakada et al., 2015; Bousquet et al., 2016; Andersen et al., 2010). Despite these findings, it remains unclear how VPS13D regulates autophagy, mitochondrial morphology and contributes to human diseases.

Here we investigate the relationship between *vps13d* and genes that regulate autophagy and mitochondrial morphology. We discover that Vps13D acts downstream of Vmp1/EPG-3, a regulator of autophagy and mitochondria and endoplasmic reticulum

(ER) contact. Like Vps13D, loss of Vmp1 disrupts autophagy and mitochondrial morphology. Through this relationship, we identify a novel role for Vps13D as a regulator of mitochondria and ER contact in *Drosophila* and human cell lines, including fibroblasts derived from patients symptomatic for *VPS13D* associated neurodegenerative disease. Importantly, we also discover that Vps13D interacts with the regulator of mitochondrial fusion Marf (Mitofusins in mammals), and that loss of either *marf* in flies or *MFN2* in patient-derived cell lines suppresses *vps13d* mutant phenotypes. Our findings establish Vmp1, Vps13D and Marf/MFN2 as important factors in a pathway that regulates inter-organelle contacts in autophagy and mitochondrial morphology, and help explain the role of *vps13d* in disease.

RESULTS

Vmp1 regulates autophagy, mitophagy and mitochondrial morphology

The essentiality **(Figure 3-1)** and unique role of Vps13D in autophagy among Vps13 family members prompted us to consider if other factors implicated in both autophagy and inter-organelle contact may possess phenotypes that are similar to *vps13d*.

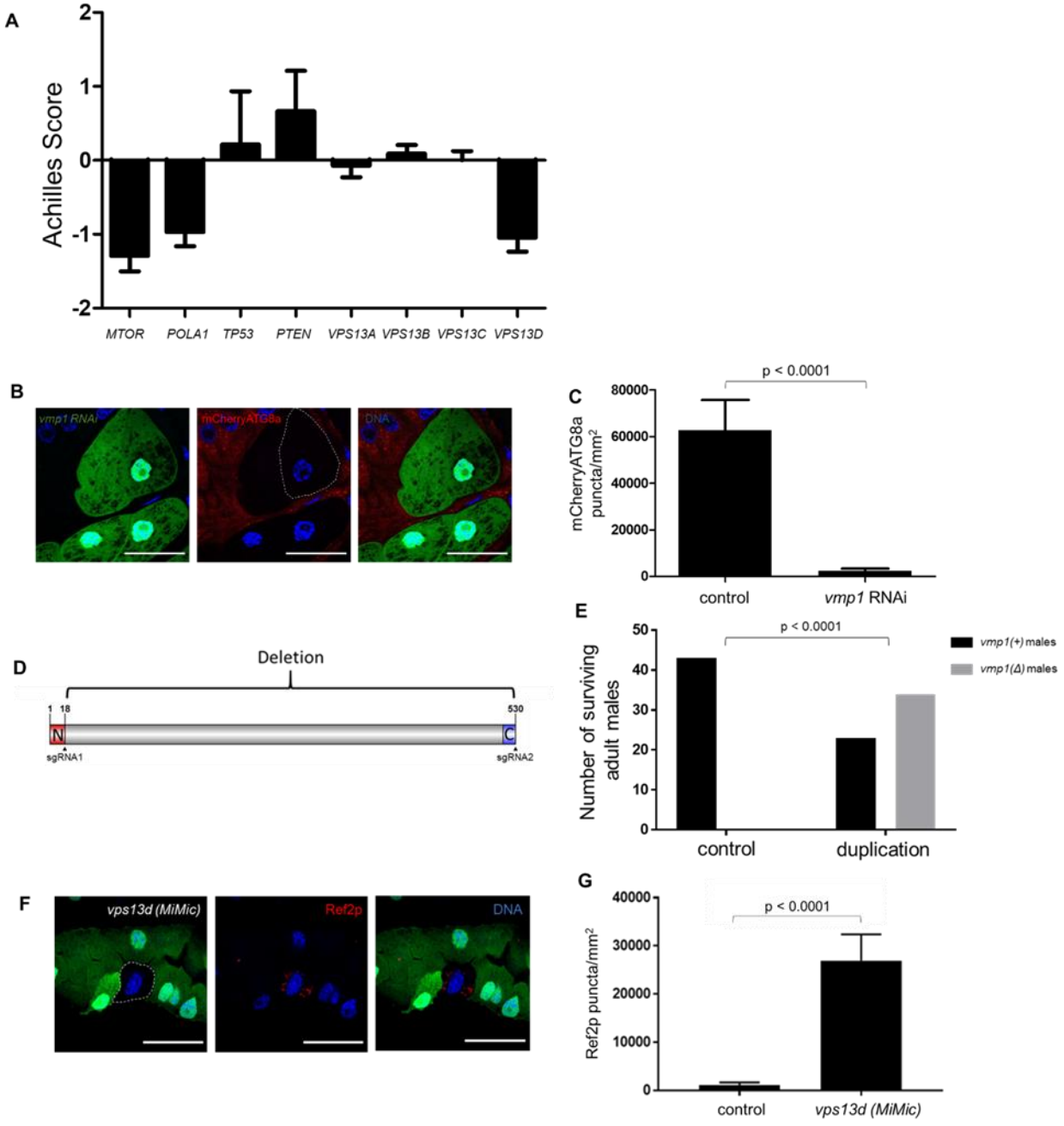

Figure 3-1: *VPS13D* is essential in human cell lines and *vmp1* and *vps13d* mutants share autophagy deficiencies in developing *Drosophila* intestines. (A) Genetic Dependency Data from the CRISPR Cancer Dependency Map[42,43] was compiled for essential genes, tumor suppressors, *VPS13D,* and other Vps13 family members. As expected, essential genes *mechanistic target of rapamycin* (*MTOR)* and *DNA polymerase alpha catalytic subunit (POLA1)* received Achilles Scores near -1, suggesting strong dependency for survival in cultured cell lines. Tumor suppressors *tumor protein p53* (*TP53)* and *phosphatase and tensin homolog (PTEN),* which may

result in enhanced cell survival in cultured cell lines when lost, received positive scores indicating non-essentiality. While *vacuolar protein sorting 13A-C* (*VPS13A-C)* scores indicate that they are not required for survival, *vacuolar protein sorting 13 d (VPS13D)* is similar to other essential genes and is required for survival. (B) *vmp1* RNAi (VDRC line #46667) intestine cells (green, white dotted line) exhibit decreased mCherryATG8a puncta formation (red) compared to neighboring control cells (non-green) 2 hours after pupation. (C) Quantification of mCherryATG8a puncta in *vmp1* (n=6) RNAi (#46667)-expressing and control (n=11) intestine cells 2 hours after pupation. (D) Design of the *Drosophila vmp1(Δ)* mutant using sgRNA1 and sgRNA2. Numbers represent amino acid sequence. (E) Number of surviving *vmp1(Δ)* loss of function mutant and *vmp1(+)* control adult male flies with or without a duplication of the genomic region that contains *vmp1*. Results compiled from 100 eclosed male flies. p value derived from the Fisher Exact Test. (F) *vps13d (MiMic)* loss of function intestine cells (non-green) were stained with antibody against Ref2p (red) and compared with neighboring *vps13d (MiMic)/+* control cells. (G) Quantification of Ref2p puncta in *vps13d (MiMic)* loss of function intestine cells (n=7) compared to *vps13d (MiMic)*/+ control intestine cells (n=12). Scale bars in (B) and (F) represent 40μm. Error bars in (A) (C) and (G) represent SEM. Representative of 3 or more independent biological experiments.

Vmp1 (EPG-3 in *C. elegans*) is a conserved regulator of autophagy in worms and mammals, and also influences inter-organelle contacts (Tian et al., 2010; Zhao et al., 2017). To test if *Drosophila* Vmp1 (also known as Tango5) has a similar function to Vps13D, we analyzed the function of *vmp1* in larval intestine cells where *vps13d* functions in autophagy, cell size reduction, mitochondrial clearance and maintenance of mitochondrial size. Like *vps13d* mutant cells (Anding et al., 2018), cells with reduced Vmp1 function that express *vmp1* RNAi and green fluorescent protein (GFP) did not accumulate mCherryAtg8a autophagy reporter puncta and were unable to reduce in size, unlike neighboring GFP-negative control cells **(Figure 3-2A and B).** This was the same phenotype seen in *vps13d* RNAi-expressing and loss of function intestine cells (Anding et al., 2018). Similar results were obtained using a distinct RNAi targeting a different *vmp1* sequence **(Figure 3-1B and C).**

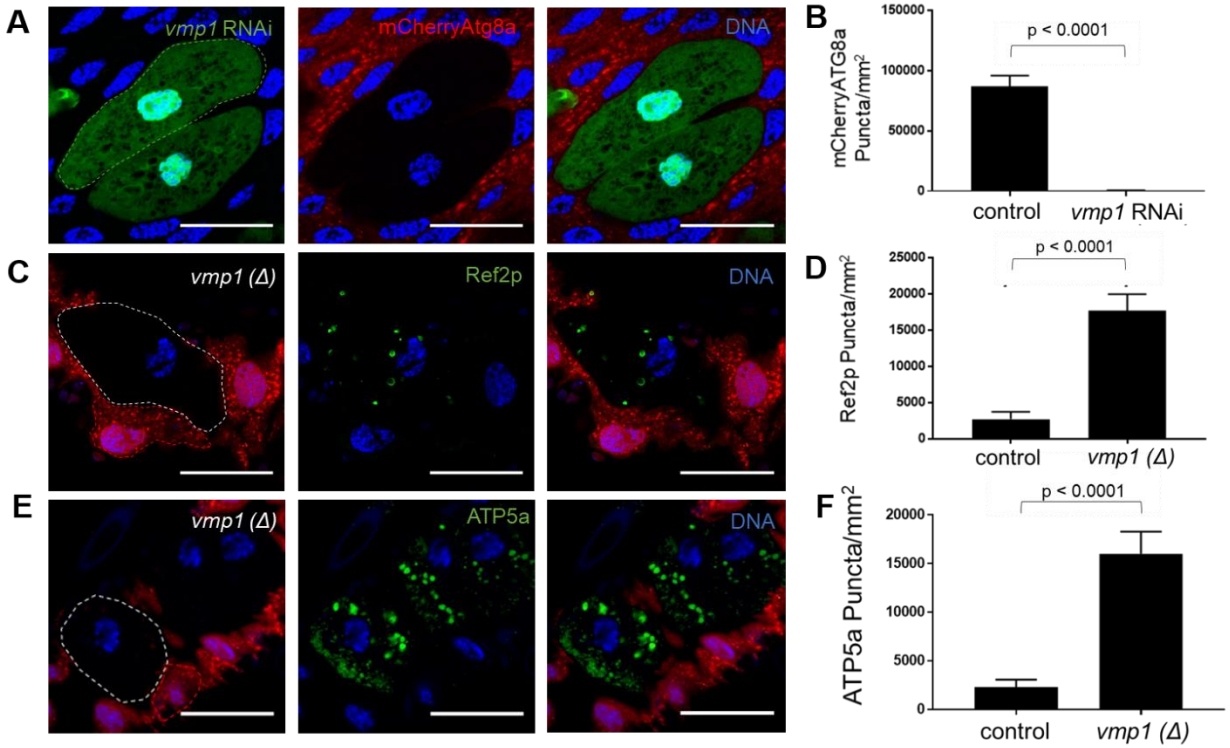

Figure 3-2: Vmp1 is required for autophagy in *Drosophila* intestines. (A) *vmp1* RNAi intestine cells (green) 2 hours after pupariation exhibit decreased mCherryAtg8a puncta formation (red) compared to neighboring control cells (non-green). (B) Quantification of mCherryAtg8a puncta in *vmp1* RNAi cells (n=8) compared to control cells (n=16). (C) *vmp1(Δ)* mutant cells (non-red, white dotted line) possess increased Ref2p/p62 puncta (green) compared to neighboring control cells (red) in intestines 2 hours after pupariation. (D) Quantification of Ref2p puncta in *vmp1(Δ)* mutant (n=9) and control cells (n=8) 2 hours after pupariation. (E) *vmp1(Δ)* loss-of-function mutant cells (non-red, white dotted line) possess elevated mitochondrial ATP5a puncta (green) compared to neighboring control cells (red) in intestines 2 hours after pupariation. (F) Quantification of ATP5a puncta in *vmp1(Δ)* mutant (n=6) and control cells (n=16) 2 hours after pupariation. Scales bars in (A), (C) and (E) represent 40 μm. Error bars in (B), (D) and (F) are SEM. Representative of 3 or more independent biological experiments.

We next used CRISPR/CAS9 gene editing to create a loss-of-function *vmp1* mutant *Drosophila* named *vmp1(Δ)* **(Figure 3-1D).** Homozygous *vmp1(Δ)* mutant animals die during development with a small number of animals surviving until the 3rd

instar larval stage. Importantly, an X chromosome duplication containing the *vmp1* open reading frame complemented the *vmp1(Δ)* lethal phenotype **(Figure 3-1E).**

We analyzed *vmp1(Δ)* mutant cells for phenotypes that are similar to homozygous *vps13d* mutant intestine cells. Consistent with *vmp1* RNAi knockdown, intestines with homozygous *vmp1(Δ)* mutant cells lacking red fluorescent protein (RFP) accumulated the autophagic cargo receptor Ref2p (p62 in mammals) compared to neighboring control cells that possess RFP **(Figure 3-2C and D),** indicating that autophagy is impaired. Similar to homozygous *vmp1(Δ)* mutant cells, Ref2p accumulated in *vps13d (MiMic)* mutant cells **(Figure 3-1F and G).**

Mitochondria are cleared by autophagy during intestine development (Chang et al., 2013). Therefore, we investigated if Vmp1, like Vps13D, is required for clearance of mitochondria in the intestine. Significantly, homozygous *vmp1(Δ)* mutant intestine cells lacking RFP were unable to clear mitochondria compared to neighboring control cells that express RFP based on persistence of the mitochondrial protein ATP5a **(Figure 3-2E and F).** Combined, these data indicate that Vmp1 has similar functions to Vps13D, including the regulation of autophagy and clearance of mitochondria.

We next investigated if the presence of mitochondria in homozygous *vmp1(Δ)* mutant intestine cells was due to a defect in mitophagy. We used the mito-QC system which utilizes a mitochondrial protein tagged with GFP and RFP to detect when mitochondria are delivered to autolysosomes (McWilliams et al., 2018; Lee et al., 2018). Control intestines that expressed control *luc* RNAi throughout the intestine cleared most mitochondria by 2 hours after pupariation as shown by the presence of RFP-positive and GFP-negative puncta **(Figure 3-3A and B).**

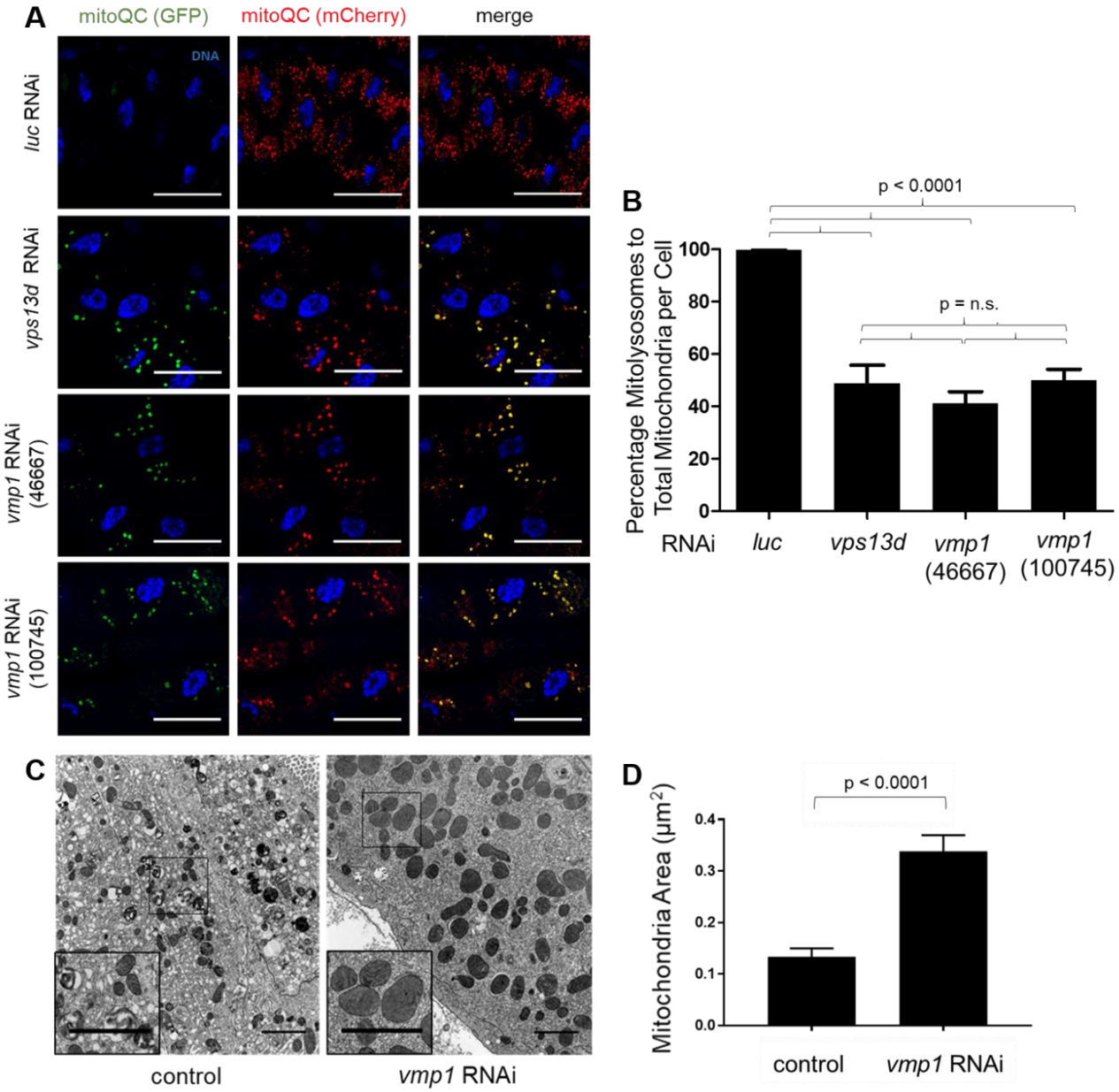

Figure 3-3: Vmp1 is required for mitophagy and normal mitochondrial morphology in *Drosophila* intestines. (A) Mito-QC was expressed in different genotypes and analyzed in all intestine cells 2 hours after pupariation. Control *luciferase (luc)* RNAi-expressing cells possessed mostly red puncta (reflecting mitochondria in autolysomes, mitolysosomes), while intestine cells expressing RNAi against either *vps13d* or 2 distinct *vmp1* RNAi expressing constructs (#46667 and #100745) all exhibited yellow puncta, reflecting mitochondria that failed to get cleared by mitophagy. (B) Quantification of the percentage of mitolysosomes to total mitochondria puncta in *luc* (n=10) RNAi-, *vps13d* (n=10) RNAi-, *vmp1* (#46667) (n=10) RNAi-, and *vmp1* (#100745) (n=8) RNAi-expressing cells 2 hours after pupariation. (C) TEM images of cells from intestines expressing either control *luciferase (luc)* RNAi or *vmp1* RNAi (#100745) 2

hours after pupariation. Enlarged regions are outlined by a black box. (D) Quantification of the size of mitochondria in either control *luc* (n=53) RNAi- or *vmp1* (n=51) RNAi-expressing intestine cells 2 hours after pupariation. Scales bars in (A) represent 40 μm. Scale bars in (C) represent 2.0 μm. Error bars in (B) and (D) are SEM. Representative of 3 or more independent biological experiments.

By contrast, intestines that expressed *vps13d* RNAi or expressed either of two distinct *vmp1* RNAi constructs retained mitochondria that were both RFP- and GFP-positive 2 hours after pupariation **(Figure 3-3A and B).** In addition, transmission electron microscopy (TEM) analyses revealed enlarged mitochondria in *vmp1* RNAi-expressing intestine cells compared to control intestine cells at 2 hours after pupariation **(Figure 3-3C and D).** Larger mitochondria were also observed by TEM analyses of intestine cells expressing a different *vmp1* RNAi **(Figure 3-4).** These data indicate that Vmp1 and Vps13D have similar functions in regulating autophagy, mitophagy and mitochondrial morphology in *Drosophila* intestines.

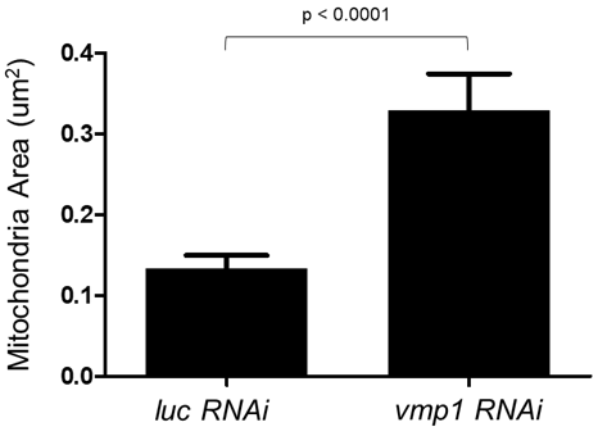

Figure 3-4: *vmp1* RNAi-expressing larval intestine cells have increased mitochondria size 2 hours after pupation. Quantification of mitochondria area in TEM sections of either control *luc* (n=53) RNAi- or *vmp1* (n=50) RNAi (VDRC line #46667)-expressing intestine cells 2 hours after pupation. Error bars represent SEM. Representative of 3 or more independent biological experiments

Vps13D regulates mitochondria and endoplasmic reticulum contact

Vmp1 is a repressor of membrane contact, and the failure to disassemble mitochondria and endoplasmic reticulum (ER) contact alters mitochondrial morphology in *vmp1* mutant mammalian and *C. elegans* cells (Zhao et al., 2017). We investigated if Vmp1 influences mitochondria and ER contact in *Drosophila* through TEM analyses of intestines 2 hours after pupariation. Intestines with decreased Vmp1 function that express *vmp1* RNAi possessed increased contact between mitochondria and ER compared to *luciferase (luc)* RNAi control cells **(Figure 3-5A and B).**

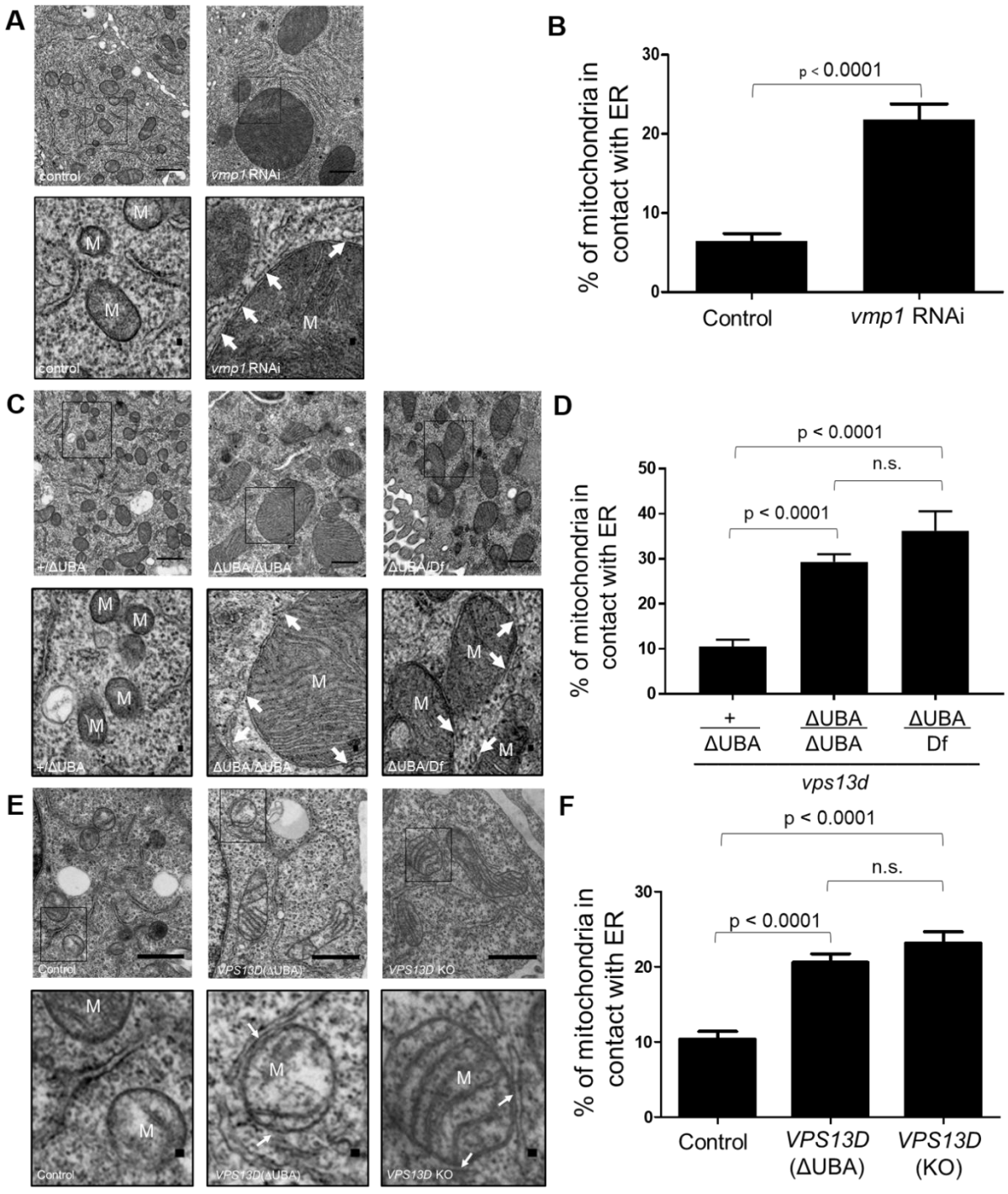

Figure 3-5: Vmp1 and Vps13D regulate mitochondria and ER contact. (A) TEM images of cells from intestines expressing either control *luciferase (luc)* RNAi or *vmp1* RNAi (#100745) 2 hours after pupariation. Enlarged regions are outlined by a black box. Mitochondria (M) and ER (arrows) are indicated. (B) Quantification of mitochondria and ER contact in either control *luc* (n=100) RNAi- or *vmp1* (n=78) RNAi-expressing

intestine cells 2 hours after pupariation. Contact between the mitochondria and ER is defined as a distance of less than 0.03 μm and contact length of at least 0.02 μm *(16)*. (C) TEM images of cells from either control +/*vps13d (*ΔUBA), *vps13d (*ΔUBA)/*vps13d (*ΔUBA), or *vps13d (*ΔUBA)/*Df* intestines 2 hours after pupariation. (D) Quantification of mitochondria and ER contact in either control +/*vps13d (*ΔUBA) (n=50), *vps13d (*ΔUBA)/*vps13d (*ΔUBA) (n=50), or *vps13d (*ΔUBA)/*Df* (n=50) intestines 2 hours after pupariation. (E) TEM images of either wild-type control, *VPS13D (*ΔUBA), or *VPS13D* KO (exon 3 deletion) HeLa cells. (F) Quantification of mitochondria and ER contact in either control (n=96), *VPS13D (*ΔUBA) (n=116), or *VPS13D* KO (exon 3 deletion) (n=100) HeLa cells. In (A), (C), and (E), arrows represent regions of contact between mitochondria (M) and ER. Scale bars in top panels represent 0.5 μm and bottom panels represent 0.03 μm. Error bars in (B), (D), and (F) are SEM. Representative of 3 or more independent biological experiments.

Similar results were obtained with a different *vmp1* RNAi line **(Figure 3-6).** These results indicate that Vmp1 regulates mitochondria and ER contact in *Drosophila.*

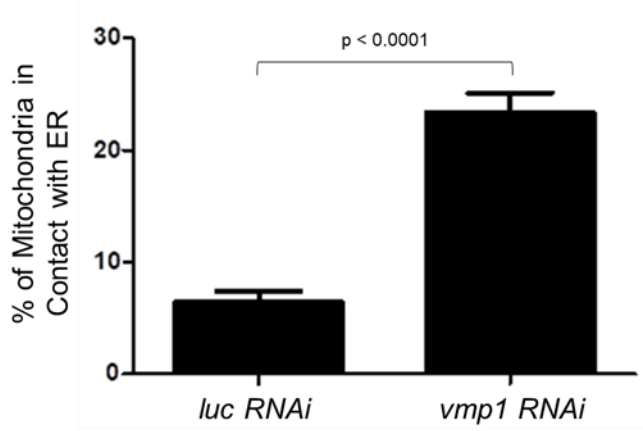

Figure 3-6: *vmp1* RNAi-expressing larval intestine cells have increased mitochondria and ER contact 2 hours after pupation. The percentage of contact between mitochondria and ER in TEM sections of either control *luc* RNAi (n=53) or *vmp1* RNAi (VDRC line #46667)-expressing intestine cells 2 hours after pupation. Error bars represent SEM. Representative of 3 or more independent biological experiments.

Given the role of Vmp1 in mitochondria and ER contact, as well as the similarities between *vmp1* and *vps13d* mutant cell phenotypes, we investigated if *vps13d* functions in mitochondria and ER contact by TEM analyses. Intestine cells of either homozygous

vps13d (ΔUBA), a mutant lacking the ubiquitin binding domain, or *vps13d(ΔUBA)*/chromosome deficiency (*Df*) for the *vps13d* genomic region had significantly increased mitochondria and ER contact compared to heterozygous *vps13d (ΔUBA)/*wild type control cells 2 hours after pupariation **(Figure 3-5C and D).**

The function of Vps13D in the regulation of mitochondria and ER contact in *Drosophila* prompted us to consider if this phenotype is conserved in humans. Therefore, we analyzed HeLa cells that either lack the ubiquitin binding domain, *VPS13D(ΔUBA),* or are thought to be a strong loss-of-function mutant, *VPS13D(KO)*. Significantly, we found that mitochondria and ER contact were increased in both *VPS13D* mutant human HeLa cell lines **(Figure 3-5E and F).** These results indicate that both *vmp1* and *vps13d* regulate mitochondria and ER contact in *Drosophila* and human cells.

Mutations in *VPS13D* have been associated with familial neurological movement disorders, including ataxia, dystonia, and chorea (Seong et al., 2018; Gauthier et al., 2018). Given the conserved function of VPS13D in inter-organelle contact between fly and human HeLa cells, we investigated if patient-derived cells with *VPS13D* mutations have altered mitochondria and ER contact by TEM. Remarkably, mitochondria in fibroblasts that were derived from the symptomatic *VPS13D* mutant (G1190D/Q1106*) patient had increased mitochondria and ER contact compared to the mitochondria in fibroblasts derived from a relative (G1190D/+) and unrelated control **(Figure 3-7A and B)** (Seong et al., 2018).

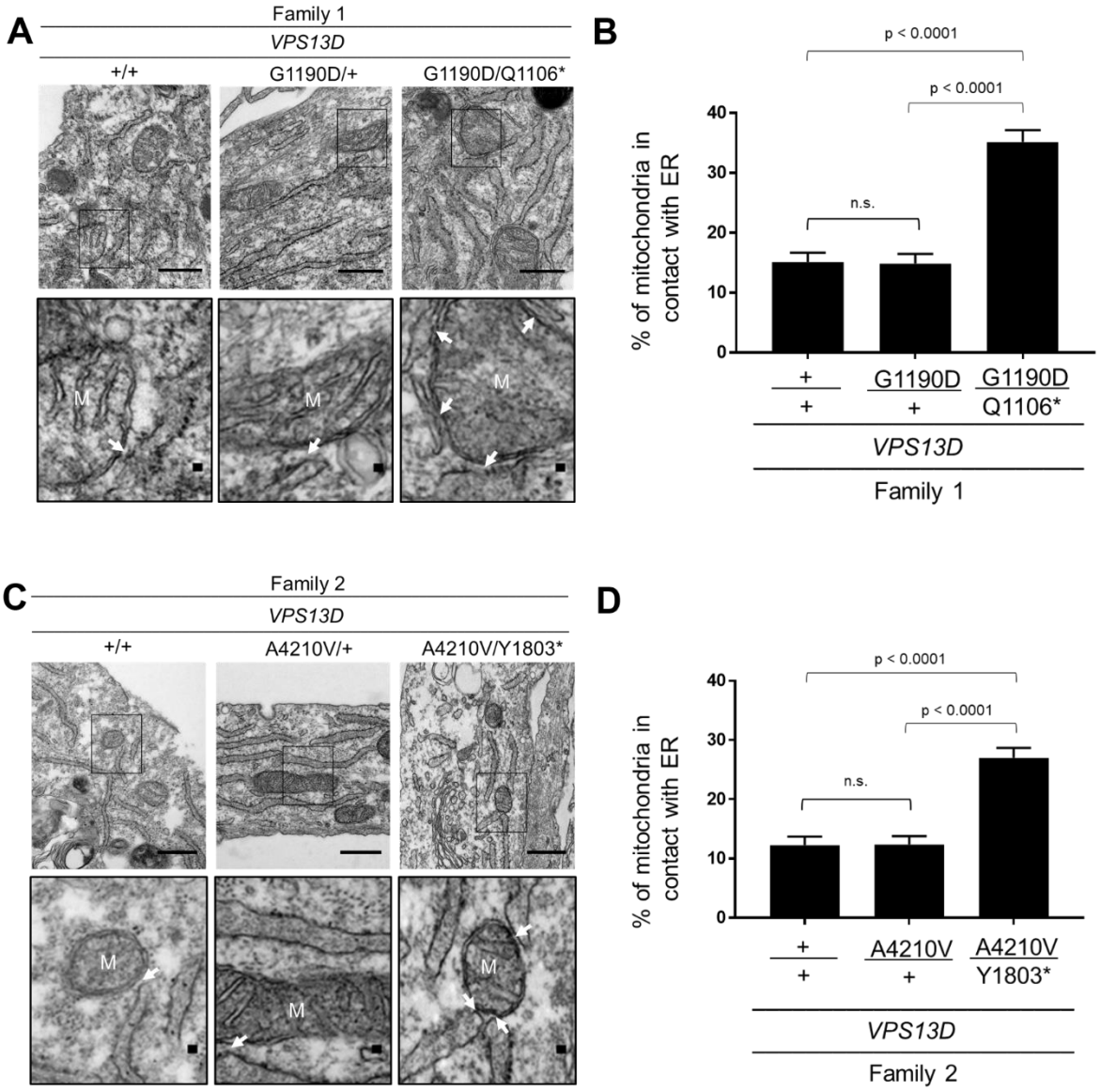

Figure 3-7: Fibroblasts derived from patients with neurological symptoms associated with *VPS13D* mutations have increased mitochondria and ER contact. (A) TEM images of fibroblast cells derived from a family with mutations in *VPS13D* (Family 1). Cells were derived from either an unrelated donor without mutations in *VPS13D* (+/+), a relative carrying the G1190D allele for *VPS13D* (G1190D/+), or a patient with neurological symptoms carrying the G1190D and Q1106* mutations in *VPS13D* (G1190D/Q1106*). Enlarged regions are outlined by a black box, mitochondria (M) and ER (arrows) are indicated. (B) Quantification of mitochondria and ER contact in *VPS13D* (+/+) (n=54), (G1190D/+) (n=50), and (G1190D/Q1106*) (n=50) fibroblasts derived from Family 1. (C) TEM images of fibroblast cells derived from a family with mutations in *VPS13D* (Family 2). Cells were derived from either an unrelated donor

without mutations in *VPS13D* (+/+), a relative carrying the A4210V allele for *VPS13D* (A4210V/+), or the patient with neurological symptoms carrying the A4210V and Y1803* mutations in *VPS13D* (A4210V and Y1803*). (D) Quantification of mitochondria and ER contact in *VPS13D* (+/+) (n=50), (A4210V/+) (n=56), and (A4210V/Y1803*) (n=50) fibroblasts derived from Family 2. In (A) and (C), scale bars in top panels are 0.5 μm and in bottom panels are 0.03 μm. Error bars in (B) and (D) are SEM. Representative of 3 or more independent biological experiments.

In addition, we analyzed mitochondria and ER contact in a second set of fibroblasts derived from an unrelated family with symptoms associated with the *VPS13D* mutations (Seong et al., 2018). Mitochondria from the symptomatic *VPS13D* mutant patient from this family (A4210V/Y1803*) also exhibited increased mitochondria and ER contact compared to mitochondria in fibroblasts derived from both an asymptomatic relative (A4210V/+) and a separate unrelated control **(Figure 3-7C and D).** Therefore, VPS13D regulates mitochondria and ER contact, this function is conserved from flies to humans, and this phenotype likely contributes to cell health and neurological disease.

Vps13D functions downstream of Vmp1 to regulate mitochondrial morphology and mitophagy

The similarities between *vmp1* and *vps13d* mutant phenotypes suggests that these genes may be in the same genetic pathway regulating mitophagy and mitochondrial size. We analyzed Vps13D protein localization in control and homozygous *vmp1(Δ)* mutant intestine cells 2 hours after pupariation, and found that Vps13D protein puncta were significantly decreased in *vmp1* mutant cells compared to neighboring control cells **(Figure 3-8A and B).**

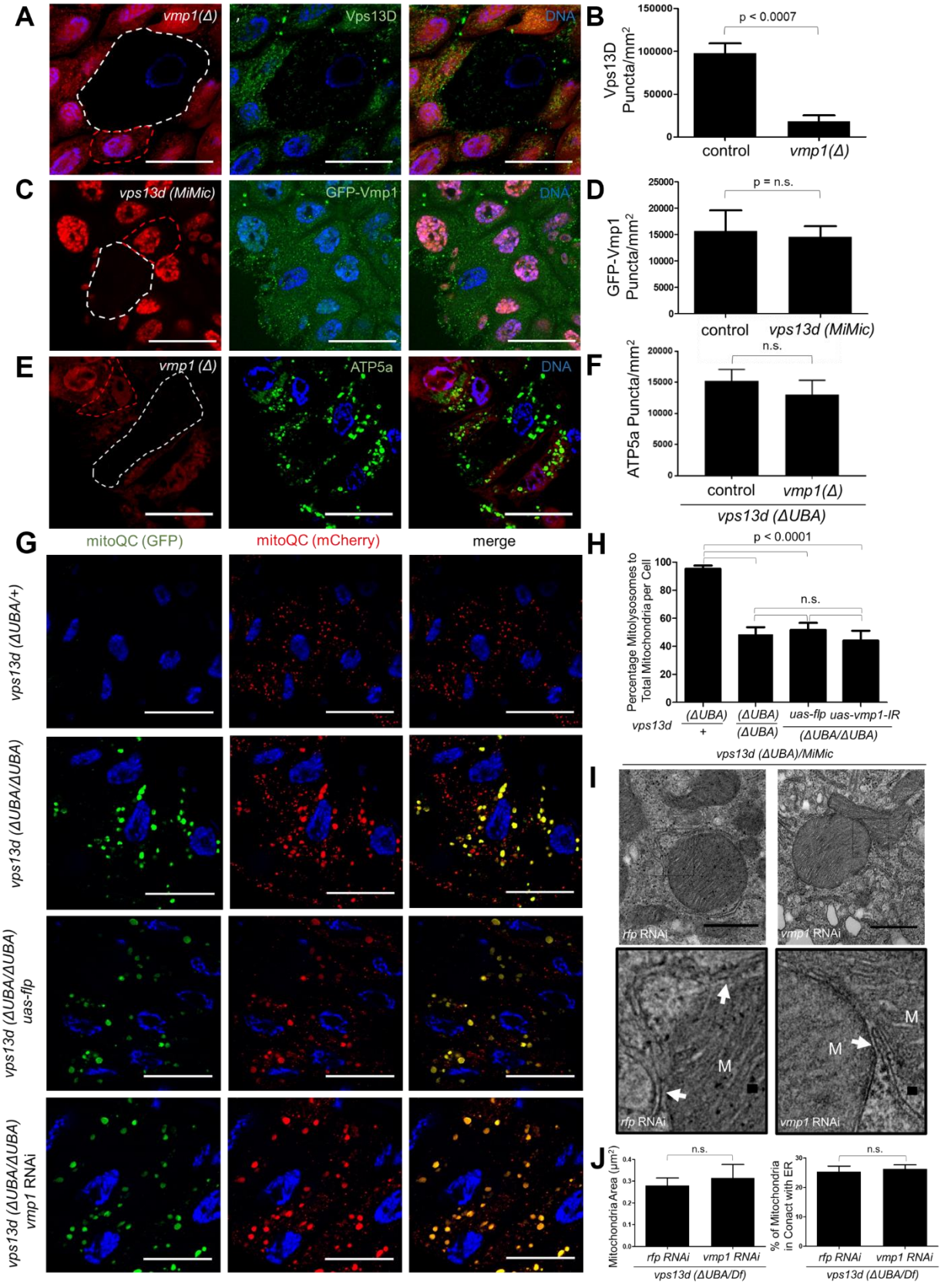
A
vmp1(Δ)
Vps13D
DNA
B
p < 0.0007
Vps13D Puncta/mm2
150000
100000
50000
0
control
vmp1(Δ)
C
vps13d (MiMic)
GFP-Vmp1
DNA
D
p = n.s.
GFP-Vmp1 Puncta/mm2
25000
20000
15000
10000
5000
0
control
vps13d (MiMic)
E
vmp1 (Δ)
ATP5a
DNA
F
n.s.
ATP5a Puncta/mm2
20000
15000
10000
5000
0
control
vmp1(Δ)
vps13d (ΔUBA)
G
mitoQC (GFP)
mitoQC (mCherry)
merge
vps13d (ΔUBA/+)
vps13d (ΔUBA/ΔUBA)
vps13d (ΔUBA/ΔUBA) uas-flp
vps13d (ΔUBA/ΔUBA) vmp1 RNAi
H
p < 0.0001
n.s.
Percentage Mitolysosomes to Total Mitochondria per Cell
100
80
60
40
20
0
vps13d
(ΔUBA) +
(ΔUBA) (ΔUBA)
uas-flp uas-vmp1-IR (ΔUBA/ΔUBA)
vps13d (ΔUBA)/MiMic
I
rfp RNAi
vmp1 RNAi
M
J
n.s.
Mitochondria Area (μm2)
0.4
0.3
0.2
0.1
0.0
rfp RNAi
vmp1 RNAi
vps13d (ΔUBA/Df)
% of Mitochondria in Conact with ER
30
20
10
0

Figure 3-8: Vps13d and Vmp1 function in a pathway to regulate mitophagy and mitochondrial morphology. (A) *vmp1 (∆)* loss-of-function mutant cells (non-red, white dotted line) possess fewer Vps13D puncta (green) compared to neighboring control cells (red) in intestines 2 hours after pupariation. (B) Quantification of Vps13D puncta in *vmp1(∆)* mutant (n=6) and control (n=16) intestine cells 2 hours after pupariation. (C) *vps13d (MiMic)* mutant cells (lacking nuclear RFP, white dotted line) do not have altered GFP-Vmp1 in larval intestines 2 hours after pupariation. Antibody against GFP was used to enhance GFP-Vmp1 signal. (D) Quantification of GFP-Vmp1 puncta in *vps13d (MiMic)* mutant (n=8) and control (n=14) intestine cells 2 hours after pupariation. (E) *vmp1*(∆) and *vps13d (∆UBA)* double mutant cells (non-red, white dotted line) exhibit similar levels of mitochondrial ATP5a protein compared to neighboring control *vmp1(∆)*/+ and *vps13d (∆UBA)* single mutant cells (red) 2 hours after pupariation. (F) Quantification of ATP5a puncta in *vmp1*(∆) and *vps13d (∆UBA)* double mutant (n=8) and *vmp1(∆)*/+ and *vps13d (∆UBA)* single mutant (n=14) control intestine cells 2 hours after pupariation. (G) Mito-QC was expressed in different genotypes and analyzed in intestine cells 2 hours after pupariation. Control *vps13d (ΔUBA)/+* cells possessed mostly red puncta (reflecting mitochondria in autolysomes, mitolysosomes), while *vps13d (ΔUBA/ΔUBA)* homozygous mutant, *vps13d (ΔUBA/ΔUBA)* mutant expressing *flp*, and *vps13d (ΔUBA/ΔUBA)* mutant with *vmp1* RNAi-expressing intestine cells all exhibited large yellow puncta (reflecting mitochondria that fail to be cleared by mitophagy). (H) Quantification of the percentage of mitolysosomes to total mitochondria puncta in *vps13d (ΔUBA)/+* (n=10), *vps13d (ΔUBA/ΔUBA)* (n=10), *vps13d (ΔUBA/ΔUBA), UAS-flp* (n=11), and *vps13d (ΔUBA/ΔUBA), vmp1* RNAi (100745) (n=10), cells 2 hours after pupariation. (I) TEM images of cells from either control *vps13d (∆UBA)/MiMic* expressing *rfp* RNAi or *vps13d (∆UBA)/MiMic* expressing *vmp1* RNAi intestines 2 hours after pupariation. Enlarged regions are outlined by a black box, mitochondria (M) and ER (arrows) are indicated. (J) Quantification of either mitochondrial size or mitochondria and ER contact in either control *vps13d (∆UBA)/MiMic* expressing *rfp* RNAi (n=55) or *vps13d (∆UBA)/MiMic* expressing *vmp1* RNAi (#100745) (n=62) intestine cells 2 hours after pupariation**.** Scale bars in (A), (C), (E), and (G) are 40 µm. Scale bars in top panel of (I) represent 0.5 µm while scale bars in bottom panels represent 0.03µm. Error bars in (B), (D), and (F), (H), and (J) are SEM. Representative of 3 or more independent biological experiments.

These results indicate that Vps13D puncta are dependent on Vmp1. We next investigated if Vps13d influences Vmp1. Antibodies do not exist to detect Vmp1 in *Drosophila.* Therefore, CRISPR/CAS9 was used to tag Vmp1 with GFP on the N terminus (GFP-Vmp1) **(Figure 3-9A).**

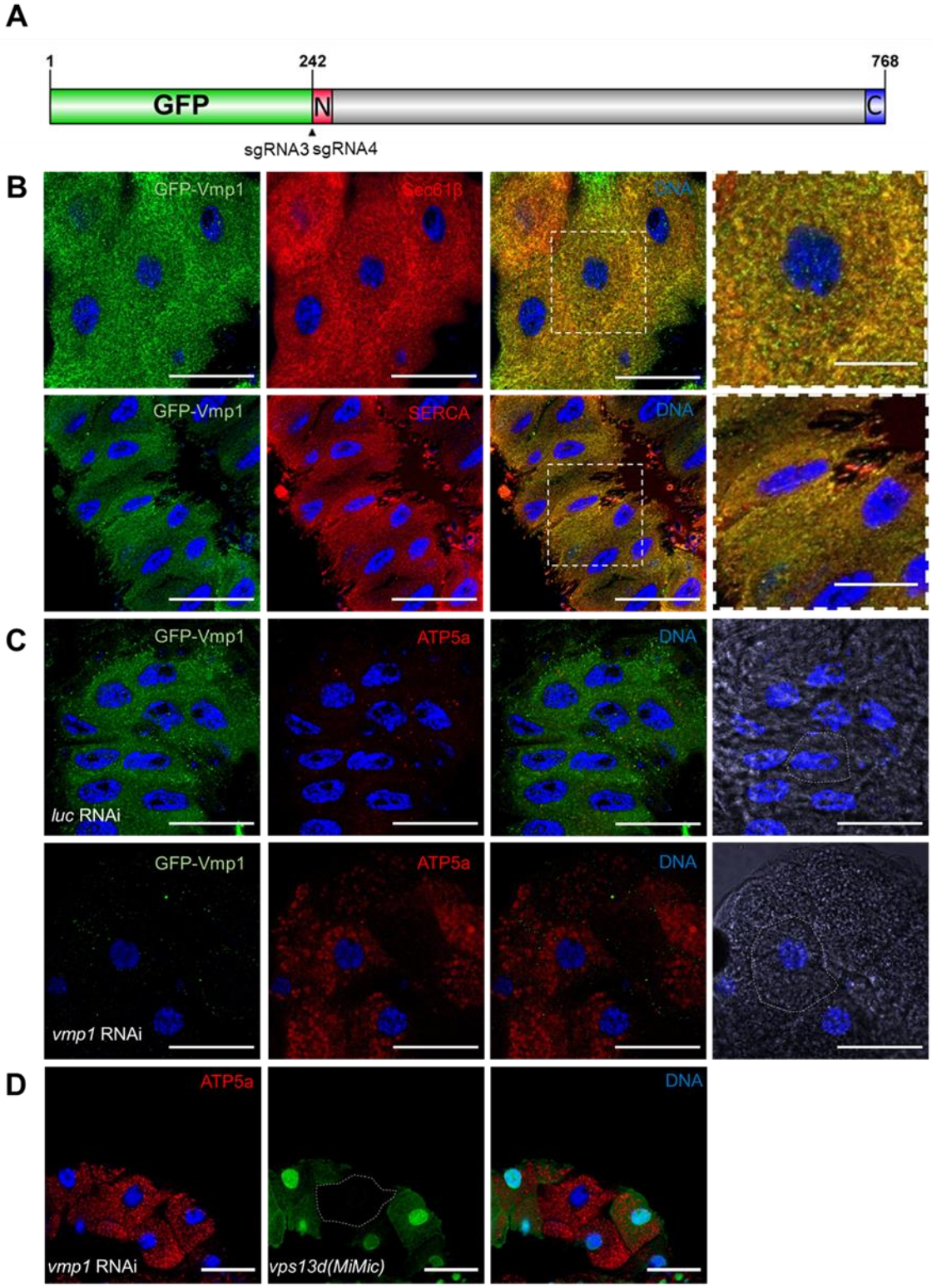
A
1
242
768
GFP
N
C
sgRNA3 sgRNA4
B
GFP-Vmp1
Sec61β
DNA
GFP-Vmp1
SERCA
DNA
C
GFP-Vmp1
ATP5a
DNA
luc RNAi
GFP-Vmp1
ATP5a
DNA
vmp1 RNAi
D
ATP5a
DNA
vmp1 RNAi
vps13d(MiMic)

Figure 3-9: Design and characterization of *gfp-vmp1.* (A) Design of the *Drosophila gfp-vmp1* using sgRNA3 and sgRNA4. Numbers represent amino acid sequence. (B) *gfp-vmp1* intestine cells were dissected from early 3rd instar larvae (top) and 2 hours after pupation (bottom). Early 3rd instar larvae expressed tdTomato-Sec61β while intestines 2 hours after pupation were stained with antibody against SERCA, both of which are associated with ER. GFP specific antibody was used to enhance *gfp-vmp1* signal. GFP-Vmp1 colocalized with the ER at both stages. (C) *gfp-vmp1* larval intestine cells have distinct GFP-Vmp1 puncta (green), are able to clear most mitochondrial ATP5a protein (red) and have reduced cell size (white dotted line) in intestines that express control *luc* RNAi throughout the intestine 2 hours after pupation (top). By contrast, animals that express *vmp1* RNAi in intestines (bottom) possess depleted GFP-Vmp1 puncta, retained mitochondria ATP5a protein, and enlarged cells (dotted white line). Antibody against GFP was used to enhance GFP-Vmp1 signal. D) *vps13d(MiMic)* mutant cells (non-GFP, white dotted line) in intestines that express *vmp1* RNAi in all cells and stained for mitochondrial ATP5a protein 2 hours after pupation. Scale bars in enlarged images in (B) (bordered with dotted lines) represent 8μm. All other scale bars represent 40μm. Representative of 3 or more independent biological experiments.

These flies are viable, fertile and complemented the lethal phenotype associated with the *vmp1(∆)* mutant. GFP-Vmp1 co-localizes with the ER markers Sec61β and SERCA in intestine cells **(Figure 3-9B).** In addition, *vmp1* RNAi expression in the entire GFP-Vmp1 larval intestine resulted in retention of mitochondria and increased cell size compared to controls. *vmp1* RNAi throughout the intestine also caused an almost complete ablation of GFP signal, verifying that the GFP puncta were indeed GFP-Vmp1 **(Figure 3-9C).** Interestingly, *vps13d(MiMic)* loss-of-function mutant cells did not possess altered GFP-Vmp1 localization **(Figure 3-8C and D),** indicating that Vmp1 localization is not dependent on *vps13d* function. Combined, these results suggest that Vps13d functions downstream of Vmp1.

We investigated the relationship between Vmp1 and Vps13d in the clearance of mitochondria. We compared mitochondrial clearance in *vmp1(Δ)* and *vps13d(ΔUBA)* double mutant intestine cells with *vmp1(Δ)/+* and *vps13d(ΔUBA)* single mutant control

cells 2 hours after pupariation. Double mutant cells had similar amounts of mitochondrial ATP5a protein compared to neighboring control cells **(Figure 3-8E and F),** suggesting that these genes function in the same pathway to clear mitochondria. Consistent with these findings, loss of *vps13d* function failed to enhance the mitochondrial clearance phenotype caused by expression of *vmp1* RNAi throughout the intestine **(Figure 3-9D).**

We next used mito-QC to investigate if Vmp1 and Vps13D function in a shared mitophagy pathway. Control intestines that were heterozygous for the *vps13d (ΔUBA)* mutation cleared most mitochondria by 2 hours after pupariation as shown by the presence of RFP-positive and GFP-negative puncta. By contrast, intestines that were homozygous for the *vps13d (ΔUBA)* mutation retained mitochondria that were both RFP- and GFP-positive 2 hours after pupariation **(Figure 3-8G and H).** Combined knockdown of *vmp1* by RNAi in a homozygous *vps13d (ΔUBA)* mutant background failed to enhance the *vps13d* mutant mito-QC phenotype **(Figure 3-8G and H),** further indicating that *vmp1* and *vps13d* function in the same mitophagy pathway.

To investigate if Vps13D and Vmp1 function in the same pathway to regulate mitochondria and ER contact, we analyzed *vps13d (ΔUBA)*/*Df* expressing either *vmp1* or control *rfp* RNAi by TEM. Importantly, the combined reduction of both *vmp1* and *vps13d* function failed to enhance either the increased mitochondrial size or mitochondria and ER contact phenotypes compared to the loss of *vps13d* alone **(Figure 3-8I and J).** These findings indicate that Vps13D and Vmp1 function in the same

pathway to regulate mitophagy and mitochondria and ER contact, and that Vps13D functions downstream of Vmp1.

marf/MFN2 suppresses *vps13d* and *vmp1* mutant phenotypes

The role of Vps13D in regulating mitochondria and ER contact sites prompted us to consider the relationship between Vps13D and known regulators of inter-organelle contact. Mfn2 (Marf in flies) has been implicated in mitochondria and ER contact (de Brito and Scorrano, 2008; Naon et al., 2016; McLelland et al., 2018), and knockdown of *marf* suppressed the *vps13d* knockdown mitochondria size phenotype (Anding et al., 2018). Therefore, we investigated how loss of Vps13D influences Marf in *Drosophila*. Antibodies against Marf do not work for immunohistochemistry, but can be used for immunoblotting **(Figure 3-10A).**

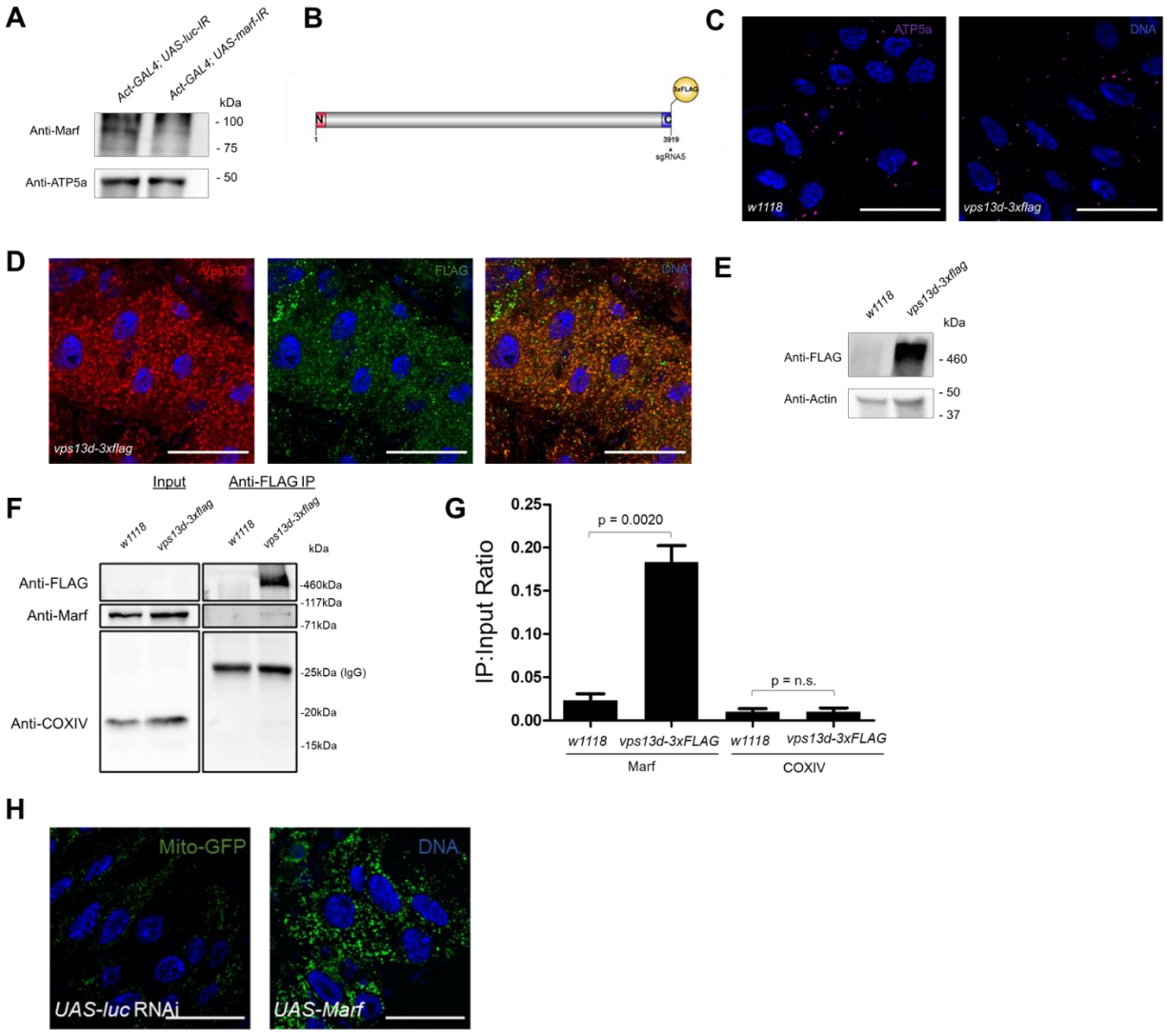

Figure 3-10: *vps13d-3xflag* flies have normal mitochondrial morphology and clearance and overexpression suppresses mitochondrial clearance. (A) 2-hour pupal lysates from either control *luc* or *marf* RNAi driven by the Act-gal4 driver were analyzed by western Blot with antibodies against Marf and ATP5a. B) Design of the *Drosophila vps13d-3xflag* using sgRNA5. Numbers represent amino acid sequence. (C) Intestines dissected from control *w1118* and *vps13d-3xflag* animals 2 hours after pupation were stained with antibody against ATP5a. (D) Intestines dissected from *vps13d-3xflag* animals 2 hours after pupation were stained with antibodies against Vps13D and FLAG. (E) Lysates from control *w1118* and *vps13d-3xflag* 2 hours after pupation were analyzed by western Blot with antibodies against FLAG and Actin. (F) Western blot of input and eluates from a FLAG immunoprecipitation of control *w1118* and *vps13d-3xflag* pupae 2 hours after pupation that was probed with antibodies against FLAG, Marf and negative control COXIV, an outer mitochondrial membrane. Vps13D-3xFLAG levels were too low to be detected in the input with lysate conditions

suitable for immunoprecipitation, so the presence of 3xFLAG tagged Vps13D was verified using harsher lysis conditions. 1ug of 3xFLAG peptide was added to *w1118* lysate before incubating with beads to control for non-specific interactions with 3xFLAG. (G) Quantification of the relative levels of Marf and COXIV in the CoIP compared to input in control *w1118* and *vps13d-3xFLAG* pupae. (H) Intestines dissected from animals 2 hours after pupation expressing either control *luc* RNAi or *marf* RNAi driven by the Myo31DFNP0001driver and expressing UAS-mito-GFP, were compared by immunofluorescence.

Therefore, we analyzed Marf levels in intestines isolated from control and *vps13d* mutant animals 2 hours after pupariation. Intestines from *vps13d (ΔUBA)/Df* trans-heterozygous mutants have increased levels of Marf and ATP5a compared to *vps13d (ΔUBA)/+* and *Df/+* controls 2 hours after pupariation **(Figure 3-11A and B)**, suggesting that Vps13D influences Marf levels. The increase in Marf levels were greater than that of ATP5a, suggesting that increased Marf was not simply due to a failure to clear mitochondria.

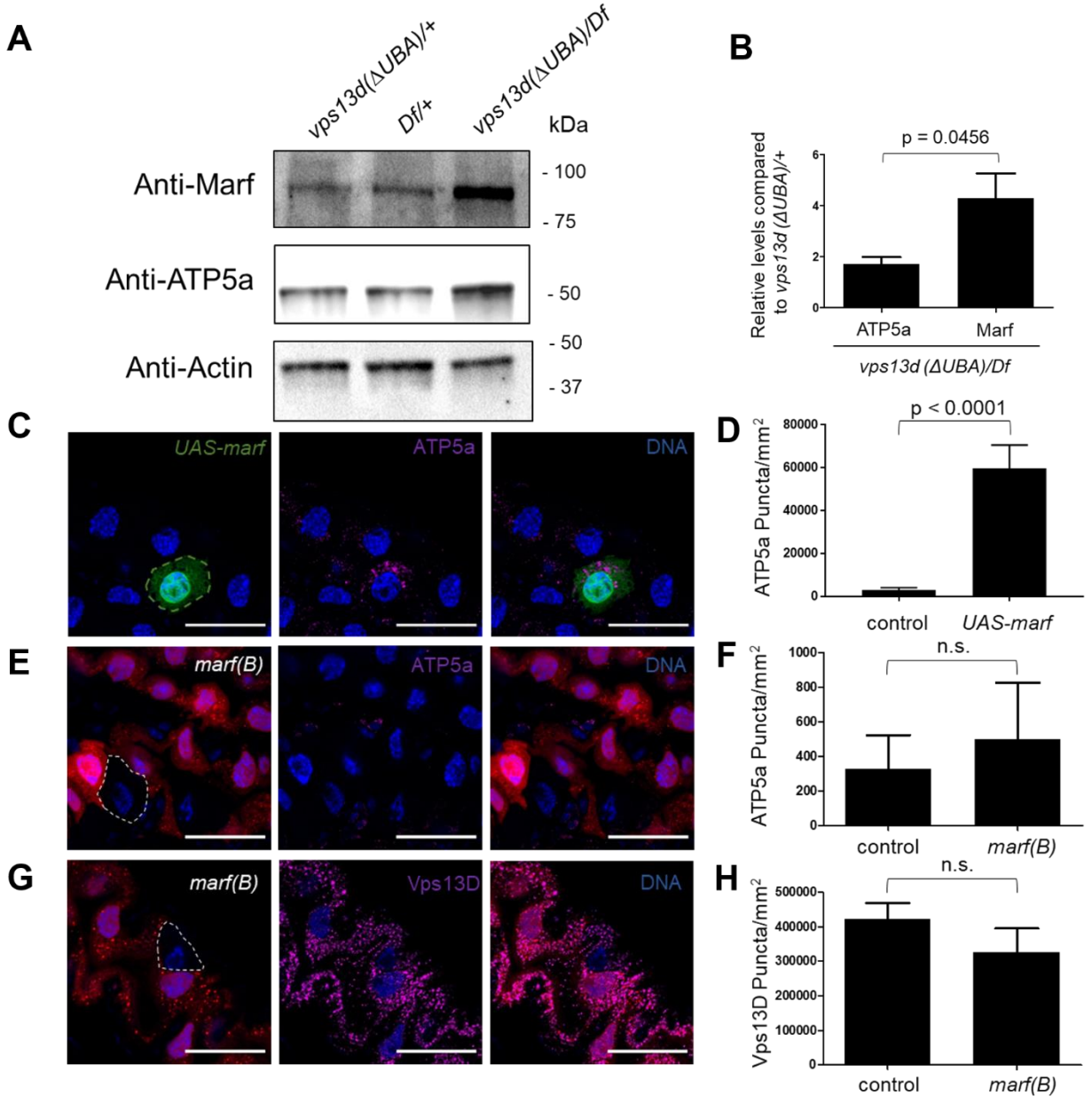

Figure 3-11: Vps13d functions upstream of Marf to mediate mitochondrial clearance. (A) Western blot of lysates from *vps13d(ΔUBA)/+, Df/+,* and *vps13d(ΔUBA)/Df* intestines 2 hours after pupariation that was probed with antibodies against Marf, ATP5a and Actin. (B) Quantification of relative levels of Marf and ATP5a in *vps13d(ΔUBA)/+, Df/+,* and *vps13d(ΔUBA)/Df* intestines 2 hours after pupariation compared to Actin. (C) Intestine cells that overexpress *marf* using the Act-GAL4 (green) were stained with antibodies against ATP5a (purple) and compared to neighboring control cells (non-green). (D) Quantification of levels of ATP5a puncta in *marf* overexpressing intestine cells 2 hours after pupariation compared to control cells. (E)

Intestines 2 hours after pupariation containing *marf(B)* loss-of-function mutant cells (non-RFP) were stained with antibody against ATP5a (purple). (F) Quantification of levels of ATP5a puncta in *marf(B)* loss-of-function mutant cells (n=6) 2 hours after pupariation compared to control cells (n=14). (G) Intestines 2 hours after pupariation containing *marf(B)* loss-of-function mutant cells (non-RFP) were stained with antibody against Vps13D (purple). (H) Quantification of levels of Vps13D puncta in *marf(B)* loss-of-function mutant cells (n=6) 2 hours after pupariation compared to control cells (n=13). Scale bars in (C), (E), and (G) represents 40 μm. Error bars in (B), (D), (F), and (H) are SEM. Representative of 3 or more independent biological experiments.

We next investigated if Marf interacts with Vps13D in *Drosophila.* The large size of Vps13D made it difficult to conduct biochemical experiments using exogenous expression in animal and cell culture models. Thus, we used CRISPR to tag the endogenous *Drosophila vps13d* gene with *3xflag* on the C terminus of the open reading frame **(Figure 3-10B).** Unlike *vps13d* mutants, these flies are viable, fertile, and do not have altered mitochondrial morphology in intestine cells at 2 hours after pupariation **(Figure 3-10C).** Co-staining of intestine cells with anti-FLAG and anti-Vps13D at 2 hours after pupariation revealed co-localization **(Figure 3-10D).** Furthermore, *vps13d-3xFLAG* pupal lysates had a unique band at the approximate weight of Vps13d-3xFLAG that was absent in the untagged *w1118* pupae **(Figure 3-10E).** The 3xFLAG epitope was used to immuno-precipitate Vps13D and potential interacting proteins. We used a Marf-specific antibody to reveal the presence of a band corresponding to endogenous Marf in the *vps13d-3xflag* eluate that was absent in the *w1118* negative control eluate **(Figure 3-10F and G).** We did not obtain significant enrichment of endogenous COXIV, an outer mitochondrial membrane protein like Marf, in the *vps13d-3xFLAG* eluate. These results suggest a specific physical interaction between Vps13d and Marf.

We next sought to characterize the role that Marf may play in mitochondrial clearance in intestines 2 hour after pupariation. Interestingly, over-expression of Marf inhibited mitochondrial clearance **(Figure 3-11C and D),** a phenotype that is similar to *vps13d* loss-of-function mutants. Similar results were obtained by expression of Marf in all intestine enterocyte cells 2 hours after pupariation **(Figure 3-10H).** Unlike *vps13d* loss-of-function mutants, *marf(B)* loss-of-function mutant cells did not possess a defect in mitochondrial clearance **(Figure 3-11E and F).** In addition, *marf(B)* mutant cells did not have altered Vps13d puncta **(Figure 3-11G and H),** suggesting that Vps13D functions upstream of Marf in the regulation mitochondrial clearance and morphology.

MFN2 is an established mitochondria and ER tether that regulates mitochondrial dynamics and mitophagy contact (de Brito and Scorrano, 2008; Naon et al., 2016; McLelland et al., 2018). Given the physical and genetic relationship between Vps13d, Vmp1, and Marf, we hypothesized that Vmp1 and Vps13D may regulate mitochondria morphology and mitochondria and ER contact sites upstream of Marf. Knockdown of *marf* suppressed the enlarged mitochondrial phenotypes seen in *vps13d (ΔUBA/MiMic)* mutants and *vmp1* knockdown intestine cells **(Figure 3-12A and B).**

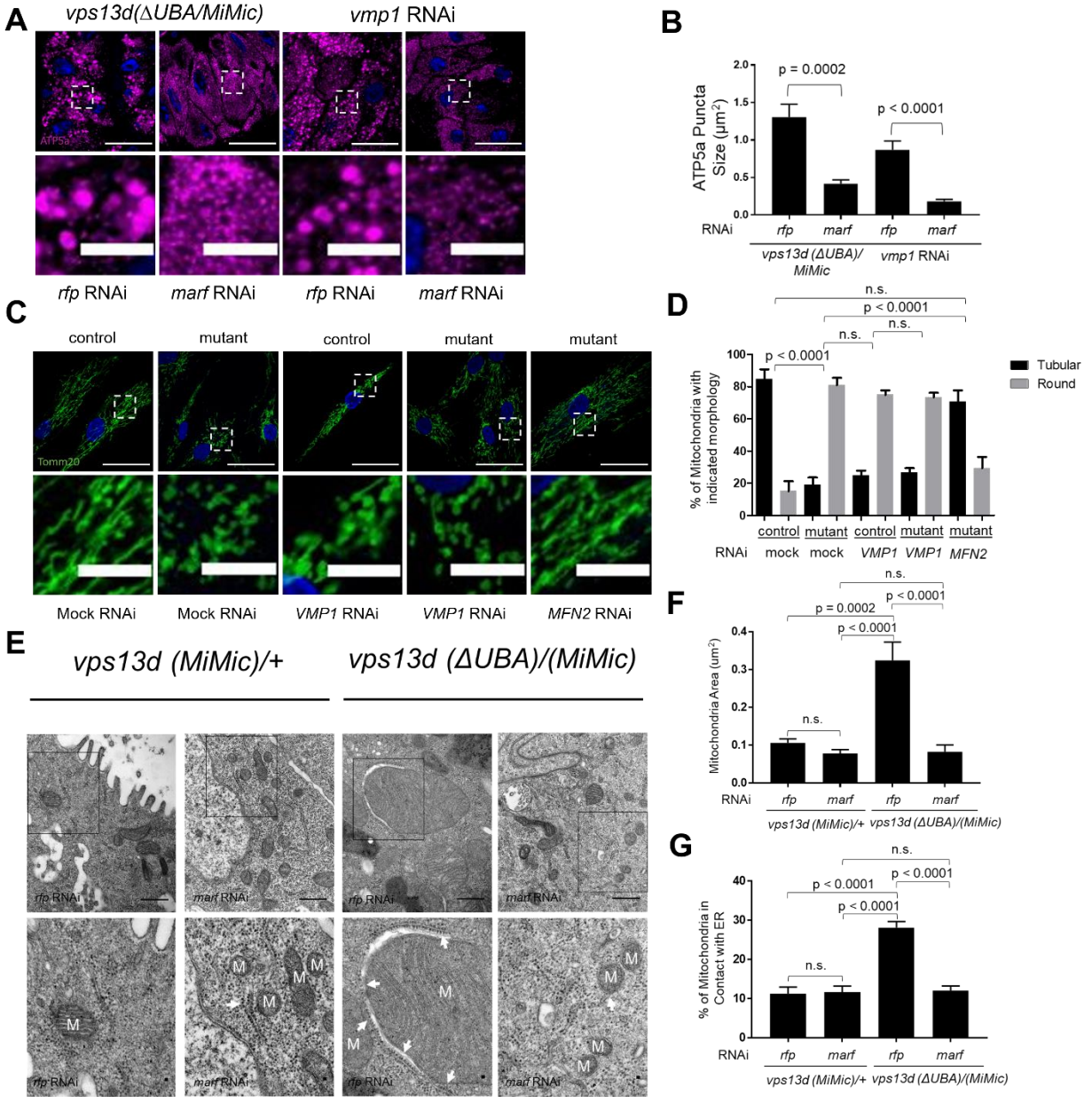

Figure 3-12: Reduction of Marf/Mfn2 function suppresses Vps13D and Vmp1 phenotypes. (A) *vps13d (ΔUBA/MiMic)* and *vmp1* RNAi-expressing intestines 2 hours after pupariation were stained with antibody against ATP5a (purple) with control *rfp* RNAi or *marf* RNAi expression. (B) Quantification of ATP5a puncta size in *vps13d (ΔUBA/MiMic)* and *vmp1* RNAi-expressing intestines 2 hours after pupariation with control *rfp* RNAi (n=13 for *vps13d*, n=11 for *vmp1*) or *marf* RNAi (n=12 for *vps13d* and *vmp1*) expression. (C) Fibroblasts from a patient (mutant) with transheterozygous *VPS13D* mutations (G1190D/Q1106*) were stained with TOMM20 antibody (green) and compared to heterozygous control (G1190D/+) fibroblasts (control). Control fibroblasts were transfected with negative control mock and *VMP1* RNAi and mutant fibroblasts

were transfected with mock, *MFN2* and *VMP1* RNAi. (D) Quantification of mitochondria morphology in control fibroblasts transfected with mock RNAi (n=11) and *VMP1* RNAi (n=10) compared to mutant fibroblasts transfected with mock RNAi (n=11), *VMP1* RNAi (n=15), and *MFN2* RNAi (n=14). E) TEM images of cells from control *vps13d (MiMic)/+* intestine cells expressing either *rfp* or *marf* RNAi (left panels) or *vps13d (*ΔUBA)/(*MiMic)* intestine cells expressing either *rfp* or *marf* RNAi (right panels)2 hours after pupariation. Enlarged regions are outlined by a black box, mitochondria (M) and ER (arrows) are indicated. (F) Quantification of mitochondrial size in*vps13d (MiMic)/+* (n=62) intestine cell expressing *rfp* RNAi, *vps13d (*ΔUBA)/(*MiMic)* (n=84) intestine cell expressing *rfp* RNAi, *vps13d (MiMic)/+* (n=82) intestine cells expressing *marf* RNAi, and *vps13d (*ΔUBA)/(*MiMic)* (n=72) intestine cells expressing *marf* RNAi 2 hours after pupariation**.** (G) Quantification mitochondria and ER contact in *vps13d (MiMic)/+* (n=62) intestine cells expressing *rfp* RNAi, *vps13d (*ΔUBA)/(*MiMic)* (n=84) intestine cells expressing *rfp* RNAi, *vps13d (MiMic)/+* (n=82) intestine cells expressing *marf* RNAi, and *vps13d (*ΔUBA)/(*MiMic)* (n=72) intestine cells expressing *marf* RNAi 2 hours after pupariation**.** Scale bar in top panels of A) and C) represents 40 μm, bottom panels represent 10μm. Scale bars in the upper panels of (E) represent 0.5 μm while scale bars in bottom panels represent 0.03μm. Error bars in (B), (D), (F) and (G) are SEM. Representative of 3 or more independent biological experiments.

Consistent with findings in other cell lines (Zhao et al., 2017), knockdown of *VMP1* in heterozygous control fibroblasts increased the number of round mitochondria, similar to the *VPS13D* mutant patient-derived fibroblasts. *VMP1* knockdown in patient-derived fibroblasts did not significantly increase the ratio of round mitochondria to tubular mitochondria, suggesting that like in *Drosophila* intestines, *VMP1* and *VPS13D* are functionally linked in a pathway in human fibroblasts. Significantly, *MFN2* knockdown in patient-derived fibroblasts **(Figure 3-13)** also suppressed the abnormal mitochondrial phenotype in *VPS13D* mutant patient-derived fibroblasts **(Figure 3-12C and D).** These findings suggest that the mechanistic relationship between *VPS13D, VMP1*, and *Marf/MFN2* are conserved from *Drosophila* to humans, and that this relationship likely contributes to disease pathology.

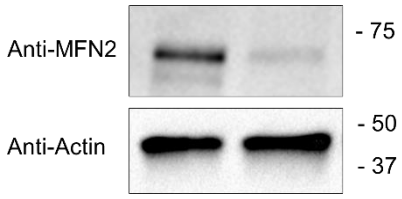

Figure 3-13: Pooled *MFN2* siRNAs reduce MFN2 levels in human fibroblasts. Human derived fibroblasts from the UMCtrl1 cell line were transfected with MFN2 siRNA SMARTpool for 48 hours, lysed, and probed for MFN2 and Actin. Representative of 3 or more independent biological experiments.

We next investigated if decreased *marf* function can suppress the *vps13d* mutant intestine cell mitochondria and ER contact phenotype. Consistent with our previous TEM analyses of mitochondria in *vps13d* RNAi-expressing intestine cells (Anding et al., 2018), reduction of *marf* function by RNAi suppresses the enlarged mitochondrial phenotype in *vps13d (ΔUBA)/MiMic* mutants **(Figure 3-12E and F).** Significantly, expression of *marf* RNAi also suppressed the increased mitochondria and ER contact phenotype in *vps13d* mutant intestine cells **(Figure 3-12E and G).** Importantly, control knockdown of *marf* alone did not alter any of the mitochondrial phenotypes compared to other controls. Therefore, these data indicate that Vps13d mechanistically regulates mitochondria and ER contact sites through Marf.

DISCUSSION

Mitophagy plays an important role in organism health and disease. *vps13d* is not only a regulator of mitophagy, but is also required for proper mitochondrial morphology (Anding et al,. 2018). However, the pathway and mechanism by which *vps13d* regulates mitochondrial size and clearance, and subsequently why *vps13d* is crucial for cell health

and its associated diseases, remains elusive. Here, we establish *vmp1* as a regulator of *vps13d* mediated mitophagy and regulation of mitochondria morphology. In doing so, we identify a new function of Vps13D as a regulator of mitochondria and ER contact in multiple systems, including fibroblasts derived from patients with *vps13d*-associated neurological symptoms.

The regulation of mitochondria and ER contact sites plays important roles in autophagy and mitochondrial morphology. Autophagosomes form at mitochondria and ER contact sites (Hamasaki et al., 2013), making these sites crucial for autophagy. In yeast, it has been shown that mitochondria and ER contact sites are required for mitophagy (Böckler, S., and Westermann, 2014). Furthermore, mitochondria and ER contact regulate mitochondrial dynamics in cultured human cells (Friedman et al., 2011), and altered mitochondrial dynamics influences *vps13d* mutant intestine cell mitochondrial size and clearance (Anding et al., 2018). The inability to disassemble mitochondria and ER contact sites, such as is required in Pink1/Parkin mitophagy (McLelland et al., 2018), can explain the mitophagy deficiency and altered mitochondrial morphology phenotypes that we observe in diverse *vps13d* mutant models.

Here we have identified the first direct link between Vmp1 and the Vps13D family. Vmp1 is an ER localized transmembrane protein that regulates autophagy through disassembly of inter-organelle membrane contacts, where loss of Vmp1 leads to failure in the disassembly of these contact sites (Zhao et al., 2017). Vps13d interacts with proteins that localize to mitochondria and ER contact sites, including Marf (de Brito and Scorrano, 2008; Antonicka et al., 2020; Hung et al., 2017). Consistent with our data

in *Drosophila*, Vps13D was recently reported to interact with Mfn2 in 293 human embryonic kidney cells (Antonicka et al., 2020). Marf has been linked to mitophagy by being degraded by the PINK1/PARKIN pathway (McLelland et al., 2018; Ziviani et al., 2010). It may thus be possible that Vps13D facilitates Marf degradation to decrease mitochondria and ER contact sites, enabling better access for Pink1/Parkin substrates during mitophagy (McLelland et al., 2018). Recent studies have shown that other proteins known to regulate mitophagy and mitochondrial dynamics also localize to mitochondria and ER contact sites (Antonicka et al., 2020; Hung et al., 2017). Along with Marf, these proteins provide a possible mechanism by which Vps13d regulates mitophagy and mitochondrial morphology.

Our data indicate that Vps13d functions as a link between Vmp1 and regulators of mitochondrial dynamics such as Marf. In mammalian cell lines, failure to disassemble mitochondria and ER contact sites is believed to contribute to the abnormal spherical mitochondria in *vmp1* mutant cells (Zhao et al., 2017). Similarly, *VPS13D* mutant HeLa cells display a spherical mitochondrial morphology (Anding et al., 2018). Since Vps13d acts downstream of Vmp1, it is thus likely that Vps13d helps mediate disassembly of membranes at mitochondria and ER contact sites via a mechanism that is similar to Vmp1. Thus, Vps13d may function at a nodal point that links mitochondria and ER contact to influence both mitochondrial dynamics and mitophagy, processes that are mostly studied in isolation. Curiously, Vmp1 also regulates membrane contacts between the ER and other organelles, including endosomes and lipid droplets. The influence of Vmp1 on these organelles does not appear to impact autophagy, suggesting that Vmp1 also has autophagy-independent functions (Zhao et al., 2017). Furthermore, unlike

Vps13D, Vmp1 appears to be required for starvation induced autophagy (Anding et al., 2018; Zhao et al., 2017). Thus, while Vps13D appears to function downstream of Vmp1 in some cellular contexts, it is likely that Vmp1-dependent and Vps13D-independent processes exist.

Vps13 family members are known to act as lipid transfer proteins (Kumar et al., 2018; Gao and Yang, 2018). Autophagosomes form at mitochondria and ER contact sites, and lipids from both organelles are thought to contribute to the autophagosome membrane (Hamasaki et al., 2013; Hailey et al., 2010). As a lipid transporter, Vps13D could facilitate the transfer of important lipids to the forming autophagosome membrane. Given the importance of lipid transfer in organelle signaling pathways (Muallem et al., 2017), Vps13D could also play a role in membrane disassembly by allowing the formation of the autophagosome between the mitochondria and ER.

Vmp1 may also function in a pathway with other Vps13 family members. Although cells lacking *VPS13A* have decreased mitochondria and ER contact, they do not have spherical mitochondria, which is in direct contrast to phenotypes in *VMP1* and *VPS13D* mutant cells (Zhao et al., 2017; Yeshaw et al., 2019). Furthermore, VPS13C does not localize to mitochondria and ER contact sites (Kumar et al., 2018). These findings suggest VMP1 functions in a pathway with VPS13D, but not other VPS13 family members. In *Drosophila*, only loss of *vps13d*, and neither *vps13a* nor *vps13b*, results in the same autophagy deficiency phenotype as loss of *vmp1* (Anding et al., 2018). In addition to being the only VPS13 family member that is essential for survival, VPS13D is the only VPS13 protein with a ubiquitin binding domain, which is crucial for

regulating mitochondria morphology and clearance. Even the single yeast VPS13 does not have this ubiquitin binding domain (Anding et al., 2018; Velayos-Baeza et al., 2004), hinting that the divergence of VPS13D from other VPS13 family members may have been the result of an evolutionary need for regulating more complex functions in higher life forms. These observations further illustrate the unique role that VPS13D plays compared to other VPS13 family members.

Mitochondria and ER contact sites are responsible for a wide range of cellular processes. In addition to autophagy, these sites are crucial for mitochondrial biogenesis, stress response, lipid exchange, calcium signaling, intracellular trafficking and immune responses (Paillusson et al., 2016). As many cells depend on these processes, it is possible that mitochondria and ER contact disruption in *vps13d* mutants is why *vps13d* is such an essential gene **(Figure 3-1A)** (Anding et al., 2018). Dysfunction of mitochondria and ER contacts is believed to contribute to neurodegenerative conditions through impairment of these processes (Friedman et al., 2011; Chakrabarti et al., 2018; Giorgi et al., 2015; Schon et al., 2013). Individuals with *VPS13D* mutations possess a range of symptoms, from asymptomatic to early childhood onset neurological disabilities (Seong et al., 2018; Gauthier et al., 2018), raising the possibility that the severity of disease may be proportional to the extent of altered mitochondria and ER contact. There are no known treatments for patients experiencing symptoms from *VPS13D* mutation-driven diseases. However, the relationship between *vps13d* and *marf* raises the possibility that therapies designed to reduce MARF/MFN2 activity could alleviate such symptoms. The link between *vps13d* and *vmp1* also raises the novel possibility that *VMP1* may play a role in neurological

disease. This link not only includes the diseases *VPS13D* is involved in, but unique diseases that *MARF* is involved in, such as Charcot-Marie-Tooth disease (Houlden et al., 2006). Future studies will determine if the membrane contact function of *vps13d* and relationship to either *vmp1* or *marf* contributes to other associated diseases.

MATERIALS AND METHODS

Drosophila strains

Drosophila melanogaster strains used in this study are listed in the Key Resources Table. w^{1118} were used as controls. All flies were raised on standard cornmeal/molasses/agar media at 25ºC.

Human cell lines

All cells used in this study are listed in Key Resources Table. Cells were cultured at 37°C in 5% CO_2 in DMEM supplemented with 5% FBS and Penicillin/Streptomycin, as previously described (Anding et al., 2018). Cells were transfected with the Lipofectamine™ RNAiMAX Transfection Reagent (Invitrogen) following manufacturer protocol and processed 2 days later.

vmp1(Δ), *gfp-vmp1, and vps13d-3xFLAG* fly construction

vmp1 loss-of-function, *vmp1(Δ),* and N terminal GFP-tagged (*gfp-vmp1) vmp1* strains were edited using CRISPR/Cas9.[39] All germline injections were done by the UMass Medical School CRISPR Core. All primers and oligonucleotides used in this study are

listed in Key Resources Table. For *vmp1(Δ)*, the following sgRNA targeting sequences were used (5’ to 3’): sgRNA1: TGTTGTTGTGACGATTGCTC, sgRNA2: TTACGGGACTAGAAAATCAG. A 200bp ultramer donor with 100bp regions flanking the site of the deletion designed by IDT (San Diego, California) was used to facilitate the deletion, resulting in a single female fly with the deletion that was validated by DNA sequence. Dp(1;3)RC025 from the Bloomington Duplication Project was used to verify that lethality was due to loss of the *vmp1.* For *gfp-vmp1*, the following sgRNA targeting sequences were used (5’ to 3’): sgRNA3: TGCTGTGACATTTAAGCGGT, sgRNA4: CGAATGCTGTGACATTTAAG. A 2kb gblock with 1kb regions flanking the site of insertion and the GFP open reading frame was designed by IDT (San Diego, California) and used to tag the N terminal of *vmp1* with *gfp*. A single female fly containing the insertion was collected, and validated by DNA sequencing. For vps13d-3xflag, the following sgRNA targeting sequence was used (5’ to 3’): sgRNA5:TTTATAAAATGCAATAGGT. A 2kb region flanking the C terminal of genomic *vps13d* was amplified by PCR and site-directed mutagenesis was used to insert the 3xflag sequence in frame immediately before the stop codon. This fragment was inserted into a TOPO vector via TOPO cloning and sequenced to ensure no additional mutations were present and was used to tag the C terminal of vps13d with 3xflag. A single female fly containing the insertion was collected and validated by DNA sequencing.

Induction of mosaic RNAi and mutant cell clones

Mosaic GFP positive RNAi-expressing cell clones were induced as described (Anding et al, 2018). To induce mosaic *vmp1(∆)* and *vps13d(MiMic)* loss-of-function clones, we used the *hsflp, FRT19A, mRFP* and *hsflp;;FRT2A, Ubi-nlsGFP* flies and crossed them with *vmp1(∆) FRT19A/ FM7i-pAct-GFP* and *vps13d(MiMic) FRT2A/TM6B* flies, respectively. Mosaic clonal analyses were only used as indicated, otherwise entire mutant or organ specific RNAi animals were used. 8-hour eggs lays were heat shocked for 90 minutes at 37°C.

Dissection and immuno-labeling of Drosophila larval intestines and Cell Lines

White prepupae were collected and allowed to develop on wet filter paper for 2 hours prior to dissection. Intestines were immuno-stained as previously described with modifications (Anding et al., 2018). Intestines were removed in cold PBS before being placed in 4% paraformaldehyde solution for fixation at 4°C overnight. Intestines were washed twice with PBS and then twice with 0.1% PBSTx before blocking in 5% normal goat serum for 90 minutes and incubation with primary antibody in 0.1% PBSTx overnight. Intestines were then stained with secondary antibody for 3 hours before nuclei staining and mounting. All antibodies used in this study are listed in Key Resources Table. The following primary antibodies were used: rabbit anti-ref(2)p (1:1000, from Gabor Juhasz), mouse anti-ATP synthase complex V (1:1000, Abcam #ab14748), anti-GFP (1:1000, Abcam # ab13970), rabbit anti-TOMM20 (1:200, Abcam # ab78547), rabbit anti-SERCA (1:1000, from Mani Ramaswami) and anti-VPS13D (1:50; Anding et al. 2018). The following secondary antibodies were used: anti-mouse AlexaFluor 647 (Invitrogen #A-21235), anti-rabbit Alexafluor 546 (Invitrogen # A-11035)

and anti-chicken AlexaFluor 488 (#A-11039). Nuclei were stained with Hoescht (Invitrogen) and samples were mounted with Vectashield (Vector Lab). Intestines expressing mCherryAtg8a puncta were fixed overnight at 4°C in 4% paraformaldehyde before being imaged the next day. Cell lines were fixed in 4% paraformaldehyde for 30 minutes at room termperature, permeabilized with digitonin for 15 minutes, and blocked in 5% normal goat serum in PBS before overnight staining with primary antibody overnight at 4°C. Cells were then washed and stained with secondary antibody before mounting in Vectashield with DAPI. Images were acquired using a Zeiss LSM 700 confocal microscope.

Transmission electron microscopy

Transmission electron microscopy (TEM) was conducted as previously described with modifications (Anding et al., 2018). Intestines were dissected in PBS (GIBCO) 2 hours after pupariation and fixed in a solution of 2.5% glutaraldehyde and 2% paraformaldehyde in 0.1M sodium cacodylate buffer, pH 7.4 (Electron Microscopy Sciences) for 1 hour at room temperature followed by overnight fixation at 4°C in fresh fix. Intestines were washed in 0.1M sodium cacodylate buffer, pH 7.4, post-fixed in 1% osmium tetroxide in distilled water for 1 hour at room temperature and washed in distilled water. Preparations were stained en bloc in 1% aqueous uranyl acetate for 1 hour at 4°C in the dark, washed in distilled water, dehydrated through a graded ethanol series, treated with propylene oxide and infiltrated in SPI-pon/Araldite for embedding. We cut ultrathin sections on a Leica UC7 microtome. Sections were stained with uranyl acetate and lead citrate and examined on a Phillips CM10 TEM. Images were taken

down the length of the anterior region of the midgut to ensure an unbiased approach. For each genotype, at least 3 intestines were embedded and sectioned for analyses and quantification. We reviewed all images and selected representative images for analyses.

For cell culture, plated cells were prefixed in 50% media: 50% fix, 2.5% glutaraldehyde and 2% paraformaldehyde in 0.1M sodium cacodylate buffer, pH 7.4 (Electron Microscopy Sciences) for 5 minutes followed by fixation in full fix for 1 hour at room temperature. Cells were then washed with 0.1M cacodylate buffer, pH 7.4, post-fixed in 1% osmium tetroxide in distilled water for 1 hour at room temperature and washed in distilled water. Preparations were stained en bloc in 1% aqueous uranyl acetate over night at 4°C in the dark and then washed in distilled water. The cells were then scraped and pelleted. Cell pellets were embedded in agarose, dehydrated through a graded ethanol series, treated with propylene oxide and infiltrated in SPI-pon/Araldite for embedding. We cut ultrathin sections on a Leica UC7 microtome. Sections were stained with uranyl acetate and lead citrate and examined on a Phillips CM10 TEM. For each cell line, at least (3) 10 cm^2 dishes at 60-80% confluency were embedded independently of each other and sectioned in an unbiased manner for analyses and quantification.

Western Blot and Immunoprecipitation

Tissue was lysed in 1X Laemli Sample Buffer diluted in RIPA lysis buffer (10mM Tris-Cl PH 8.0, 1mM EDTA PH 8.0, 0.5mM EGTA, 2.4mM Sodium Deoxycholate 140mM Sodium Chloride) at a ratio of 10µL lysis buffer per intestine and 30µL per whole pupa.

Samples were crushed in solution using a plastic pestle for 30 seconds before being boiled at 99°C for 6 minutes. Samples were run on 7.5% polyacrylamide gel, transferred onto 0.45µm PVDF membranes (Millipore Sigma), and probed with antibodies using standard protocols. Primary antibodies used were mouse anti-FLAG (1:1000, Millipore Sigma), rabbit anti-Marf (1:1000, from Alexander Whitworth) mouse anti-CoxIV (1:1000, Abcam), mouse anti-Actin (1:1000, Proteintech), and mouse anti-ATP synthase complex V (1:1000, Abcam).

For immunoprecipitations, 2-hour-old pupae were lysed in RIPA lysis buffer supplemented with 1mM NEM, 1mM PMSF and Halt Protease Inhibitor Cocktail (Thermo Fisher) at a ratio of 16 pupae per 250µL lysis buffer. Pupae were crushed with a plastic pestle for 30 seconds and incubated on ice for 30 minutes before being centrifuged at 4°C at 13,000rpm for 10 minutes. Supernatant was filtered through 0.45µm Cellulose Acetate filters (Millipore Sigma). 30µL of filtered supernatant was diluted in 10µL of 4x Laemli Sample Buffer (Biorad), boiled for 6 minutes at 99°C and used as input. 200µL of filtered supernatant (approximately 1mg protein) was used for immunoprecipitation. 40µL of anti-FLAG M2 magnetic bead slurry (Millipore Sigma) warmed to room temperature was washed twice with RIPA buffer before incubation with filtered supernatant for 2 hours at 4°C on a rotator. Following incubation, supernatant was discarded and beads were washed 4 times with 1mL 0.1% PBST. Beads were eluted with 20µL 1X Laemli Sample Buffer diluted in RIPA lysis buffer and boiled for 6 minutes at 99°C. 20µL of input and eluate was run on 7.5% polyacrylamide gel for Western Blot analysis.

QUANTIFICATION AND STATISTICAL ANALYSES

Quantification of mitochondria morphology in fibroblasts were blindly characterized as tubular or spherical. All other quantifications, including cell size and puncta in immunofluorescence images were conducted using ImageJ, as described previously (Anding et al., 2018). Sample sizes (n) in immunofluorescent experiment quantifications represent number of cells.

TEM analyses of mitochondria area was manually calculated by individually analyzing mitochondria using ImageJ. For determination of mitochondria and ER contact sites, mitochondria and ER were individually identified on TEM sections and distance between mitochondria and ER was manually measured using ImageJ. Regions of ER that were within 30nm of mitochondria and had a contact length of at least 20nm were identified as mitochondria and ER contact sites as previously defined.[20] The length of these sites of contact were manually measured for each mitochondria and compared with the entire mitochondria perimeter to determine the percentage in contact. Regions for analyses were randomly selected from embedded blocks for each sample. For each analysis, at least 50 mitochondria from at least 20 sections and 3 independent experiments were used for quantifications. Sample sizes (n) for TEM quantifications represent number of mitochondria.

All experiments are representative of 3 independent replicates. No statistical methods were used to predetermine sample sizes. Preliminary experiments were conducted to achieve similar sample sizes as previous published studies using our model systems. Animals were not excluded for statistical analyses. Researchers were

not blinded. Unless otherwise stated, p values were calculated using the two-tailed student t-test without Welch's correlation. p values greater than 0.05 were considered non-significant (n.s.). All bars are means and error bars are SEM unless otherwise.

Table 3-1: Key Resources Table

REAGENT or RESOURCE	SOURCE	IDENTIFIER
Antibodies		
Vps13D	Eric Baehrecke	[7]
ref(2)p	Gabor Juhasz	[40]
ATP synthase complex V	Abcam	Ab14748
GFP	Abcam	ab13970
SERCA	Mani Ramaswami	[41]
Actin	Proteintech	60008-1-Ig
TOMM20	Abcam	ab78547
MFN2	Abnova	H00009927-M03
COX IV	Abcam	ab14744
anti-mouse AlexaFluor 647	Invitrogen	A-21235
anti-rabbit Alexafluor 546	Invitrogen	A-11035
anti-chicken AlexaFluor 488	Invitrogen	A-11039
anti-mouse Alexa Fluor 488	Invitrogen	A-11029
Oregon Green 488 goat anti-rabbit	Molecular Probes	O-6381
Bacterial and Virus Strains		
E. coli/One Shot TOP10	Invitrogen	C404010
Biological Samples		
Chemicals, Peptides, and Recombinant Proteins		
Fetal bovine serum	Gemini Bio Products	100-106
DMEM	Life Technologies	31053-028
Penicillin-streptomycin	GIBCO	15140122
PBS	GIBCO	70011
25% Glutaraldehyde	Electron Microscopy Sciences	16220
Sodium cacodylate	Electron Microscopy Sciences	11650
osmium tetroxide	SPI	2601
propylene oxide	SPI	75-56-9
SPI-pon/Araldite 6005 epoxy embedding kit	SPI	02635-AB
paraformaldehyde	Electron Microscopy Sciences	15710
Triton x-100	Sigma	T8787
Vectashield	Vector Laboratories	H-1200
Tris-HCl	Sigma	T3253
NaCl	Fisher	BP358-212
Goat serum	Sigma	G9023
EDTA	Quality Biological	351-027-101

3xFLAG peptide	Sigma	F4799-4MG
Critical Commercial Assays		
Deposited Data		
Project Achiles	Broad Institute	[42]
Experimental Models: Cell Lines		
HeLa	ATCC	CCL-2
HeLa *VPS13D* ΔUBA deletion (ΔUBA)	Eric Baehrecke	[7]
HeLa *VPS13D* exon 3 deletion (KO #45)	Eric Baehrecke	[7]
Family 1 Patient Fibroblasts (G1190D/Q1106*): UM1.2	Margit Burmeister	[8]
Family 1 Heterozygote Fibroblasts (Q1106*/+): UM1.17	Margit Burmeister	[8]
Family 1 Unrelated Fibroblasts (+/+): UMCtrl1	Margit Burmeister	[8]
Family 2 Patient Fibroblasts (A4210V/Y1803*): LUB1.1	Katja Lohmann	[8]
Family 2 Heterozygote Fibroblasts (Y1803*/+): LUB1.3	Katja Lohmann	[8]
Family 2 Unrelated Fibroblasts (+/+): LUBCtrl1	Katja Lohmann	[8]
Experimental Models: Organisms/Strains		
Drosophila Melanogaster/*w^{1118}*	Bloomington *Drosophila* stock center	5905
Drosophila Melanogaster/w^{1118}; P{GD15932}v46667	VDRC	46667
Drosophila Melanogaster/w^{1118}; P{KK108366}VIE-260B	VDRC	100745
Drosophila Melanogaster/ y^{1} sc* v^{1} sev21; P{TRiP.HMS01784}attP2	Bloomington *Drosophila* stock center	38320
Drosophila Melanogaster/ y^{1} v^{1}; P{TRiP.JF01355}attP2	Bloomington *Drosophila* stock center	31603
Drosophila Melanogaster/ y^{1} sc* v^{1} sev^{21}; P{TRiP.HMS05713}attP40	Bloomington *Drosophila* stock center	67852
Drosophila Melanogaster/ y^{1} w*; Mi{MIC}Vps13DMI11101	Bloomington *Drosophila* stock center	56282
Drosophila Melanogaster/ w^{1118}; Df(3L)BSC631/TM6C, cu^{1} Sb^{1}	Bloomington *Drosophila* stock center	25722
Drosophila Melanogaster/w^{1118}; Dp(1;3)RC025, PBac{RC025}VK00033/TM6C, Sb1	Bloomington *Drosophila* stock center	38486
Drosophila Melanogaster / w^{1118}; P{20XUAS-tdTomato-Sec61β}attP2	Bloomington *Drosophila* stock center	64747
Drosophila Melanogaster/w*; P{w[+mW.hs]=FRT(w[hs])}2A	Bloomington *Drosophila* stock center	1997
Drosophila Melanogaster/w^{1118}; P{w[+mC]=Ubi-mRFP.nls}3L P{ry[+t7.2]=neoFRT}80B	Bloomington *Drosophila* stock center	30852
Drosophila Melanogaster/w*; P{w[+mC]=Ubi-GFP.D}61EF P{w[+mW.hs]=FRT(w[hs])}2A	Bloomington *Drosophila* stock center	1626

Drosophila Melanogaster/w*; P{w[+mC]=UAS-FLP.D}JD2	Bloomington *Drosophila* stock center	4540
Drosophila Melanogaster/w*; P{GawB}Myo31DFNP0001 / CyO, P{UAS-lacZ.UW14}UW14	*Drosophila* Genetic Resource Center	112001
Drosophila Melanogaster/ P{UAS-mito-QC}attP16	Alexander J. Whitworth	[5]
Drosophila Melanogaster/ *vps13d (ΔUBA)/TM6B*	Eric Baehrcke	[7]
Drosophila Melanogaster/ *vmp1(Δ)*	This paper	N/A
Drosophila Melanogaster/ *gfp-vmp1*	This paper	N/A
Oligonucleotides		
Primer to design sgRNA1: TGTTGTTGTGACGATTGCTC	Integrated DNA Technologies	N/A
Primer to design sgRNA2: TTACGGGACTAGAAAATCAG	Integrated DNA Technologies	N/A
Primer to design sgRNA3: TGCTGTGACATTTAAGCGGT	Integrated DNA Technologies	N/A
Primer to design sgRNA4: CGAATGCTGTGACATTTAAG	Integrated DNA Technologies	N/A
Single-stranded donor DNA to design *vmp1(Δ)*: CAAAAACCGTGAAAAACACAGCCGCTTGCAAGCCA ACCGCTTAAATGTCACAGCATTCGAAAAAGGAAACC ACCAGCAGCAGCGGTAGCCATGCGGCCCAAAAATC AGTGGATCAGTCTTCTGTTGATCTTTTTCCCCAACC CTTGGTTTTCGTTTAAATTATTTTGTATATTGCGGCT TTCGCTCTTAGTCAAATGATG	Integrated DNA Technologies	N/A

G-block donor DNA to design *gfp-vmp1*: TCTCTTTTTTACGCGCATGTGGATTCATTTTATTGGT GCTCAAGTATCGCATGATAATCTCACGCTACGTCCC TCGTAATTGTTGTTGTAATCGCTGTCGTTCTGTCAG CAGAATGTCTTTATTGTTATTGTTGTTGTTGTGCTTT TCCGCCTAACACACACTAACACGCGCACACACAGG CACACTTGCCGAAAAATTGAAGCCATTCTCGCCGCA AATCAAATTCAATTGAGGGAAACTATCAACTAACCC GCATAAAAGTGAGAAAAAAAACATACAGAGAAACAG CCGACACTTTTATACACTTCCAGTTAAAAAAAAAAAT AAAACAGTCAGTAATATAAGTTATTAATATAATTACC CAACAATAAGTTTCATTACAAAAATACAGTTTTTATG TTATATTATTTGAGATTATCATGACGAGTTCCTACAT TTCTTGAATAATTCGGTGTATATGTTTAATAGCAATA TCTGCTAGTTCTTATCACTACTATAGTTTTCATATTTT TCTAAGCTGTGACACATACGTACATAAGTCGTATGT AGCATAATTTTTATATTATTTTTAAAGACCATTATTTC TTAGTTTGCCCTGTGAAATAATCTGACACCTTAACTG GGGATTACAAATTAGCCTACTATCAGTTGGGAACTT ATCCCCTTATCAGTGCTAGTGAAAACCGGCTACCTA AGCGATCTCCAAATTATCATTACCCGTTGTGGCACG CCCGACGAAGCAACCTTAGAGTGGAACGTATATAG AGAGAGAGAGAGCTTCTACACCTTACACCATCACTC ATTTGAAGCTTATCAGTTTATCAGTGGCCTACGACG ATTTGAAATTTCAGTTTCATTTCCATTTCCTACATCG CGTCACCGTCGTGTGTTCAAAATTAATAAATTCTTTT CGAATCGCCGGCATTTACATCACTATTATTTTGTATT TTCATTGCAAAAACCGTGAAAAACACAGCCGCTTGC AAGCCAACCGCTTAAATGGTGAGCAAGGGCGAGGA GCTGTTCACCGGGGTGGTGCCCATCCTGGTCGAGC TGGACGGCGACGTAAACGGCCACAAGTTCAGCGTG TCCGGCGAGGGCGAGGGCGATGCCACCTACGGCA AGCTGACCCTGAAGTTCATCTGCACCACCGGCAAG CTGCCCGTGCCCTGGCCCACCCTCGTGACCACCCT GACCTACGGCGTGCAGTGCTTCAGCCGCTACCCCG ACCACATGAAGCAGCACGACTTCTTCAAGTCCGCCA TGCCCGAAGGCTACGTCCAGGAGCGCACCATCTTC TTCAAGGACGACGGCAACTACAAGACCCGCGCCGA GGTGAAGTTCGAGGGCGACACCCTGGTGAACCGCA TCGAGCTGAAGGGCATCGACTTCAAGGAGGACGGC AACATCCTGGGGCACAAGCTGGAGTACAACTACAA CAGCCACAACGTCTATATCATGGCCGACAAGCAGA AGAACGGCATCAAGGTGAACTTCAAGATCCGCCAC AACATCGAGGACGGCAGCGTGCAGCTCGCCGACCA CTACCAGCAGAACACCCCCATCGGCGACGGCCCCG TGCTGCTGCCCGACAACCACTACCTGAGCACCCAG TCCGCCCTGAGCAAAGACCCCAACGAGAAGCGCGA TCACATGGTCCTGCTGGAGTTCGTGACCGCCGCCG GGATCACTCTCGGCATGGACGAGCTGTACAAGGGT GGATCTGGAGGTTCCGGCGGCTCAGGGGGTAGTAT GTCACAGCATTCGAAAAAGGAAACCACCAGCAGCA GCGGTAGCCATGCGGCCCAGAGCAATCGTCACAAC AACATCGGCGGCGGCGGCGGAAACGGCAATAGCA ACAGCATCAGCGGTAGCAGCAACAACAAGAGCCAC AAGCGGCAGGCGGCCAATGGCAGTCTAAAGTCGCC	Integrated DNA Technologies	N/A

ACTCCTGACAATCACCAACATCAACTCCCACAGCCA AAAAGGCGCTTTGAAATCGCCCGTCAGCAAAGTCAA GCAGAGCAGCAACAGCAGCAGTAGCAACAGTAACA GCAAAACCCTCAGCGGGAGCAGCATGCAGGAGACC GGCTCATCCGCCACATCCTTGCTGGCCGCTGGCGG CAAGGCGAAGAAGAACCAAAAAGACAAGCAGCGCG AGCGGGAACGCTTGGAACGCGGCCAGCTGGTCCT CTGGCGTCGTCCCCTGCAGACCACCAAGTACTGCG GCCTCGAGCTGTTCACCTTGCTGCGCACGTGGAGC ACCAGGTAGGATCGAAAGTAGCCCCATTTTGAAACC ATTTAACCAACGCTTTCCTCGCAGATTGCTGCAACA GCGTCTCCTGTTGGCCACTCTGATAGTATTAAGCAT CGTATTTAGCGTAATTTACAAGATAGACGGTCCCCA TCAGTTGGCCATCGAGTTTGTGCGCCGGAACACCT GGTTCTTTGTCTACTGGTTGGGTCTGGGCGTGCTCT CCTCGGTGGGCTTGGGCACCGGACTGCACACGTTT CTGCTCTATCTGGGGCCGCACATAGCCAGTGTCAC GCTGGCCGCCTACGAGTGCAATTCCCTGCGATTCC CACAGCCACCGTATCCCGATGAGTAAGTACATGTAG GTTCTCTTCCTCATTGCTTGATAACTAACTGCCTGTT CTTGCTTACTCCTACAGTATTATCTGTCCCGAGGAG CCGTACGACAAACATGTGCCAAATATCTGGTCCATT ATGTCCAAGGTGCGCCTGGAGGCCTTCCTCTGGGG AGCGGGCA		
Primer to screen and verify 5’ of *vmp1(Δ)* and *gfp-vmp1*: CTTTTCGAATCGCCGGCATTTACATCAC	Integrated DNA Technologies	N/A
Primer to screen and verify 3’ of *vmp1(Δ)* and *gfp-vmp1*: CATCATTTGACTAAGAGCGAAAGCCGC	Integrated DNA Technologies	N/A
Primer to verify 3’ N terminus *vmp1* of *gfp-vmp1*: CTGATGCTGTTGCTATTGCCGTTTCC	Integrated DNA Technologies	N/A
siRNA NC negative (mock) control: UUCUCCGAACGUGUCACGUTT	Hong Zhang	[20]
siRNA Human *VMP1*: 5’-GGAAUGGACCUCAAAAUUATT-3’	Hong Zhang	[20]
siRNA SMARTpool for *Human MFN2*: GACUAUAAGCUGCGAAUUA CAUGAGGCCUUUCUCCUUA GCAACUCUAUCGUCACAGU GGUGGACGAUUACCAGAUG	Dharmacon	N/A
Recombinant DNA		
Plasmid: U6droBsagRNA	Drosophila Genomics Resource Center	1341
Plasmid: pCR™2.1-TOPO® vector	Thermo Fisher Scientific	K450002
Software and Algorithms		
ImageJ	NIH	https://imagej.nih.gov/ij/
Zen Black	Zeiss	N/A
Prism	Graphpad Software, Inc.	https://www.graphpad.com/scientific-software/prism/

Other

Acknowledgments

We thank the Baehrecke and Zhang laboratories, R. Youle, C. Wang, G. Juhasz, M. Ramaswami, A.J. Whitworth, the Vienna Drosophila Resource Center, the Bloomington Stock Center, the Kyoto Drosophila Genetic Resource Center, and the Electron Microscopy Core Facility at UMass Medical School for advice, flies, antibodies, cell lines and technical support. We would like to thank the VPS13D-patients and their relatives, and K. Lohmann, J.E. Gudjonsson,, E. Seong, and L. Gates with establishing or maintaining iPSCs of VPS13D patients and relatives. This work was supported by R35GM131689 to E.H.B. and F30CA239374 to J.L.S.

Author contributions

J.L.S., Y.G.Z. and E.H.B. designed experiments, J.L.S. and T.M.F. performed experiments, R.W. and M.B. provided resources, J.L.S. and E.H.B. wrote the manuscript and all authors commented on it.

Chapter IV

Discussion and Conclusions

Mitochondria play critical roles in cell metabolism, signaling and homeostasis. The ability to remove mitochondria in response to stress and developmental stimuli is a crucial factor in maintaining animal health and preventing disease. My thesis utilizes the physiological mitophagy machinery in pupating *Drosophila* larval intestines to investigate the role of Vps13D in mitophagy. I identify that in the core autophagy machinery, Vps13D acts downstream of autophagy initiators, but upstream of the Atg8a conjugation pathway. I discover that Vps13D regulates ubiquitin and Atg8a localization around mitochondria in mitophagy. Vps13D acts downstream of Pink1-mediated phosphorylation and conjugation of ubiquitin around mitochondria. Furthermore, Vps13D and Pink1 regulate mitochondrial size in a shared pathway. This process acts independently of Park, which when ablated, does not have the abnormal mitochondrial and autophagy phenotypes seen in *pink1* and *vps13d* mutants.

Vps13D belongs to the Vps13 family of proteins, which act as lipid transporters at membrane contacts between organelles. This connection between Vps13D and membrane contacts led me to identify a functional interaction between Vps13D and Vmp1, a regulator of the disassembly between mitochondria and ER membrane contacts. Vmp1 functions upstream of Vps13D in a shared pathway to regulate autophagy, mitochondrial size, and mitochondria and ER contact sites. *Vps13d* mutants in *Drosophila* and human cell culture models, including fibroblasts from patients suffering neurological symptoms associated with *VPS13D* mutations, had increased

mitochondria and ER contact. Further investigation revealed that this regulation of mitochondria and ER contact sites depended on Marf/Mfn2, a positive regulator of mitochondrial fusion that tethers mitochondria and ER membranes. I identify that Marf physically interacts with Vps13D in *Drosophila,* loss of Marf suppresses the mitochondrial and membrane contact phenotypes in *vps13d* loss-of-function mutants*,* and loss of Vps13D has increased Marf levels in pupating larval intestine cells. Taken together, I characterize the pathways in which Vps13D regulates mitophagy, mitochondrial size, and membrane contacts.

Regulation of Vps13D by the Core Autophagy Machinery

Mitophagy in the pupating larval intestine depends on autophagy genes and *vps13d* (Chang et al., 2013; Anding et al., 2018), with *vps13d* mutants having enlarged Atg8a puncta surrounding uncleared mitochondria. Loss of certain core autophagy genes depletes Vps13D puncta and suppresses the abnormal Atg8a localization in *vps13d* mutants. This suggests that the core autophagy machinery and Vps13D act in a shared pathway in this process. However, loss of Atg8a-conjugating proteins do not seem to affect Vps13D puncta formation. These proteins act downstream of other autophagy regulating complexes in the core autophagy machinery, suggesting that Vps13D may be recruited in a relatively upstream step. The accumulation of Atg8a and conjugated ubiquitin around mitochondria in *vps13d* mutants suggests that functionally, Vps13D is required for a process in mitophagy after these proteins are already localized to mitochondria **(Figure 4-1)**.

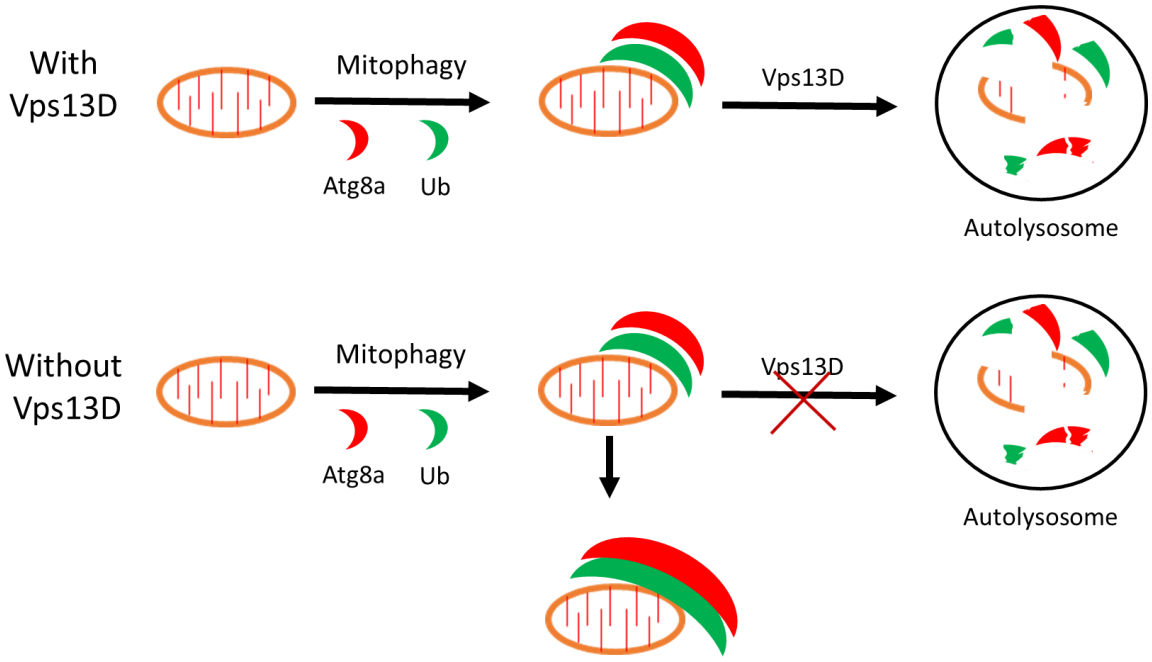

Figure 4-1: General model of where Vps13D acts in mitophagy. Vps13D is required for mitophagy in a step between recruitment of Atg8a and ubiquitin to mitochondria and formation of the autolysosome. Please refer to text for possible mechanisms.

Investigating how loss of Vps13D function results in an accumulation of conjugated ubiquitin and Atg8a around the mitochondria is an important future direction. There are a number of possibilities given what we currently know about Vps13D localization and known roles of other Vps13 family members. *atg2* mutants in *C elegans* have abnormal, enlarged autophagosomal structures similar to those we see in *vps13d* mutants (Lu et al., 2011). Atg2 acts as a lipid transporter in autophagy, providing phospholipids for the growing phagophore (Valverde et al., 2019). This function depends on the Chorein_N domain, which has high conservation with the Vps13D Chorein_N domain. It is possible that Vps13D, like Atg2, may act as a lipid transporter at the site of autophagosome formation. Vps13D could be recruited to ubiquitin localized

around the mitochondria and facilitate transfer of lipids to the expanding autophagosome membrane as it encapsulates the mitochondria. The enlarged Atg8a structures surrounding mitochondria in *vps13d* mutants could thus be the result of stalled autophagosome formation around mitochondria. Designing and characterizing *vps13d* mutants with alterations in this Chorein_N domain, particularly those that are known to impair function in Atg2, will be important for determining if this is the case. Further biochemical studies, including assays to measure lipid transfer activity in Vps13D, are also necessary to test this hypothesis.

Loss of core autophagy genes important for the initiation of autophagosome formation, including *atg1* and *atg6*, decreases Vps13D puncta. As Vps13D puncta normally localizes to ubiquitin, it is thus likely that the core autophagy machinery regulates recruitment of Vps13D to ubiquitin. Conjugated ubiquitin localization depends on which core autophagy gene is ablated. Knockdown of *atg1* suppresses the formation of conjugated ubiquitin puncta while knockdown of *atg8a* results in enlarged, conjugated ubiquitin puncta (Anding et al., 2018). It is thus possible that Vps13D could act as a mediator between the core autophagy and ubiquitin. Additional studies looking into the mechanism of these phenotypes, including ubiquitin localization in *vps13d* and core autophagy gene double mutants, will help clarify how the core autophagy machinery regulates ubiquitin localization with Vps13D.

An important future direction will be to investigate how localization of Vps13D affects function. Yeast Vps13 is highly dynamic, localizing to membrane contact sites at endosomes, vacuoles, endoplasmic reticulum, mitochondria, and the prospore

membrane depending on the which adaptors bind with Vps13 (Bean et al., 2018). The divergence of yeast Vps13 into four paralogs in higher eukaryotes is suggested to have compartmentalized Vps13 family member localization (Kumar et al., 2018). However, Vps13D still appears to localize to many different intracellular components. Proteomic studies in mammalian cells suggest that Vps13D can be recruited to mitochondria and ER contact sites (Hung et al., 2017; Antonicka et al., 2020). Studies in *Drosophila* suggest that Vps13D localizes to the ER-Golgi intermediate compartment (ERGIC), a structure that serves as a transport hub between the ER and Golgi Body (Wang et al., unpublished). Furthermore, Vps13D localizes to Lamp1, a reporter for late endosomes/lysosomes (Anding et al., 2018). Vps13D interacts with rab6 and rab9, two endosomal localizing proteins, in *Drosophila* S2 cells (Gillingham et al., 2014). Establishing a better understanding of context-dependent Vps13D localization, such as immuno-TEM of *vps13d-3xFLAG* larvae, before and after pupariation, will be invaluable in this aspect.

One mechanism not pursued in my thesis is the role of the ESCRT pathway, which regulates trafficking of endosomes and lysosomes, in Vps13D recruitment. Loss of Vps25 and Tsg101, two core components ESCRT, have depleted Vps13D puncta (Anding et al., 2018; Wang et al., unpublished). Endosomes play an important role in the maturation of autophagosomes and eventual fusion with lysosomes (Hyttinen et al., 2013; Birgisdottir and Johansen, 2020). Inhibition of endosome formation has been shown to impair autophagy and cause an accumulation of autophagic structures (Razi et al., 2009; Lefebvre et al., 2018), consistent with the accumulation of Atg8a and conjugated ubiquitin around mitochondria in *vps13d* mutants. The failure to clear

mitochondria and accumulation of enlarged Atg8a puncta similar in morphology to loss-of-function *vps13d* mutants was also present in ESCRT loss-of-function mutants (data not shown). Further studies into the role of ESCRT on Vps13D, such as determining Vps13D localization in cells depleted of certain ESCRT proteins and endosome/lysosome recruitment to mitochondria in *vps13d* mutants, are required to investigate these possibilities.

Relationship between Pink1 and Vps13D

I demonstrate that Pink1, like certain core autophagy genes, is required for Vps13D puncta formation. Loss of Pink1 also phenocopies the autophagy, Atg8a localization, and mitochondrial clearance phenotypes in *vps13d* mutants. These findings suggest that, in the pupating larval intestine cells, Pink1 and Vps13D function in a shared mitophagy pathway. One potential mechanism is that Pink1 could recruit Vps13D to conjugated ubiquitin through the core autophagy machinery. It has been shown that during mitophagy, Pink1 interacts with and recruits Atg6 to the mitochondria and ER contact sites, which may then recruit other factors to this site, including Vps13D (Michiorri et al., 2010; Gelmetti et al., 2017). Consistent with this hypothesis, Vps13D appears to regulate mitochondria and ER contact sites in multiple experimental models. While Parkin is also recruited to this site, the recruitment of Atg6 to the mitochondria and ER contact sites acts independently of Parkin (Gelmetti et al., 2017). These findings are consistent with Vps13D acting through this mechanism as *park* loss-of-function mutants fail to phenocopy *vps13d* loss-of-function mutants in pupating larval intestines.

Another mechanism is direct phosphorylation of Vps13D by Pink1 or downstream kinases (Auburger et al., 2019), which could potentially recruit or activate Vps13D. Proteomic studies that investigate Vps13D phosphorylation in a Pink1 loss-of-function background and if Pink1 and Vps13D physically interact will help address this possibility.

I demonstrate that Vps13D has a context-dependent interaction with ubiquitinated proteins 2 hours after pupariation. Consistent with these findings, Vps13D and ubiquitin co-localize specifically during pupariation and deletion of the UBA domain, shown to interact with K63 ubiquitin chains *in vitro* (Anding et al., 2018), is crucial for this co-localization. Conjugated ubiquitin seems to accumulate around mitochondria in *vps13d* mutants, consistent with a model where Vps13D regulates mitophagy after ubiquitin recruitment to the mitochondria. The loss of Pink1 suppresses this localization, which could be explained by Pink1 playing a role in recruitment of conjugated ubiquitin to mitochondria. Pink1 phosphorylates ubiquitin conjugated to OMM proteins, which inhibits de-ubiquitination and leads the further ubiquitination of OMM substrates (Wauer et al., 2015). Pink1 also phosphorylates Parkin, facilitating a feed-forward mechanism that accelerates ubiquitination and labeling of mitochondria for mitophagy (Koyano et al., 2014; Ordureau et al., 2014). It is possible that these expanding ubiquitin chains recruit Vps13D, placing Vps13D downstream of ubiquitin phosphorylation and conjugation around the mitochondria. Additional biochemical studies, such as testing if Vps13D binds with phosphorylated ubiquitin or ubiquitinated forms of OMM proteins, will be required to investigate this model.

I have characterized a previously unknown relationship between Pink1 and Vps13D in the regulation of mitochondrial size. *pink1* and *vps13d* single mutants both have enlarged mitochondria, with *pink1* and *vps13d* double mutants failing to have an additive increase in mitochondrial size compared to single mutants. These abnormal, large mitochondria are unable to be cleared by mitophagy, as they are present 2 hours after pupariation when most mitochondria are already cleared. Thus, Vps13D and Pink1 could also act in a shared pathway that regulates mitochondrial dynamics. Pink1 promotes mitochondrial fission while inhibiting mitochondrial fusion, which could explain the enlarged mitochondria in *pink1* loss-of-function mutants (Pryde et al., 2016; Deng et al., 2008; McLelland et al. 2018; Burman et al., 2017). Drp1 facilitates Pink1-mediated mitophagy by regulating mitochondrial fission (Burman et al., 2017). In *VPS13D* mutant HeLa cells, the amount of phosphorylated Drp1 at the S616 residue is increased, which is the same site that Pink1 phosphorylates Drp1 to enhance mitochondrial fission (Han et al., 2020). *drp1* loss-of-function mutants also have many of the same phenotypes as *vps13d* loss-of-function mutants, including enlarged mitochondria and a cell size reduction deficiency in pupating larval intestine cells (Anding et al., 2018). Further investigation between the roles of Vps13D and Drp1 through approaches such as double mutant analysis, in addition to other factors implicated in Pink1-mediated mitophagy such as MTX1 (Le Guerroué et al., 2017), will help address this possibility.

One aspect of autophagy that is often overlooked is the process of autophagosome engulfment of the cargo (Xie and Klionsky, 2007; Shaid and Brandts 2013). The mitochondria in *pink1* and *vps13d* loss-of-function mutants are enlarged, and this would require the autophagic machinery to expand the autophagosome more

than in the case of normal-sized mitochondria. This would require additional recruitment of resources, including autophagy proteins and autophagosome membrane components, to the forming autophagosome. This increased resource burden to degrade mitochondria could siphon resources necessary for the clearance of other cargo and organelles, indirectly impairing more than just mitophagy. The excessive removal of membranes and resources from other organelles could also affect functions beyond autophagy. If this is the case, it would be an example of how impairing selective autophagy could affect multiple cellular processes.

Vmp1 and Vps13D Regulation of Mitochondria and ER Contact Sites

In my thesis, I show that Vmp1 and Vps13D are functionally linked through regulation of mitophagy, mitochondrial size, and mitochondria and ER contact sites. In pupating larval intestine cells, *vmp1* and *vps13d* loss-of-function mutants have enlarged mitochondria that are unable to be cleared. Loss of Vmp1 in mammalian cell lines results in increased contact between the mitochondria and ER (Zhao et al., 2017), similar to what we see in loss-of-function *vps13d* mutant cell lines. In *Drosophila* intestines, *vmp1* and *vps13d* double mutant cells do not have an additive mitochondrial clearance phenotype. *vmp1* mutant intestine cells have decreased Vps13D puncta, suggesting that Vps13D acts downstream of Vmp1. However, the mechanistic details defining the relationship between these two genes remains unexplored. Vmp1 regulates the local Ca^{2}+ levels between membranes through an interaction with the calcium channel SERCA (Zhao et al., 2017). Biochemical experiments investigating if Vps13D

interacts with Vmp1, or downstream proteins like SERCA, will help elucidate this mechanism.

The enlarged mitochondria seen in Vmp1 and Vps13D depleted intestine cells are suppressed by *marf* knockdown, suggesting that Marf functions downstream of Vps13D in this pathway. *vps13d* mutant intestine cells have more Marf than control cells, which is consistent with Vps13D facilitating Marf degradation during mitophagy. It is known that Pink1 regulates the ubiquitination of Mfn2 to facilitate degradation during mitophagy (Chen and Dorn, 2013). As Vps13D interacts with both ubiquitinated cargo and Marf, one possibility is that Vps13D interacts with ubiquitinated Marf to facilitate degradation, suppressing mitochondrial fusion and mitochondria and ER tethering. Further biochemical analysis will be required to test this hypothesis.

The role of Vps13D as a disassembler of membrane contacts is surprising, as Vps13A and Vps13C seem to act as membrane tethers (Kumar et al., 2018). These findings suggest that Vps13D plays a distinct role compared to other Vps13 family members. This is consistent with the many unique aspects of Vps13D, including being the only Vps13 family member that is essential (Wang et al., 2015; Blomen et al., 2015; Meyers et al., 2017) and having an ubiquitin binding domain (Anding et al., 2018). This role in disassembling membrane contacts between the mitochondria and ER is consistent with the phenotypes observed in *vps13d* mutants. Mitochondria and ER membrane contact sites are sites of autophagosome formation and are essential for mitophagy (Hamasaki et al., 2013; Böckler and Westermann, 2014). Ubiquitin and regulators of autophagy could be recruited to these sites, but without membrane

disassembly to allow the forming autophagosome to expand, these factors would simply accumulate. This could explain the increase in Atg8a and ubiquitin around the mitochondria **(Figure 4-2)**. Furthermore, mitochondria and ER contact sites are sites that regulate mitochondrial fission and fusion (Friedman et al., 2011; Moltedo et al., 2019). Regulation of these processes could be disrupted when disassembly is impaired, especially given the dynamic nature of membrane contact site formation. Studies investigating how disassembly of mitochondria and ER membrane contact sites affect autophagosome formation and mitochondrial dynamics will provide additional models for the mechanism of Vps13D function.

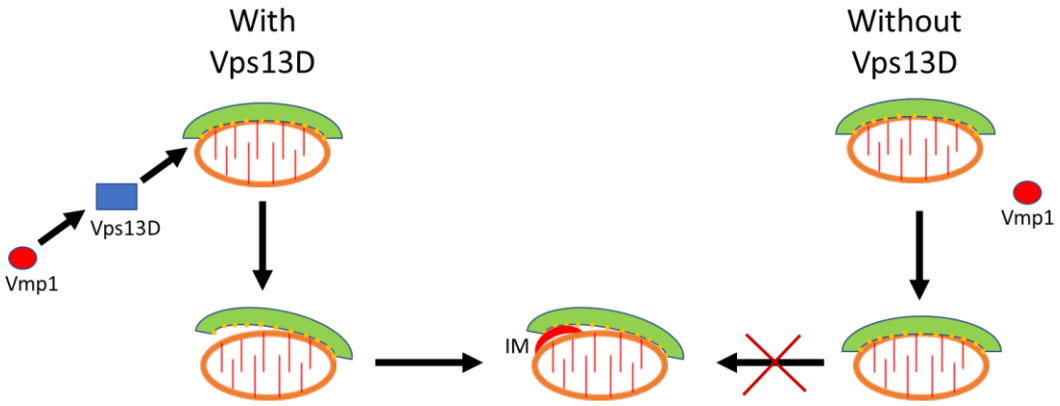

Figure 4-2: Proposed model of the relationship between Vmp1 and Vps13D. Vmp1 and Vps13D regulate disassembly of mitochondria and ER membrane contacts, enabling formation of the isolation membrane (IM)

Connection between the Core Autophagy Machinery, Pink1, and Vmp1

In my thesis, I characterize the role that Vps13D plays in mitophagy pathways regulated by the core autophagy machinery, Pink1, and Vmp1. These pathways are highly connected with multiple overlapping functions, including regulation of autophagy and

mitochondria and ER contact sites. Vmp1 is known to interact with Atg6, and this interaction is important for the autophagy functions of both proteins (Molejon et al., 2013). This is consistent with recruitment of Atg6 by Pink1 to the mitochondria and ER contact sites in mitophagy, which places Pink1, Atg6, and Vmp1 in the same intracellular localization (Michiorri et al., 2010; Gelmetti et al., 2017; Zhao et al., 2017). Loss of Vmp1 increases mitochondria and ER contact sites in mammalian cell lines (Zhao et al., 2017). Similarly, loss of Pink1 in *Drosophila* neurons and human cell lines also increases mitochondria and ER contact sites (Valadas et al., 2018; Lee et al., 2018; McLelland et al., 2018). It has been proposed that Pink1 decreases mitochondria and ER contact sites through degradation of mitochondria and ER tethering proteins, including Mfn2 and Miro, which are suggested to interact with Vps13D (Wang et al., 2011; McLelland et al., 2018; Antonicka et al., 2020). Given how Vps13D is involved in several pathways mediated by these proteins, it begs the question of if there is a distinct pathway involving Pink1, Atg6, Vmp1, and Vps13D. The overlap in function, loss-of-function phenotypes, and potential localization of all these factors to the mitochondria and ER contact sites could suggest that they all serve in an identical complex or mechanism. Investigating this possibility will not only improve our understanding of these proteins, but also expand our understanding of how membrane contacts, mitochondrial dynamics, and autophagy are connected.

Given that many of the molecular mechanisms of the core autophagy machinery, Pink1, and Vmp1 are well characterized, a similar characterization of Vps13D on a molecular level is an important future direction. Regulation of Atg8a localization could be coordinated by a direct interaction between Vps13D and Atg8a, as there are multiple

predicted Atg8a-interacting motifs (AIMs) on Vps13D (Anding et al., 2018). However, an *in vivo* interaction between Atg8a and Vps13D has not yet been identified. If Vps13D and Atg8a do interact, this interaction is unlikely to have the same purpose as Atg8a interactions with autophagy receptors, which play an important role in recruiting Atg8a to mitochondria during mitophagy(Lazarou et al., 2015). This hypothesis is supported by data showing that Atg8a is still able to localize to mitochondria in *vps13d* mutants. Rather, given the presence of the Chorein_N domain on Vps13D, Vps13D may play an important role in the distribution of Atg8a-associated membranes around the mitochondria, similar to Atg2 (Osawa and Noda, 2019). The disassembly of mitochondria and ER contact sites may play an important role in this process. Failure to expose portions of the mitochondria in contact with the ER may limit the ability of Pink1 to target outer mitochondrial membrane proteins for ubiquitination, thus preventing the core autophagy machinery from engulfing the mitochondria. Vmp1 is known to regulate the disassembly of mitochondria and ER membrane contact sites through calcium channel signaling by SERCA (Zhao et al., 2017). It is possible that Vps13D could also regulate these membrane contact sites through calcium channel signaling, as immunoprecipitation assays have identified an interaction between Vps13D and SERCA in *Drosophila* (data not shown). While speculative, testing these hypotheses will be crucial for better understanding the molecular functions of Vps13D.

D. Significance of Findings

VPS13D is also associated with multiple diseases, including neurological movement disorders and septic shock. However, these associations are poorly characterized on

the mechanistic level. Furthermore, it is unknown why *Vps13D* is such an essential gene when other *Vps13* family members are not. Here, I have characterized multiple aspects of Vps13D function. Vps13D acts in a Vmp1-regulated pathway of disassembling mitochondria and ER membrane contact sites, which are crucial sites for autophagosome generation, lipid metabolism, calcium signaling, and organelle function. Vps13D acts in the core autophagy machinery and regulates Atg8a and ubiquitin localization. Vps13D also regulates mitochondrial dynamics and functions downstream of Pink1-mediated mitophagy. These functions are crucial for cell health and survival, and thus my findings provide multiple possible explanations for how *VPS13D* plays a role in these diseases and survival. The regulation of autophagy, mitochondrial dynamics, and mitochondria and ER membrane contacts are often studied in isolation despite being connected through common regulatory pathways. A better understanding of Vps13D not only helps us better understand these functions individually, but can also explain how all of these functions are connected. Further mechanistic studies into these newly defined functions will be critical to understanding the significance of this vital gene.

Appendix

Table A1: Screen for genes required for Vps13D puncta formation in pupating larval intestines.

Gene	Abberation	Bloomington/VDRC #	Misc Identification	Vps13D Puncta Phenotype	Comments
atg1	Loss-of-function mutant, *atg1(1)*	N/A	Toda et al., 2008	Less	
atg2	RNAi	27706		Less	
atg3	RNAi	24359		No change	
atg5	RNAi	27551		No change	Cell size reduction phenotype present
	RNAi	10655		No change	Cell size reduction phenotype present
atg6	Loss-of-function mutant, *atg6(Δ)*	N/A	Shravage et al., 2013	Less	
atg7	RNAi	27707		No change	
atg8a	Hypomorph, *atg8a (MiMic)*	59357		No change	Cell size reduction phenotype present
atg8b	RNAi	27554		No change	
atg9	Loss-of-function mutant, *atg9(d51)*	N/A	Wen et al., 2013	Less	
atg12	RNAi	34675		No change	Cell size reduction phenotype present
	RNAi	27552		No change	Cell size reduction phenotype present
atg16	Loss-of-function mutant, *atg16(1)*	N/A	Shen et al., 2021 (unpublished)	No change	Cell size reduction phenotype present
	Loss-of-function mutant, *atg16 (d67)*	N/A	Juhasz et al., 2017	No change	Cell size reduction phenotype present
rab5	RNAi	30518		Less	
rab6	RNAi	27490		Less	
rab7	RNAi	v40338		Less	
	RNAi	20751		Less	
rab9	RNAi	31688		No change	
	RNAi	v36201		No change	
vmp1	Loss-of-function mutant, *vmp1(Δ)*	N/A	Shen et al., 2021 (unpublished)	Less	Remaining Puncta is Enlarged
pink1	Loss-of-function mutant, *pink1 (B9)*	34749	Park et al., 2006	Less	
mff	RNAi	43116		No change	Mild cell size reduction phenotype presen
park	Loss-of-function mutant, *park(25)*	N/A	Greene et al., 2003	No change	Non-clonal analysis
mul1	Loss-of-function mutant, *mul1(A6)*	N/A	Yun et al., 2014	No change	Non-clonal analysis

Bibliography

Akutsu, M., Dikic, I., and Bremm, A. (2016). Ubiquitin chain diversity at a glance. J Cell Sci *129*, 875-880.

Allen, G.F., Toth, R., James, J., and Ganley, I.G. (2013). Loss of iron triggers PINK1/Parkin-independent mitophagy. EMBO Rep *14*, 1127-1135.

Anding, A.L., and Baehrecke, E.H. (2015). Autophagy in Cell Life and Cell Death. Curr Top Dev Biol *114*, 67-91.

Anding, A.L., Wang, C., Chang, T.-K., Sliter, D.A., Powers, C.M., Hofmann, K., Youle, R.J., and Baehrecke, E.H. (2018). Vps13D Encodes a Ubiquitin-Binding Protein that Is Required for the Regulation of Mitochondrial Size and Clearance. Curr Biol *28*, 287-295.e286.

Antonicka, H., Lin, Z.-Y., Janer, A., Aaltonen, M.J., Weraarpachai, W., Gingras, A.-C., and Shoubridge, E.A. (2020). A High-Density Human Mitochondrial Proximity Interaction Network. Cell Metab *32*, 479-497.e479.

Arakawa, S., Tsujioka, M., Yoshida, T., Tajima-Sakurai, H., Nishida, Y., Matsuoka, Y., Yoshino, I., Tsujimoto, Y., and Shimizu, S. (2017). Role of Atg5-dependent cell death in the embryonic development of Bax/Bak double-knockout mice. Cell Death Differ *24*, 1598-1608.

Araki, Y., Ku, W.C., Akioka, M., May, A.I., Hayashi, Y., Arisaka, F., Ishihama, Y., and Ohsumi, Y. (2013). Atg38 is required for autophagy-specific phosphatidylinositol 3-kinase complex integrity. J Cell Biol *203*, 299-313.

Armstrong, M.J., and Okun, M.S. (2020). Diagnosis and Treatment of Parkinson Disease: A Review. JAMA *323*, 548-560.

Auburger, G., Gispert, S., Torres-Odio, S., Jendrach, M., Brehm, N., Canet-Pons, J., Key, J., and Sen, N.-E. (2019). SerThr-PhosphoProteome of Brain from Aged PINK1-KO+A53T-SNCA Mice Reveals pT1928-MAP1B and pS3781-ANK2 Deficits, as Hub between Autophagy and Synapse Changes. Int J Mol Sci *20*, 3284.

Axe, E.L., Walker, S.A., Manifava, M., Chandra, P., Roderick, H.L., Habermann, A., Griffiths, G., and Ktistakis, N.T. (2008). Autophagosome formation from membrane compartments enriched in phosphatidylinositol 3-phosphate and dynamically connected to the endoplasmic reticulum. J Cell Biol *182*, 685-701.

Bean, B.D.M., Dziurdzik, S.K., Kolehmainen, K.L., Fowler, C.M.S., Kwong, W.K., Grad, L.I., Davey, M., Schluter, C., and Conibear, E. (2018). Competitive organelle-specific adaptors recruit Vps13 to membrane contact sites. J Cell Biol *217*, 3593-3607.

Berry, D.L., and Baehrecke, E.H. (2007). Growth arrest and autophagy are required for salivary gland cell degradation in Drosophila. Cell *131*, 1137-1148.

Bhujabal, Z., Birgisdottir, Å.B., Sjøttem, E., Brenne, H.B., Øvervatn, A., Habisov, S., Kirkin, V., Lamark, T., and Johansen, T. (2017). FKBP8 recruits LC3A to mediate Parkin-independent mitophagy. EMBO Rep *18*, 947-961.

Birgisdottir, Å.B., and Johansen, T. (2020). Autophagy and endocytosis – interconnections and interdependencies. J Cell Sci *133*, jcs228114.

Blomen, V.A., Májek, P., Jae, L.T., Bigenzahn, J.W., Nieuwenhuis, J., Staring, J., Sacco, R., van Diemen, F.R., Olk, N., Stukalov, A.*, et al.* (2015). Gene essentiality and synthetic lethality in haploid human cells. Science *350*, 1092.

Böckler, S., and Westermann, B. (2014). ER-mitochondria contacts as sites of mitophagosome formation. Autophagy *10*, 1346-1347.

Böckler, S., and Westermann, B. (2014). Mitochondrial ER Contacts Are Crucial for Mitophagy in Yeast. Dev Cell *28*, 450-458.

Bousquet, M., Noirot, C., Accadbled, F., Sales de Gauzy, J., Castex, M.P., Brousset, P., and Gomez-Brouchet, A. (2016). Whole-exome sequencing in osteosarcoma reveals important heterogeneity of genetic alterations. Ann Oncol *27*, 738-744.

Brickner, J.H., and Fuller, R.S. (1997). SOI1 encodes a novel, conserved protein that promotes TGN-endosomal cycling of Kex2p and other membrane proteins by modulating the function of two TGN localization signals. J Cell Biol *139*, 23-36.

Burman, J.L., Pickles, S., Wang, C., Sekine, S., Vargas, J.N.S., Zhang, Z., Youle, A.M., Nezich, C.L., Wu, X., Hammer, J.A.*, et al.* (2017). Mitochondrial fission facilitates the selective mitophagy of protein aggregates. J Cell Biol *216*, 3231-3247.

Burman, J.L., Pickles, S., Wang, C., Sekine, S., Vargas, J.N.S., Zhang, Z., Youle, A.M., Nezich, C.L., Wu, X., Hammer, J.A.*, et al.* (2017). Mitochondrial fission facilitates the selective mitophagy of protein aggregates. J Cell Biol *216*, 3231-3247.

Cecconi, F., and Levine, B. (2008). The role of autophagy in mammalian development: cell makeover rather than cell death. Dev Cell *15*, 344-357.

Chakrabarti, R., Ji, W.-K., Stan, R.V., de Juan Sanz, J., Ryan, T.A., and Higgs, H.N. (2018). INF2-mediated actin polymerization at the ER stimulates mitochondrial calcium uptake, inner membrane constriction, and division. J Cell Biol *217*, 251-268.

Chang, T.-K., Shravage, B.V., Hayes, S.D., Powers, C.M., Simin, R.T., Harper, J.W., and Baehrecke, E.H. (2013). Uba1 functions in Atg7- and Atg3-independent autophagy. Nat Cell Biol *15*, 1067-1078.

Chen, G., Kroemer, G., and Kepp, O. (2020). Mitophagy: An Emerging Role in Aging and Age-Associated Diseases. Front. Cell Dev. Biol. *8*.

Chen, R.-H., Chen, Y.-H., and Huang, T.-Y. (2019). Ubiquitin-mediated regulation of autophagy. J Biomed Sci *26*, 80.

Chen, Y., and Dorn, G.W., 2nd (2013). PINK1-phosphorylated mitofusin 2 is a Parkin receptor for culling damaged mitochondria. Science *340*, 471-475.

Chino, H., and Mizushima, N. (2020). ER-Phagy: Quality Control and Turnover of Endoplasmic Reticulum. Trends Cell Biol *30*, 384-398.

Cohen, M.M., Jr., Hall, B.D., Smith, D.W., Graham, C.B., and Lampert, K.J. (1973). A new syndrome with hypotonia, obesity, mental deficiency, and facial, oral, ocular, and limb anomalies. J Pediatr *83*, 280-284.

Dasari, S.K., Bialik, S., Levin-Zaidman, S., Levin-Salomon, V., Merrill, A.H., Jr., Futerman, A.H., and Kimchi, A. (2017). Signalome-wide RNAi screen identifies GBA1 as a positive mediator of autophagic cell death. Cell Death Differ *24*, 1288-1302.

de Brito, O.M., and Scorrano, L. (2008). Mitofusin 2 tethers endoplasmic reticulum to mitochondria. Nature *456*, 605-610.

De Tito, S., Hervás, J.H., van Vliet, A.R., and Tooze, S.A. (2020). The Golgi as an Assembly Line to the Autophagosome. Trends Biochem Sci *45*, 484-496.

Deas, E., Plun-Favreau, H., Gandhi, S., Desmond, H., Kjaer, S., Loh, S.H., Renton, A.E., Harvey, R.J., Whitworth, A.J., Martins, L.M.*, et al.* (2011). PINK1 cleavage at position A103 by the mitochondrial protease PARL. Hum Mol Genet *20*, 867-879.

Dempster, J.M., Rossen, J., Kazachkova, M., Pan, J., Kugener, G., Root, D.E., and Tsherniak, A. (2019). Extracting Biological Insights from the Project Achilles Genome-Scale CRISPR Screens in Cancer Cell Lines. bioRxiv, 720243.

Deng, H., Dodson, M.W., Huang, H., and Guo, M. (2008). The Parkinson's disease genes pink1 and parkin promote mitochondrial fission and/or inhibit fusion in Drosophila. Proc Natl Acad Sci U S A *105*, 14503-14508.

Deng, Z., Purtell, K., Lachance, V., Wold, M.S., Chen, S., and Yue, Z. (2017). Autophagy Receptors and Neurodegenerative Diseases. Trends Cell Biol *27*, 491-504.

Denton, D., and Kumar, S. (2019). Autophagy-dependent cell death. Cell Death Differ *26*, 605-616.

Denton, D., Shravage, B., Simin, R., Mills, K., Berry, D.L., Baehrecke, E.H., and Kumar, S. (2009). Autophagy, not apoptosis, is essential for midgut cell death in Drosophila. Curr Biol *19*, 1741-1746.

Duplomb, L., Duvet, S., Picot, D., Jego, G., El Chehadeh-Djebbar, S., Marle, N., Gigot, N., Aral, B., Carmignac, V., Thevenon, J.*, et al.* (2013). Cohen syndrome is associated with major glycosylation defects. Hum Mol Genet *23*, 2391-2399.

Dupont, N., Chauhan, S., Arko-Mensah, J., Castillo, E.F., Masedunskas, A., Weigert, R., Robenek, H., Proikas-Cezanne, T., and Deretic, V. (2014). Neutral lipid stores and lipase PNPLA5 contribute to autophagosome biogenesis. Curr Biol *24*, 609-620.

Farré, J.-C., and Subramani, S. (2016). Mechanistic insights into selective autophagy pathways: lessons from yeast. Nat. Rev. Mol. Cell Biol. *17*, 537-552.

Friedman, J.R., Lackner, L.L., West, M., DiBenedetto, J.R., Nunnari, J., and Voeltz, G.K. (2011). ER tubules mark sites of mitochondrial division. Science *334*, 358-362.
Friedman, J.R., and Nunnari, J. (2014). Mitochondrial form and function. Nature *505*, 335-343.

Galluzzi, L., Vitale, I., Aaronson, S.A., Abrams, J.M., Adam, D., Agostinis, P., Alnemri, E.S., Altucci, L., Amelio, I., Andrews, D.W.*, et al.* (2018). Molecular mechanisms of cell death: recommendations of the Nomenclature Committee on Cell Death 2018. Cell Death Differ *25*, 486-541.

Gao, M., and Yang, H. (2018). VPS13: A lipid transfer protein making contacts at multiple cellular locations. J Cell Biol *217*, 3322-3324.

Gauthier, J., Meijer, I.A., Lessel, D., Mencacci, N.E., Krainc, D., Hempel, M., Tsiakas, K., Prokisch, H., Rossignol, E., Helm, M.H.*, et al.* (2018). Recessive mutations in VPS13D cause childhood onset movement disorders. Ann Neurol *83*, 1089-1095.

Ge, L., Melville, D., Zhang, M., and Schekman, R. (2013). The ER-Golgi intermediate compartment is a key membrane source for the LC3 lipidation step of autophagosome biogenesis. Elife *2*, e00947.

Gelmetti, V., De Rosa, P., Torosantucci, L., Marini, E.S., Romagnoli, A., Di Rienzo, M., Arena, G., Vignone, D., Fimia, G.M., and Valente, E.M. (2017). PINK1 and BECN1

relocalize at mitochondria-associated membranes during mitophagy and promote ER-mitochondria tethering and autophagosome formation. Autophagy *13*, 654-669.

Gillingham, A.K., Sinka, R., Torres, I.L., Lilley, K.S., and Munro, S. (2014). Toward a comprehensive map of the effectors of rab GTPases. Dev Cell *31*, 358-373.

Giorgi, C., Missiroli, S., Patergnani, S., Duszynski, J., Wieckowski, M.R., and Pinton, P. (2015). Mitochondria-associated membranes: composition, molecular mechanisms, and physiopathological implications. Antioxid Redox Signal *22*, 995-1019.

Gonçalves, P.R., Rocha-Brito, K.J., Fernandes, M.R., Abrantes, J.L., Durán, N., and Ferreira-Halder, C.V. (2016). Violacein induces death of RAS-mutated metastatic melanoma by impairing autophagy process. Tumour Biol *37*, 14049-14058.

Guarente, L., and Kenyon, C. (2000). Genetic pathways that regulate ageing in model organisms. Nature *408*, 255-262.

Hailey, D.W., Rambold, A.S., Satpute-Krishnan, P., Mitra, K., Sougrat, R., Kim, P.K., and Lippincott-Schwartz, J. (2010). Mitochondria supply membranes for autophagosome biogenesis during starvation. Cell *141*, 656-667.

Hamasaki, M., Furuta, N., Matsuda, A., Nezu, A., Yamamoto, A., Fujita, N., Oomori, H., Noda, T., Haraguchi, T., Hiraoka, Y.*, et al.* (2013). Autophagosomes form at ER-mitochondria contact sites. Nature *495*, 389-393.

Hamasaki, M., Furuta, N., Matsuda, A., Nezu, A., Yamamoto, A., Fujita, N., Oomori, H., Noda, T., Haraguchi, T., Hiraoka, Y.*, et al.* (2013). Autophagosomes form at ER–mitochondria contact sites. Nature *495*, 389.

Han, H., Tan, J., Wang, R., Wan, H., He, Y., Yan, X., Guo, J., Gao, Q., Li, J., Shang, S.*, et al.* (2020). PINK1 phosphorylates Drp1S616 to regulate mitophagy-independent mitochondrial dynamics. EMBO Rep *21*, e48686.

Hara, T., Takamura, A., Kishi, C., Iemura, S.-i., Natsume, T., Guan, J.-L., and Mizushima, N. (2008). FIP200, a ULK-interacting protein, is required for autophagosome formation in mammalian cells. J Cell Biol *181*, 497-510.

Hayashi-Nishino, M., Fujita, N., Noda, T., Yamaguchi, A., Yoshimori, T., and Yamamoto, A. (2009). A subdomain of the endoplasmic reticulum forms a cradle for autophagosome formation. Nat Cell Biol *11*, 1433-1437.

Honda, S., Arakawa, S., Nishida, Y., Yamaguchi, H., Ishii, E., and Shimizu, S. (2014). Ulk1-mediated Atg5-independent macroautophagy mediates elimination of mitochondria from embryonic reticulocytes. Nat Commun *5*, 4004.

Hou, X., Watzlawik, J.O., Fiesel, F.C., and Springer, W. (2020). Autophagy in Parkinson's Disease. J Mol Biol *432*, 2651-2672.
Houlden, H., and Reilly, M.M. (2006). Molecular genetics of autosomal-dominant demyelinating Charcot-Marie-Tooth disease. Neuromolecular Med *8*, 43-62.

Hung, V., Lam, S.S., Udeshi, N.D., Svinkina, T., Guzman, G., Mootha, V.K., Carr, S.A., and Ting, A.Y. (2017). Proteomic mapping of cytosol-facing outer mitochondrial and ER membranes in living human cells by proximity biotinylation. Elife *6*, e24463.

Hyttinen, J.M.T., Niittykoski, M., Salminen, A., and Kaarniranta, K. (2013). Maturation of autophagosomes and endosomes: A key role for Rab7. Biochim Biophys Acta *1833*, 503-510.

Igarashi, R., Yamashita, S.-i., Yamashita, T., Inoue, K., Fukuda, T., Fukuchi, T., and Kanki, T. (2020). Gemcitabine induces Parkin-independent mitophagy through mitochondrial-resident E3 ligase MUL1-mediated stabilization of PINK1. Sci Rep *10*, 1465.

Jennings, B.H. (2011). Drosophila – a versatile model in biology & medicine. Mater Today *14*, 190-195.

Jia, K., Hart, A.C., and Levine, B. (2007). Autophagy genes protect against disease caused by polyglutamine expansion proteins in Caenorhabditis elegans. Autophagy *3*, 21-25.

Jia, K., and Levine, B. (2007). Autophagy is required for dietary restriction-mediated life span extension in C. elegans. Autophagy *3*, 597-599.

Jiang, P., and Mizushima, N. (2014). Autophagy and human diseases. Cell Res *24*, 69-79.

Jin, S.M., Lazarou, M., Wang, C., Kane, L.A., Narendra, D.P., and Youle, R.J. (2010). Mitochondrial membrane potential regulates PINK1 import and proteolytic destabilization by PARL. J Cell Biol *191*, 933-942.

John Peter, A.T., Herrmann, B., Antunes, D., Rapaport, D., Dimmer, K.S., and Kornmann, B. (2017). Vps13-Mcp1 interact at vacuole–mitochondria interfaces and bypass ER–mitochondria contact sites. J Cell Biol *216*, 3219-3229.

Kamada, Y., Yoshino, K., Kondo, C., Kawamata, T., Oshiro, N., Yonezawa, K., and Ohsumi, Y. (2010). Tor directly controls the Atg1 kinase complex to regulate autophagy. Mol Cell Biol *30*, 1049-1058.

Kamimoto, T., Shoji, S., Hidvegi, T., Mizushima, N., Umebayashi, K., Perlmutter, D.H., and Yoshimori, T. (2006). Intracellular inclusions containing mutant alpha1-antitrypsin Z are propagated in the absence of autophagic activity. J Biol Chem *281*, 4467-4476.

Kim, Y.-M., Jung, C.H., Seo, M., Kim, E.K., Park, J.-M., Bae, S.S., and Kim, D.-H. (2015). mTORC1 phosphorylates UVRAG to negatively regulate autophagosome and endosome maturation. Mol Cell *57*, 207-218.

Kirkin, V., and Rogov, V.V. (2019). A Diversity of Selective Autophagy Receptors Determines the Specificity of the Autophagy Pathway. Mol Cell *76*, 268-285.

Kondapalli, C., Kazlauskaite, A., Zhang, N., Woodroof, H.I., Campbell, D.G., Gourlay, R., Burchell, L., Walden, H., Macartney, T.J., Deak, M.*, et al.* (2012). PINK1 is activated by mitochondrial membrane potential depolarization and stimulates Parkin E3 ligase activity by phosphorylating Serine 65. Open Biol *2*, 120080.

Koyano, F., Okatsu, K., Kosako, H., Tamura, Y., Go, E., Kimura, M., Kimura, Y., Tsuchiya, H., Yoshihara, H., Hirokawa, T.*, et al.* (2014). Ubiquitin is phosphorylated by PINK1 to activate parkin. Nature *510*, 162-166.

Ktistakis, N.T., and Tooze, S.A. (2016). Digesting the Expanding Mechanisms of Autophagy. Trends Cell Biol *26*, 624-635.

Kubli, D.A., Cortez, M.Q., Moyzis, A.G., Najor, R.H., Lee, Y., and Gustafsson Å, B. (2015). PINK1 Is Dispensable for Mitochondrial Recruitment of Parkin and Activation of Mitophagy in Cardiac Myocytes. PLoS One *10*, e0130707.

Kumar, N., Leonzino, M., Hancock-Cerutti, W., Horenkamp, F.A., Li, P., Lees, J.A., Wheeler, H., Reinisch, K.M., and De Camilli, P. (2018). VPS13A and VPS13C are lipid transport proteins differentially localized at ER contact sites. J Cell Biol *217*, 3625-3639.

Lang, A.B., John Peter, A.T., Walter, P., and Kornmann, B. (2015). ER-mitochondrial junctions can be bypassed by dominant mutations in the endosomal protein Vps13. J Cell Biol *210*, 883-890.

Lazarou, M., Jin, S.M., Kane, L.A., and Youle, R.J. (2012). Role of PINK1 binding to the TOM complex and alternate intracellular membranes in recruitment and activation of the E3 ligase Parkin. Dev Cell *22*, 320-333.

Lazarou, M., Sliter, D.A., Kane, L.A., Sarraf, S.A., Wang, C., Burman, J.L., Sideris, D.P., Fogel, A.I., and Youle, R.J. (2015). The ubiquitin kinase PINK1 recruits autophagy receptors to induce mitophagy. Nature *524*, 309-314.

Le Guerroué, F., Eck, F., Jung, J., Starzetz, T., Mittelbronn, M., Kaulich, M., and Behrends, C. (2017). Autophagosomal Content Profiling Reveals an LC3C-Dependent Piecemeal Mitophagy Pathway. Mol Cell *68*, 786-796.e786.

Lee, C.Y., Cooksey, B.A., and Baehrecke, E.H. (2002). Steroid regulation of midgut cell death during Drosophila development. Dev Biol *250*, 101-111.

Lee, J.J., Sanchez-Martinez, A., Zarate, A.M., Benincá, C., Mayor, U., Clague, M.J., and Whitworth, A.J. (2018). Basal mitophagy is widespread in Drosophila but minimally affected by loss of Pink1 or parkin. J Cell Biol *217*, 1613-1622.

Lee, K.-S., Huh, S., Lee, S., Wu, Z., Kim, A.-K., Kang, H.-Y., and Lu, B. (2018). Altered ER-mitochondria contact impacts mitochondria calcium homeostasis and contributes to neurodegeneration in vivo in disease models. Proc Natl Acad Sci U S A *115*, E8844-E8853.

Lefebvre, C., Legouis, R., and Culetto, E. (2018). ESCRT and autophagies: Endosomal functions and beyond. Semin Cell Dev Biol *74*, 21-28.

Lesage, S., Drouet, V., Majounie, E., Deramecourt, V., Jacoupy, M., Nicolas, A., Cormier-Dequaire, F., Hassoun, Sidi M., Pujol, C., Ciura, S.*, et al.* (2016). Loss of VPS13C Function in Autosomal-Recessive Parkinsonism Causes Mitochondrial Dysfunction and Increases PINK1/Parkin-Dependent Mitophagy. Am J Hum Genet *98*, 500-513.

Levine, B., and Deretic, V. (2007). Unveiling the roles of autophagy in innate and adaptive immunity. Nat Rev Immunol *7*, 767-777.

Levine, B., and Kroemer, G. (2008). Autophagy in the pathogenesis of disease. Cell *132*, 27-42.

Li, P., Lees, J.A., Lusk, C.P., and Reinisch, K.M. (2020). Cryo-EM reconstruction of a VPS13 fragment reveals a long groove to channel lipids between membranes. J Cell Biol *219*.

Liang, C., Lee, J.S., Inn, K.S., Gack, M.U., Li, Q., Roberts, E.A., Vergne, I., Deretic, V., Feng, P., Akazawa, C.*, et al.* (2008). Beclin1-binding UVRAG targets the class C Vps complex to coordinate autophagosome maturation and endocytic trafficking. Nat Cell Biol *10*, 776-787.

Liang, X.H., Jackson, S., Seaman, M., Brown, K., Kempkes, B., Hibshoosh, H., and Levine, B. (1999). Induction of autophagy and inhibition of tumorigenesis by beclin 1. Nature *402*, 672-676.

Liesa, M., Palacín, M., and Zorzano, A. (2009). Mitochondrial dynamics in mammalian health and disease. Physiol Rev *89*, 799-845.

Lin, J., Chen, K., Chen, W., Yao, Y., Ni, S., Ye, M., Zhuang, G., Hu, M., Gao, J., Gao, C.*, et al.* (2020). Paradoxical Mitophagy Regulation by PINK1 and TUFm. Mol Cell *80*, 607-620.e612.

Lőrincz, P., Mauvezin, C., and Juhász, G. (2017). Exploring Autophagy in Drosophila. Cells *6*, 22.

Lu, Q., Yang, P., Huang, X., Hu, W., Guo, B., Wu, F., Lin, L., Kovács, A.L., Yu, L., and Zhang, H. (2011). The WD40 repeat PtdIns(3)P-binding protein EPG-6 regulates progression of omegasomes to autophagosomes. Dev Cell *21*, 343-357.

Massey, A., Kiffin, R., and Cuervo, A.M. (2004). Pathophysiology of chaperone-mediated autophagy. Int J Biochem Cell Biol *36*, 2420-2434.

Mathur, D., Bost, A., Driver, I., and Ohlstein, B. (2010). A transient niche regulates the specification of Drosophila intestinal stem cells. Science *327*, 210-213.

Matsuura, A., Tsukada, M., Wada, Y., and Ohsumi, Y. (1997). Apg1p, a novel protein kinase required for the autophagic process in Saccharomyces cerevisiae. Gene *192*, 245-250.

McLelland, G.-L., Goiran, T., Yi, W., Dorval, G., Chen, C.X., Lauinger, N.D., Krahn, A.I., Valimehr, S., Rakovic, A., Rouiller, I.*, et al.* (2018). Mfn2 ubiquitination by PINK1/parkin gates the p97-dependent release of ER from mitochondria to drive mitophagy. Elife *7*, e32866.

McWilliams, T.G., Prescott, A.R., Allen, G.F.G., Tamjar, J., Munson, M.J., Thomson, C., Muqit, M.M.K., and Ganley, I.G. (2016). mito-QC illuminates mitophagy and mitochondrial architecture in vivo. J Cell Biol *214*, 333-345.

McWilliams, T.G., Prescott, A.R., Montava-Garriga, L., Ball, G., Singh, F., Barini, E., Muqit, M.M.K., Brooks, S.P., and Ganley, I.G. (2018). Basal Mitophagy Occurs Independently of PINK1 in Mouse Tissues of High Metabolic Demand. Cell Metab *27*, 439-449.e435.

Mercer, C.A., Kaliappan, A., and Dennis, P.B. (2009). A novel, human Atg13 binding protein, Atg101, interacts with ULK1 and is essential for macroautophagy. Autophagy *5*, 649-662.

Meyers, R.M., Bryan, J.G., McFarland, J.M., Weir, B.A., Sizemore, A.E., Xu, H., Dharia, N.V., Montgomery, P.G., Cowley, G.S., Pantel, S.*, et al.* (2017). Computational

correction of copy number effect improves specificity of CRISPR-Cas9 essentiality screens in cancer cells. Nat Genet *49*, 1779-1784.

Michiorri, S., Gelmetti, V., Giarda, E., Lombardi, F., Romano, F., Marongiu, R., Nerini-Molteni, S., Sale, P., Vago, R., Arena, G.*, et al.* (2010). The Parkinson-associated protein PINK1 interacts with Beclin1 and promotes autophagy. Cell Death Differ *17*, 962-974.

Mijaljica, D., Prescott, M., and Devenish, R.J. (2011). Microautophagy in mammalian cells: revisiting a 40-year-old conundrum. Autophagy *7*, 673-682.

Molejon, M.I., Ropolo, A., Re, A.L., Boggio, V., and Vaccaro, M.I. (2013). The VMP1-Beclin 1 interaction regulates autophagy induction. Sci Rep *3*, 1055-1055.

Moltedo, O., Remondelli, P., and Amodio, G. (2019). The Mitochondria–Endoplasmic Reticulum Contacts and Their Critical Role in Aging and Age-Associated Diseases. Front Cell Dev Biol *7*.

Morselli, E., Galluzzi, L., Kepp, O., Vicencio, J.M., Criollo, A., Maiuri, M.C., and Kroemer, G. (2009). Anti- and pro-tumor functions of autophagy. Biochim Biophys Acta *1793*, 1524-1532.

Muallem, S., Chung, W.Y., Jha, A., and Ahuja, M. (2017). Lipids at membrane contact sites: cell signaling and ion transport. EMBO Rep *18*, 1893-1904.

Nagata, O., Nakamura, M., Sakimoto, H., Urata, Y., Sasaki, N., Shiokawa, N., and Sano, A. (2018). Mouse model of chorea-acanthocytosis exhibits male infertility caused by impaired sperm motility as a result of ultrastructural morphological abnormalities in the mitochondrial sheath in the sperm midpiece. Biochem Biophys Res Commun *503*, 915-920.

Nakada, T.A., Boyd, J.H., Russell, J.A., Aguirre-Hernandez, R., Wilkinson, M.D., Thair, S.A., Nakada, E., McConechy, M.K., Fjell, C.D., and Walley, K.R. (2015). VPS13D Gene Variant Is Associated with Altered IL-6 Production and Mortality in Septic Shock. J Innate Immun *7*, 545-553.

Nakatogawa, H., Suzuki, K., Kamada, Y., and Ohsumi, Y. (2009). Dynamics and diversity in autophagy mechanisms: lessons from yeast. Nat Rev Mol Cell Biol *10*, 458-467.

Naon, D., Zaninello, M., Giacomello, M., Varanita, T., Grespi, F., Lakshminaranayan, S., Serafini, A., Semenzato, M., Herkenne, S., Hernández-Alvarez, M.I.*, et al.* (2016). Critical reappraisal confirms that Mitofusin 2 is an endoplasmic reticulum-mitochondria tether. Proc Natl Acad Sci U S A *113*, 11249-11254.

Narendra, D., Tanaka, A., Suen, D.-F., and Youle, R.J. (2008). Parkin is recruited selectively to impaired mitochondria and promotes their autophagy. J Cell Biol *183*, 795-803.

Narendra, D.P., Jin, S.M., Tanaka, A., Suen, D.-F., Gautier, C.A., Shen, J., Cookson, M.R., and Youle, R.J. (2010). PINK1 Is Selectively Stabilized on Impaired Mitochondria to Activate Parkin. PLoS Biol *8*, e1000298.

Nascimbeni, A.C., Giordano, F., Dupont, N., Grasso, D., Vaccaro, M.I., Codogno, P., and Morel, E. (2017). ER-plasma membrane contact sites contribute to autophagosome biogenesis by regulation of local PI3P synthesis. EMBO J *36*, 2018-2033.

Nishimura, T., and Tooze, S.A. (2020). Emerging roles of ATG proteins and membrane lipids in autophagosome formation. Cell Discov *6*, 32.

Ohtake, F., Tsuchiya, H., Saeki, Y., and Tanaka, K. (2018). K63 ubiquitylation triggers proteasomal degradation by seeding branched ubiquitin chains. Proc Natl Acad Sci U S A *115*, E1401.

Okatsu, K., Koyano, F., Kimura, M., Kosako, H., Saeki, Y., Tanaka, K., and Matsuda, N. (2015). Phosphorylated ubiquitin chain is the genuine Parkin receptor. J Cell Biol *209*, 111-128.

Okatsu, K., Uno, M., Koyano, F., Go, E., Kimura, M., Oka, T., Tanaka, K., and Matsuda, N. (2013). A dimeric PINK1-containing complex on depolarized mitochondria stimulates Parkin recruitment. J Biol Chem *288*, 36372-36384.

Ordureau, A., Sarraf, S.A., Duda, D.M., Heo, J.M., Jedrychowski, M.P., Sviderskiy, V.O., Olszewski, J.L., Koerber, J.T., Xie, T., Beausoleil, S.A.*, et al.* (2014). Quantitative proteomics reveal a feedforward mechanism for mitochondrial PARKIN translocation and ubiquitin chain synthesis. Mol Cell *56*, 360-375.

Osawa, T., Kotani, T., Kawaoka, T., Hirata, E., Suzuki, K., Nakatogawa, H., Ohsumi, Y., and Noda, N.N. (2019). Atg2 mediates direct lipid transfer between membranes for autophagosome formation. Nat Struct Mol Biol *26*, 281-288.

Osawa, T., and Noda, N.N. (2019). Atg2: A novel phospholipid transfer protein that mediates de novo autophagosome biogenesis. Protein Sci *28*, 1005-1012.

Paillusson, S., Stoica, R., Gomez-Suaga, P., Lau, D.H.W., Mueller, S., Miller, T., and Miller, C.C.J. (2016). There's Something Wrong with my MAM; the ER-Mitochondria Axis and Neurodegenerative Diseases. Trends Neurosci *39*, 146-157.

Palikaras, K., Lionaki, E., and Tavernarakis, N. (2018). Mechanisms of mitophagy in cellular homeostasis, physiology and pathology. Nat Cell Biol *20*, 1013-1022.

Parzych, K.R., and Klionsky, D.J. (2014). An overview of autophagy: morphology, mechanism, and regulation. Antioxid Redox Signal *20*, 460-473.

Pattingre, S., Tassa, A., Qu, X., Garuti, R., Liang, X.H., Mizushima, N., Packer, M., Schneider, M.D., and Levine, B. (2005). Bcl-2 antiapoptotic proteins inhibit Beclin 1-dependent autophagy. Cell *122*, 927-939.

Peikert, K., Danek, A., and Hermann, A. (2018). Current state of knowledge in Chorea-Acanthocytosis as core Neuroacanthocytosis syndrome. Eur J Med Genet *61*, 699-705.
Pickles, S., Vigié, P., and Youle, R.J. (2018). Mitophagy and Quality Control Mechanisms in Mitochondrial Maintenance. Curr Biol *28*, R170-R185.

Pilli, M., Arko-Mensah, J., Ponpuak, M., Roberts, E., Master, S., Mandell, M.A., Dupont, N., Ornatowski, W., Jiang, S., Bradfute, S.B.*, et al.* (2012). TBK-1 promotes autophagy-mediated antimicrobial defense by controlling autophagosome maturation. Immunity *37*, 223-234.

Pryde, K.R., Smith, H.L., Chau, K.-Y., and Schapira, A.H.V. (2016). PINK1 disables the anti-fission machinery to segregate damaged mitochondria for mitophagy. J Cell Biol *213*, 163-171.

Puri, C., Renna, M., Bento, C.F., Moreau, K., and Rubinsztein, D.C. (2013). Diverse autophagosome membrane sources coalesce in recycling endosomes. Cell *154*, 1285-1299.

Qu, X., Yu, J., Bhagat, G., Furuya, N., Hibshoosh, H., Troxel, A., Rosen, J., Eskelinen, E.L., Mizushima, N., Ohsumi, Y.*, et al.* (2003). Promotion of tumorigenesis by heterozygous disruption of the beclin 1 autophagy gene. J Clin Invest *112*, 1809-1820.

Rakovic, A., Grünewald, A., Kottwitz, J., Brüggemann, N., Pramstaller, P.P., Lohmann, K., and Klein, C. (2011). Mutations in PINK1 and Parkin Impair Ubiquitination of Mitofusins in Human Fibroblasts. PLoS One *6*, e16746.

Rakovic, A., Ziegler, J., Mårtensson, C.U., Prasuhn, J., Shurkewitsch, K., König, P., Paulson, H.L., and Klein, C. (2019). PINK1-dependent mitophagy is driven by the UPS and can occur independently of LC3 conversion. Cell Death Differ *26*, 1428-1441.

Ravikumar, B., Moreau, K., Jahreiss, L., Puri, C., and Rubinsztein, D.C. (2010). Plasma membrane contributes to the formation of pre-autophagosomal structures. Nat Cell Biol *12*, 747-757.

Razi, M., Chan, E.Y., and Tooze, S.A. (2009). Early endosomes and endosomal coatomer are required for autophagy. J Cell Biol *185*, 305-321.

Rojansky, R., Cha, M.-Y., and Chan, D.C. (2016). Elimination of paternal mitochondria in mouse embryos occurs through autophagic degradation dependent on PARKIN and MUL1. Elife *5*, e17896.

Scarlatti, F., Maffei, R., Beau, I., Codogno, P., and Ghidoni, R. (2008). Role of non-canonical Beclin 1-independent autophagy in cell death induced by resveratrol in human breast cancer cells. Cell Death Differ *15*, 1318-1329.

Schäfer, J.A., Schessner, J.P., Bircham, P.W., Tsuji, T., Funaya, C., Pajonk, O., Schaeff, K., Ruffini, G., Papagiannidis, D., Knop, M.*, et al.* (2020). ESCRT machinery mediates selective microautophagy of endoplasmic reticulum in yeast. EMBO J *39*, e102586.

Scheffner, M., Nuber, U., and Huibregtse, J.M. (1995). Protein ubiquitination involving an E1-E2-E3 enzyme ubiquitin thioester cascade. Nature *373*, 81-83.

Schon, E.A., and Area-Gomez, E. (2013). Mitochondria-associated ER membranes in Alzheimer disease. Mol Cell Neurosci *55*, 26-36.

Schweers, R.L., Zhang, J., Randall, M.S., Loyd, M.R., Li, W., Dorsey, F.C., Kundu, M., Opferman, J.T., Cleveland, J.L., Miller, J.L.*, et al.* (2007). NIX is required for programmed mitochondrial clearance during reticulocyte maturation. Proc Natl Acad Sci U S A *104*, 19500-19505.

Seifert, W., Kühnisch, J., Maritzen, T., Horn, D., Haucke, V., and Hennies, H.C. (2011). Cohen Syndrome-associated Protein, COH1, Is a Novel, Giant Golgi Matrix Protein Required for Golgi Integrity*. J Biol Chem *286*, 37665-37675.

Seong, E., Insolera, R., Dulovic, M., Kamsteeg, E.-J., Trinh, J., Brüggemann, N., Sandford, E., Li, S., Ozel, A.B., Li, J.Z.*, et al.* (2018). Mutations in VPS13D lead to a new recessive ataxia with spasticity and mitochondrial defects. Ann Neurol *83*, 1075-1088.

Shaid, S., Brandts, C.H., Serve, H., and Dikic, I. (2013). Ubiquitination and selective autophagy. Cell Death Differ *20*, 21-30.

Shiba-Fukushima, K., Arano, T., Matsumoto, G., Inoshita, T., Yoshida, S., Ishihama, Y., Ryu, K.Y., Nukina, N., Hattori, N., and Imai, Y. (2014). Phosphorylation of mitochondrial polyubiquitin by PINK1 promotes Parkin mitochondrial tethering. PLoS Genet *10*, e1004861.

Shiba-Fukushima, K., Imai, Y., Yoshida, S., Ishihama, Y., Kanao, T., Sato, S., and Hattori, N. (2012). PINK1-mediated phosphorylation of the Parkin ubiquitin-like domain primes mitochondrial translocation of Parkin and regulates mitophagy. Sci Rep *2*, 1002.

Shpilka, T., Weidberg, H., Pietrokovski, S., and Elazar, Z. (2011). Atg8: an autophagy-related ubiquitin-like protein family. Genome Biol *12*, 226-226.

Stjepanovic, G., Baskaran, S., Lin, M.G., and Hurley, J.H. (2017). Vps34 Kinase Domain Dynamics Regulate the Autophagic PI 3-Kinase Complex. Mol Cell *67*, 528-534.e523.

Suzuki, K., Kubota, Y., Sekito, T., and Ohsumi, Y. (2007). Hierarchy of Atg proteins in pre-autophagosomal structure organization. Genes Cells *12*, 209-218.

Takahashi, Y., Coppola, D., Matsushita, N., Cualing, H.D., Sun, M., Sato, Y., Liang, C., Jung, J.U., Cheng, J.Q., Mulé, J.J.*, et al.* (2007). Bif-1 interacts with Beclin 1 through UVRAG and regulates autophagy and tumorigenesis. Nat Cell Biol *9*, 1142-1151.

Takeshige, K., Baba, M., Tsuboi, S., Noda, T., and Ohsumi, Y. (1992). Autophagy in yeast demonstrated with proteinase-deficient mutants and conditions for its induction. J Cell Biol *119*, 301-311.

Tian, Y., Li, Z., Hu, W., Ren, H., Tian, E., Zhao, Y., Lu, Q., Huang, X., Yang, P., Li, X.*, et al.* (2010). C. elegans Screen Identifies Autophagy Genes Specific to Multicellular Organisms. Cell *141*, 1042-1055.

Tracy, K., Dibling, B.C., Spike, B.T., Knabb, J.R., Schumacker, P., and Macleod, K.F. (2007). BNIP3 is an RB/E2F target gene required for hypoxia-induced autophagy. Mol Cell Biol *27*, 6229-6242.

Tsuboyama, K., Koyama-Honda, I., Sakamaki, Y., Koike, M., Morishita, H., and Mizushima, N. (2016). The ATG conjugation systems are important for degradation of the inner autophagosomal membrane. Science *354*, 1036-1041.

Ugur, B., Hancock-Cerutti, W., Leonzino, M., and De Camilli, P. (2020). Role of VPS13, a protein with similarity to ATG2, in physiology and disease. Curr Opin Genet Dev *65*, 61-68.

Valadas, J.S., Esposito, G., Vandekerkhove, D., Miskiewicz, K., Deaulmerie, L., Raitano, S., Seibler, P., Klein, C., and Verstreken, P. (2018). ER Lipid Defects in Neuropeptidergic Neurons Impair Sleep Patterns in Parkinson's Disease. Neuron *98*, 1155-1169.e1156.

Valverde, D.P., Yu, S., Boggavarapu, V., Kumar, N., Lees, J.A., Walz, T., Reinisch, K.M., and Melia, T.J. (2019). ATG2 transports lipids to promote autophagosome biogenesis. J Cell Biol *218*, 1787-1798.

Velayos-Baeza, A., Vettori, A., Copley, R.R., Dobson-Stone, C., and Monaco, A.P. (2004). Analysis of the human VPS13 gene family. Genomics *84*, 536-549.

Vicencio, E., Beltrán, S., Labrador, L., Manque, P., Nassif, M., and Woehlbier, U. (2020). Implications of Selective Autophagy Dysfunction for ALS Pathology. Cells *9*, 381.

Vilain, S., Esposito, G., Haddad, D., Schaap, O., Dobreva, M.P., Vos, M., Van Meensel, S., Morais, V.A., De Strooper, B., and Verstreken, P. (2012). The yeast complex I equivalent NADH dehydrogenase rescues pink1 mutants. PLoS Genet *8*, e1002456.

Vives-Bauza, C., Zhou, C., Huang, Y., Cui, M., de Vries, R.L.A., Kim, J., May, J., Tocilescu, M.A., Liu, W., Ko, H.S.*, et al.* (2010). PINK1-dependent recruitment of Parkin to mitochondria in mitophagy. Proc Natl Acad Sci U S A *107*, 378.

von Stockum, S., Marchesan, E., and Ziviani, E. (2018). Mitochondrial quality control beyond PINK1/Parkin. Oncotarget *9*, 12550-12551.

Vonk, J.J., Yeshaw, W.M., Pinto, F., Faber, A.I.E., Lahaye, L.L., Kanon, B., van der Zwaag, M., Velayos-Baeza, A., Freire, R., van Ijzendoorn, S.C.*, et al.* (2017). Drosophila Vps13 Is Required for Protein Homeostasis in the Brain. PLoS One *12*, e0170106.

Wang, T., Birsoy, K., Hughes, N.W., Krupczak, K.M., Post, Y., Wei, J.J., Lander, E.S., and Sabatini, D.M. (2015). Identification and characterization of essential genes in the human genome. Science *350*, 1096-1101.

Wang, X., Winter, D., Ashrafi, G., Schlehe, J., Wong, Y.L., Selkoe, D., Rice, S., Steen, J., LaVoie, M.J., and Schwarz, T.L. (2011). PINK1 and Parkin target Miro for phosphorylation and degradation to arrest mitochondrial motility. Cell *147*, 893-906.

Wang, Y., Liu, N., and Lu, B. (2019). Mechanisms and roles of mitophagy in neurodegenerative diseases. CNS Neurosci Ther *25*, 859-875.

Wauer, T., Swatek, K.N., Wagstaff, J.L., Gladkova, C., Pruneda, J.N., Michel, M.A., Gersch, M., Johnson, C.M., Freund, S.M., and Komander, D. (2015). Ubiquitin Ser65 phosphorylation affects ubiquitin structure, chain assembly and hydrolysis. EMBO J *34*, 307-325.

Williams, A., Jahreiss, L., Sarkar, S., Saiki, S., Menzies, F.M., Ravikumar, B., and Rubinsztein, D.C. (2006). Aggregate-prone proteins are cleared from the cytosol by autophagy: therapeutic implications. Curr Top Dev Biol *76*, 89-101.

Wilson, E.L., and Metzakopian, E. (2020). ER-mitochondria contact sites in neurodegeneration: genetic screening approaches to investigate novel disease mechanisms. Cell Death Differ.

Wong, Y.C., Ysselstein, D., and Krainc, D. (2018). Mitochondria–lysosome contacts regulate mitochondrial fission via RAB7 GTP hydrolysis. Nature *554*, 382-386.

Xie, Z., and Klionsky, D.J. (2007). Autophagosome formation: core machinery and adaptations. Nat Cell Biol *9*, 1102-1109.

Yang, J.-Y., and Yang, W.Y. (2013). Bit-by-bit autophagic removal of parkin-labelled mitochondria. Nat Commun *4*, 2428.

Yang, Y., Ouyang, Y., Yang, L., Beal, M.F., McQuibban, A., Vogel, H., and Lu, B. (2008). Pink1 regulates mitochondrial dynamics through interaction with the fission/fusion machinery. Proc Natl Acad Sci U S A *105*, 7070-7075.

Yeshaw, W.M., van der Zwaag, M., Pinto, F., Lahaye, L.L., Faber, A.I.E., Gómez-Sánchez, R., Dolga, A.M., Poland, C., Monaco, A.P., van Ijzendoorn, S.C.D.*, et al.* (2019). Human VPS13A is associated with multiple organelles and influences mitochondrial morphology and lipid droplet motility. Elife *8*, e43561.

Ylä-Anttila, P., Vihinen, H., Jokitalo, E., and Eskelinen, E.L. (2009). 3D tomography reveals connections between the phagophore and endoplasmic reticulum. Autophagy *5*, 1180-1185.

Youle, R.J., and Narendra, D.P. (2011). Mechanisms of mitophagy. Nat Rev Mol Cell Biol *12*, 9-14.

Yun, C.W., and Lee, S.H. (2018). The Roles of Autophagy in Cancer. Int J Mol Sci *19*, 3466.

Yun, J., Puri, R., Yang, H., Lizzio, M.A., Wu, C., Sheng, Z.H., and Guo, M. (2014). MUL1 acts in parallel to the PINK1/parkin pathway in regulating mitofusin and compensates for loss of PINK1/parkin. Elife *3*, e01958.

Zhao, Y.G., Chen, Y., Miao, G., Zhao, H., Qu, W., Li, D., Wang, Z., Liu, N., Li, L., Chen, S.*, et al.* (2017). The ER-Localized Transmembrane Protein EPG-3/VMP1 Regulates SERCA Activity to Control ER-Isolation Membrane Contacts for Autophagosome Formation. Mol Cell *67*, 974-989.e976.

Zhu, D., Zhou, J., Zhao, J., Jiang, G., Zhang, X., Zhang, Y., and Dong, M. (2019). ZC3H13 suppresses colorectal cancer proliferation and invasion via inactivating Ras-ERK signaling. J Cell Physiol *234*, 8899-8907.

Ziviani, E., Tao, R.N., and Whitworth, A.J. (2010). Drosophila parkin requires PINK1 for mitochondrial translocation and ubiquitinates mitofusin. Proc Natl Acad Sci U S A *107*, 5018-5023.